Groundwater salinization processes in the coastal area of the Netherlands due to transgressions during the Holocene

Post, V.E.A.

2004

document version
Publisher's PDF, also known as Version of record

Groundwater salinization processes in the coastal area of the Netherlands due to transgressions during the Holocene

ISBN 90-9017404-4

Groundwater salinization processes in the coastal area of the Netherlands due to transgressions during the Holocene. [Ph.D. thesis, Vrije Universiteit Amsterdam]

In Dutch: Processen van grondwaterverzilting in het Nederlandse kustgebied ten gevolge van transgressies tijdens het Holoceen. [ac. proefschrift, Vrije Universiteit Amsterdam]

Available on-line at http://home.hccnet.nl/vincentpost/

Cover photo: sunset at Den Helder

This project was partly funded by the Netherlands Institute of Applied Geoscience TNO - National Geological Survey.

VRIJE UNIVERSITEIT

Groundwater salinization processes in the coastal area of the Netherlands due to transgressions during the Holocene

ACADEMISCH PROEFSCHRIFT

ter verkrijging van de graad van doctor aan
de Vrije Universiteit Amsterdam,
op gezag van de rector magnificus
prof.dr. T. Sminia,
in het openbaar te verdedigen
ten overstaan van de promotiecommissie
van de faculteit der Aard- en Levenswetenschappen
op dinsdag 6 januari 2004 om 15.45 uur
in het auditorium van de universiteit,
De Boelelaan 1105

door

Vincent Eduard Alexander Post

geboren te Dordrecht

promotor: prof.dr. J.J. de Vries
copromotor: dr. H. Kooi

Se non è vera, è ben trovata

Italian proverb. Derived from: Giordano Bruno,
Gli Eroici Furori, 1585.

leescommissie: prof. W.M. Edmunds
dr. C.J. Beets
dr. J. Griffioen
dr.ir. C.R. Meinardi
dr.ir. T.N. Olsthoorn

Contents

List of Figures

List of Tables

Introduction

Background

The hydrogeology of coastal aquifers has been studied intensively during the past decades, stimulated by both scientific interest and societal relevance. Practical hydrological problems in coastal areas are typically connected to contamination of fresh water resources by seawater and include amongst others well field salinization, crop damage and surface water quality deterioration. Proper management of available groundwater reserves is impossible without knowledge of the spatial distribution of fresh and saline groundwater and the processes that determine the evolution hereof.

The traditional conception of the spatial distribution of fresh and saline groundwater in a coastal aquifer comprises a fresh water lens overlying a salt-water wedge on land and saline groundwater below the seafloor (Hubbert, 1940). Application of this concept is restricted to areas where the position of the coastline has remained stable sufficiently long to reach equilibrium. This situation, however, is the exception rather than the rule as global sea level fluctuates on a geological timescale and coastlines consequently migrate. Notably the effects of the sea level lowstand during the last glaciation (Weichselian, 110 – 10 ka BP) and the subsequent sea level rise during the Holocene (10 ka BP – present) are still recognized in coastal groundwaters today (e.g Edmunds, 2001). As a result, saline groundwater is often encountered far inland from the current coastline or, conversely, fresh groundwater is found up to tens of kilometers offshore.

As the present-day distribution of fresh and saline groundwater in coastal aquifers still reflects former environmental conditions, it is often unclear to what extent the current situation is the result of long-term effects or recent (anthropogenic) changes. Understanding the processes and factors that control the evolution of saline water in the subsurface over periods of thousands of years is an academic challenge and at the same time of important practical use for water resource evaluation and seawater intrusion studies. Insights can be based on interpretations of the observed groundwater composition and/or modelling studies. Applications of numerical codes to study fresh-salt water dynamics on a geological timescale (e.g. Oude Essink, 1996; Groen et al., 2000a; Kooi et al., 2000; Harrar et al., 2001; Person et al., 2001) are relatively rare. The paleohydrological development of coastal groundwater systems was given considerable attention, however, in hydrochemistry and isotope hydrology

(e.g. Walraevens, 1987; Beekman, 1991; Appelo, 1994; Van der Kemp et al., 2000).

In the Netherlands, interest in groundwater salinization developed during the second half of the 19th century when the search for drinking water near the city of Amsterdam revealed the occurrence of saline groundwater (Harting, 1852; Drabbe and Badon Ghijben, 1888). At present, the Pleistocene coastal aquifers are among the most heavily-investigated hydrogeological systems in the world. A dense network of observation wells and systematic geo-electrical surveys have shown that the subsurface salinity distribution is very heterogeneous.

Many authors attempted to explain the occurrence of saline groundwater in the Pleistocene aquifer system of the Dutch coastal area (Lorie, 1899; Dubois, 1903; Wintgens, 1911; Versluys, 1931; Geirnaert, 1972; De Vries, 1974; Appelo and Geirnaert, 1991; Stuyfzand, 1993; Oude Essink, 1996) and competing theories developed about the processes through which seawater entered the aquifers (Versluys, 1931; Volker, 1961; Meinardi, 1974; Pomper, 1978; Beekman, 1991; Gieske, 1991). The origin of the saline groundwater is still not fully understood, however, because many studies remained of a qualitative character, had only local applicability or did not consider and integrate all available data. This thesis strives to complement and extend previous work by adopting the quantitative methods available today, combining numerical, chemical and isotopic techniques.

End and means

The primary objective of this thesis is to develop quantitative understanding of the processes that caused salinization of groundwater in the coastal area of the Netherlands[1] during the Holocene under natural conditions. It is expected that understanding of the paleohydrological evolution and the connected processes from this extremely well-documented area has generic applicability and can be used to explain salinity patterns in aquifer systems where data are less abundant.

Even when a wealth of observations exists, the interpretation of the salinity distribution in aquifers is extremely complicated. Much of the uncertainty is related to the fact that the circumstances under which the saline waters formed are unknown or no longer exist. The timescales of reaction to changing boundary conditions differ between hydraulic and hydrochemical systems, which often means that water quality patterns are the result of multiple consecutive flow systems. Additional complications arise from the fact that man has sometimes altered the hydrogeological conditions to such an extent that it has become difficult to assess whether such patterns reflect the natural situation. This is particularly the case in the Dutch coastal area where water management and land reclamation practices have dramatically changed the hydrological and topographical conditions during the last 1 000 y.

[1] In this thesis, the coastal area of the Netherlands denotes that part of the country in which marine conditions were established during the Holocene and approximately coincides with the area that has an elevation below sea level.

An approach is used here that combines different earth-scientific disciplines in an attempt to overcome these difficulties. The disciplines comprise:

hydrochemistry and isotope hydrology to constrain age and provenance of the brackish and saline groundwater

study of the pore water composition of confining units to reconstruct former environmental conditions and identify processes that controlled salinization

numerical transport modelling to simulate the conditions that existed when the sea covered the present land surface during the Holocene

Quaternary geology to reconstruct paleogeographical developments

This thesis demonstrates that in order to understand the hydrogeology of coastal areas, insights from all these individual subdisciplines have to be taken into account.

Thesis outline

The main body of this thesis consists of six chapters. Each chapter, except chapter 6, is based on a paper that has been submitted to or accepted by peer-reviewed journals. A subdivision into three parts was made, each part containing two chapters:

Part I reviews existing observations from the Pleistocene aquifers in the coastal area. In chapter 1 the present-day salinity distribution is used to identify patterns that may be related to the processes that caused salinization. Chapter 2 focuses on establishing the age and provenance of the brackish and saline groundwater based on its stable isotope and radiocarbon signature.

Part II deals with the study of the pore water composition in confining units. Chapter 3 presents the results of a study of a formerly-fresh clay bed below the North Sea that currently becomes more saline by diffusion of dissolved salts from the overlying seawater. A similar study was undertaken on the island of Texel where anomalously-high Cl concentrations (i.e., higher than seawater) are encountered, which will be discussed in chapter 4.

Part III discusses the results of numerical transport modelling. In chapter 5 a relation between permeability and the rate of salinization by free convection is sought. The effect of complicating factors such as sedimentation and the presence of low-permeability strata in the subsurface is treated quantitatively in chapter 6

The final chapter (synthesis) summarizes the main conclusions from the foregoing chapters to provide an overview of the controls on salinization of coastal aquifers during transgressions and discusses the hydrogeological implications.

Part I: review of existing observations from the Pleistocene aquifers

Chapter 1

Relation between geological history and groundwater salinity

Abstract

A data set consisting of chemical (chlorinity) and geo-electrical measurements was compiled from existing studies and archives to obtain an overview of the large-scale subsurface salinity distribution in the coastal area of the Netherlands. A critical review of all possible salinization mechanisms shows that the origin of the brackish and saline groundwater is related to former transgressions. The vertical salinity distribution of the groundwater indicates that connate seawater dating from the Pliocene to Early-Pleistocene is not the source of the brackish to saline groundwater in the overlying Pleistocene fluvial aquifers. Instead, it derives from Holocene transgressions. The salinization mechanism is discussed in relation to the paleogeographical development during the Holocene and the occurrence of low-permeability strata. Finally, freshening of the aquifers following retreat of the sea is briefly considered.

1.1 Introduction

A very complex salinity distribution is encountered in the coastal area of the Netherlands that is not in equilibrium with present-day hydrological boundary conditions (Oude Essink, 1996). As will be elaborated in this chapter, the origin of the brackish and saline groundwater is related to the geological history of the area that included multiple transgressions during the past 2 My. Understanding the genesis of the salinity distribution requires knowledge of the hydrological processes (e.g. diffusion, compaction-driven flow, free and forced convection) that control the salinity distribution on a geological timescale ($>$ 1 ka). Identification of these processes is

This chapter is based on the paper: Post, V.E.A., Van der Plicht, H., Meijer, H.A.J., 2003. The origin of brackish and saline groundwater in the coastal area of the Netherlands. Netherlands Journal of Geosciences / Geologie en Mijnbouw 82, 131-145.

complicated because the present-day groundwater composition has been strongly affected by man-made changes of the boundary conditions during the recent past.

In the Dutch coastal area, a wealth of observations is available that are scattered across many different archives and reports. Various authors have addressed the origin of the brackish to saline groundwater (e.g. Volker, 1961; De Vries, 1981; Beekman, 1991; Gieske, 1991; Meinardi, 1991; Stuyfzand, 1993), but few publications integrate data from these various sources. Both in this chapter and in chapter 2, a conceptual model of the genesis of the current salinity distribution will be presented based on a comprehensive collection of geological, chemical, isotopic and geophysical data. The data will be presented in the form of maps and charts and the possible sources of salt will be treated in detail. From the analysis, conclusions will be drawn on the origin of the brackish to saline groundwater and the relevant hydrological processes will be identified.

1.2 Physical setting

The coastal area of the Netherlands forms a part of the southeastern North Sea coastal plain that extends more or less continuously from northern Denmark to the north of France. The morphology generally consists of a polder landscape with an elevation near or below sea level, bordered on the western side by a coastal dune belt and on the eastern side by a fresh water lake (IJsselmeer), the more elevated terrain of ice-pushed ridges and the Brabant Massif and recent river deposits of Rhine and Meuse (figure 1.1).

1.2.1 Geological history

The North Sea covered most of the Netherlands during the Early Pliocene (figure 1.2) but both the coastline and the depocenters were shifting toward the northwest at that time (Zagwijn, 1989). This shift continued into the Early-Pleistocene and by 1.6 Ma BP marine influences had disappeared from the present coastal area. The deltas of large rivers draining the Baltic region (the predecessors of the rivers Elbe, Weser and Ems, referred to as eastern rivers) and of the rivers Rhine and Meuse, merged to form one large delta complex. The expansion of the large delta continued until the early part of the Middle Pleistocene. The regression reached a maximum in the period between 900 and 450 ka BP, when the coastline was probably in the vicinity of the Dogger Bank (Zagwijn, 1989). It was not until the Holsteinian interglacial that the sea invaded the western part of the Netherlands again. Marine sediments from this period are found locally in deep valley systems that had formed during the Elsterian glacial stage (380 – 360 ka BP). During the following Saalian glacial (180 – 130 ka BP), ice sheets covered approximately half of the Netherlands (Zagwijn, 1974), which had a profound impact on the morphology of the landscape. The ice formed subglacial basins of up to 100 m deep and ice-pushed ridges with

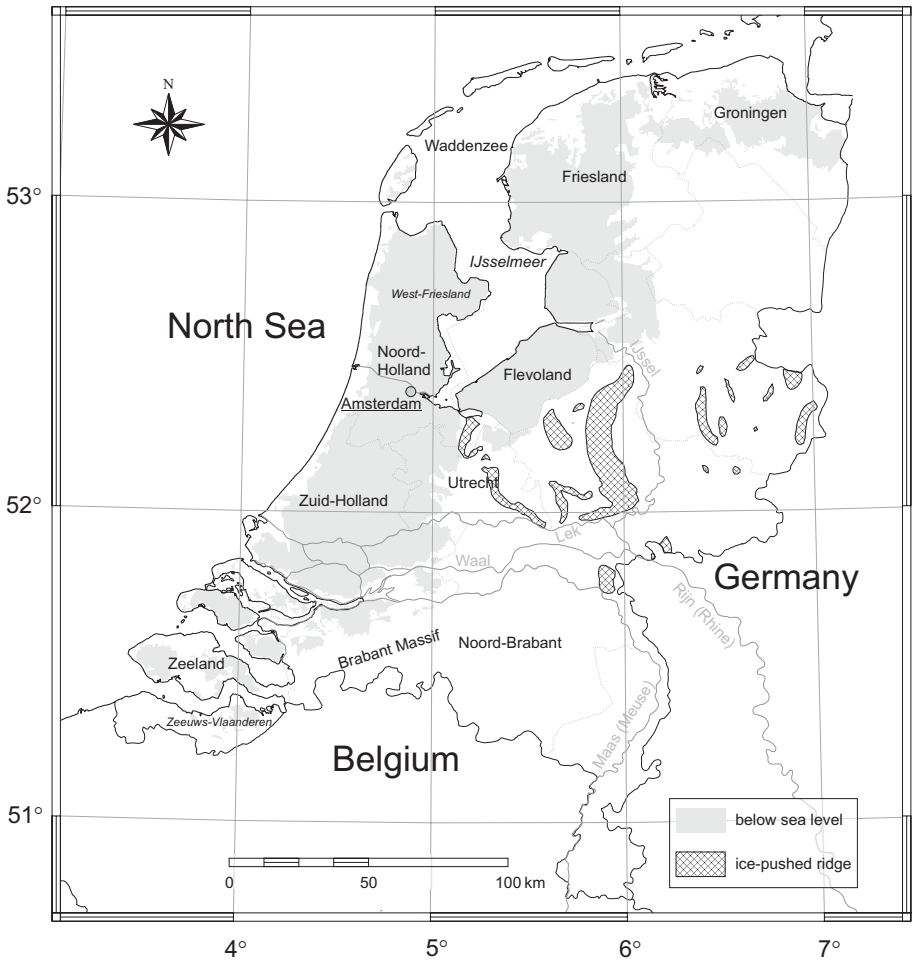

Figure 1.1: Map of the Netherlands showing the area below mean sea level, ice-pushed ridges and geographical names referred to in the text.

heights of more than 100 m (De Gans et al., 1986). Sea level rose during the Eemian (130 – 110 ka BP) and the sea penetrated the former glacial basins and deep river valleys (Zagwijn, 1983), resulting in widespread marine conditions in the western part of the Netherlands (figure 1.2). During the Weichselian glacial (110 – 10 ka BP), periglacial conditions prevailed and the Saalian relief was further levelled through the deposition of so-called drift sands (fine-grained aeolian deposits) and strong

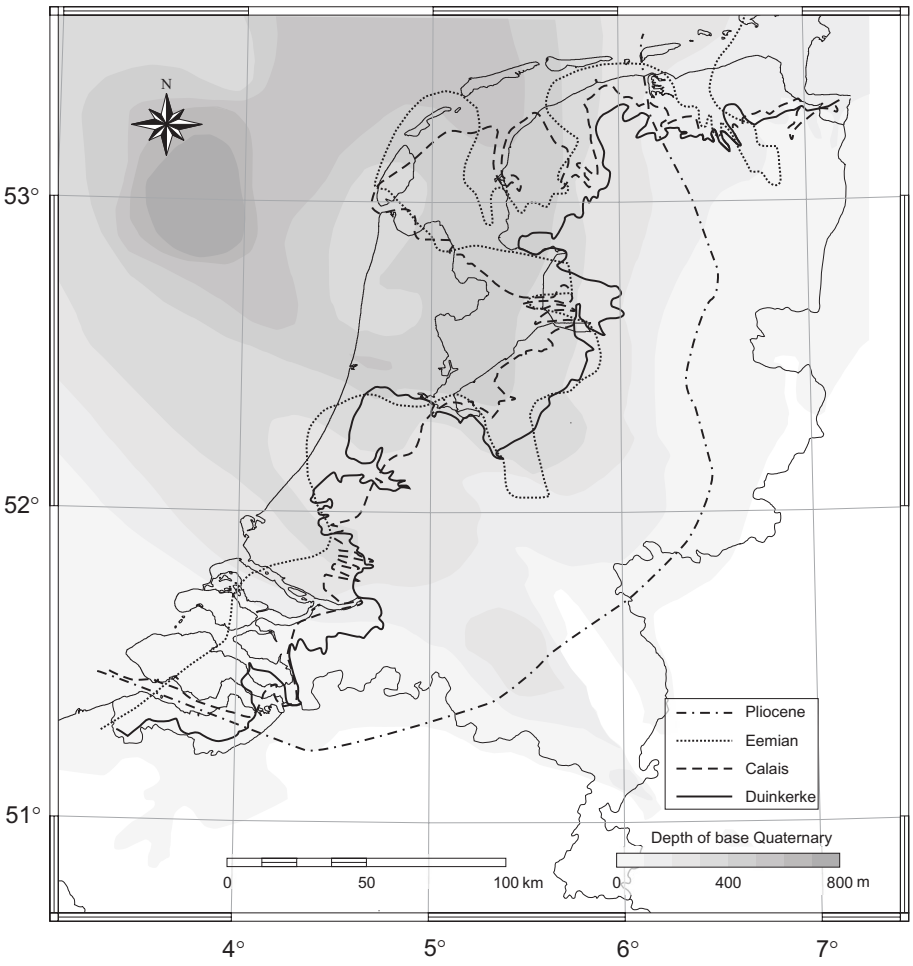

Figure 1.2: Map of the Netherlands showing the depth of the base of the Quaternary strata (Zagwijn and Doppert, 1978) and landward extent of the North Sea during the Pliocene and three Quaternary transgressions (Zagwijn, 1974; Zagwijn and Doppert, 1978; Zagwijn, 1986).

erosion of elevated terrain (Zagwijn, 1974). The rivers Rhine and Meuse eroded two extensive east-west running valleys (in the present floodplain of the Rhine and in the IJsselmeer/West-Friesland area) that were separated by an area with little relief (De Gans and Van Gijssel, 1996).

These valleys were the first areas that were inundated when the North Sea reached the present coastline approximately 7.5 ka BP. Groundwater levels increased as a result of the sea level rise and due to the poor drainage of the relatively flat area, widespread peat formation occurred (Basal peat). Sea level continued to rise (Calais transgression: 8 – 3.8 ka BP) and the sea flooded large parts of the peat areas (figure 1.2). Around 5 ka BP barrier islands had formed at almost the same position as the present coastline, inland of which sand and clay were deposited in a lagoonal and tidal flat area fringed by salt marshes. Several tidal inlets dissected the barrier islands (Beets et al., 1992) and Basal peat was eroded here. Marine influence gradually diminished inland of the barrier islands upon closure of the tidal inlets since 5.5 ka BP (Beets et al., 1992) and once again peat growth occurred (Holland peat). Large peat bogs with an elevation of up to 5 m above the present sea level developed (Pons, 1992). A fresh water lake existed in the IJsselmeer area between about 3 to 1 ka BP (Zagwijn, 1986). Although the sea level rise had decreased to about 5 10^{-4} m/y around 2 ka BP (Beets et al., 1992), large peat areas in the southwestern and northern part of the coastal area were invaded and eroded by the sea (Duinkerke transgression: 3.5 ka BP and later, figure 1.2). Dunes developed on top of the barrier islands from about 1 ka BP. An inland-sea (Zuiderzee) formed in the IJsselmeer area around 0.7 ka BP following strong erosion of the northern peat area.

Since Roman times, man has dramatically changed the natural landscape. Systematic drainage and reclamation of peat bogs and marshes started in early Medieval times. This resulted in land subsidence owing to compaction and decomposition of peat. Vast areas of peat disappeared by erosion during floods and excavation for fuel, as a result of which many large lakes came into being. Several of these lakes have been reclaimed since the Middle Ages. Land reclamation also occurred on tidal flats in the southwestern and northern part of the coastal area, where dikes were built to reclaim these areas from the sea. Dikes were also necessary to prevent rivers from flooding. Due to compaction, decomposition, erosion and sea level rise the elevation of the polders is currently below sea level. This way the characteristic polder landscape of the Dutch coastal area was created.

1.2.2 Stratigraphy

The study area is part of the subsiding North Sea basin that is filled with unconsolidated Cenozoic sediments, varying in thickness from 400 to over 1000 m, overlying Mesozoic strata (Zagwijn, 1989). The upper part of the Tertiary deposits consists of marine sand, sandy clay and clay (Zagwijn and Van Staalduinen, 1975). The depth of the base of the Quaternary sediments is shown in figure 1.2. The oldest Pleistocene layers consist of fine-grained marine deposits that reach a thickness of up to 200 m (Zagwijn and Van Staalduinen, 1975). A thick sequence of continental deposits is overlying these marine sediments. In the northern part of the area, these consist of coarse-grained fluvial deposits of the eastern rivers and the river Rhine.

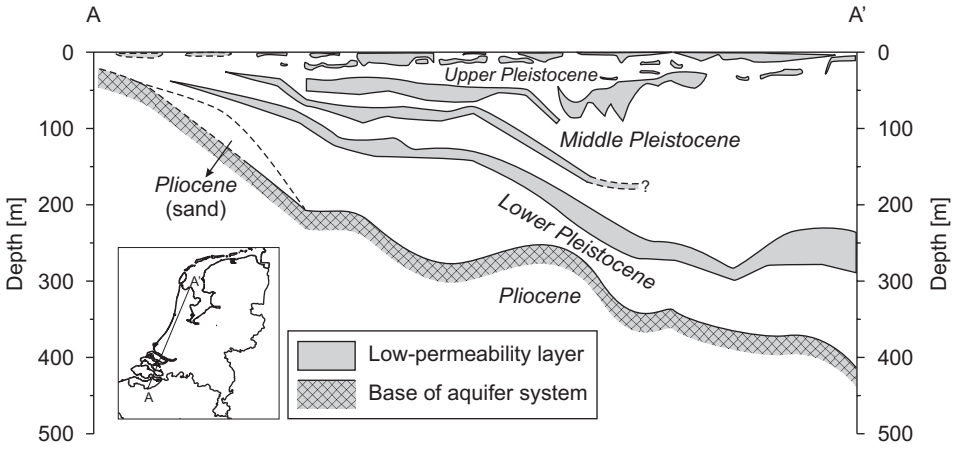

Figure 1.3: Schematic diagram of the generalized subdivision of the subsurface in aquifers and aquitards. Section is roughly 200 km in length. Depths are approximate.

The total thickness of these deposits locally exceeds 200 m. In the southern part, the sequence has a maximum thickness of approximately 100 m and consists of fluvial sand and clay of the rivers Rhine and Meuse. In both the north and the south, the upper part of the Pleistocene sequence consists of Eemian marine sediments, as well as aeolian and fluvial sediments from the Weichselian. Their total thickness generally does not exceed 20 to 30 m. Peat, lagoonal and marine clay together with fine-grained sand from the Holocene are found at the surface throughout most of the study area. Their average thickness amounts to 20 m although it increases from a few meters in the eastern part of the area to over 50 m in former tidal inlets.

1.2.3 Hydrogeology

Significant lateral variations in lithology prohibit a simple subdivision of the subsurface into aquifers and aquitards that is valid for the entire area (Dufour, 1998). In general, six aquifers are discerned which are shown schematically in a south-north cross section in figure 1.3. Locally, subaquifers exist where clay layers of significant thickness and extent occur (Van Rees Vellinga et al., 1981).

In the largest part of the area, the base of the aquifer system is formed by clays of Pliocene and locally, clays of Early-Pleistocene age (Pomper, 1983). In the province of Zeeland, the Tertiary marine sediments show a sandy facies and constitute an aquifer (figure 1.3). Here, Oligocene clay forms the low-permeability base.

Fine-grained layers that form more or less continuous aquitards in the south (for example, Early-Pleistocene fluvial clays), are absent in the northern part of the area. Conversely, confining units such as Saalian glacial deposits or Eemian marine

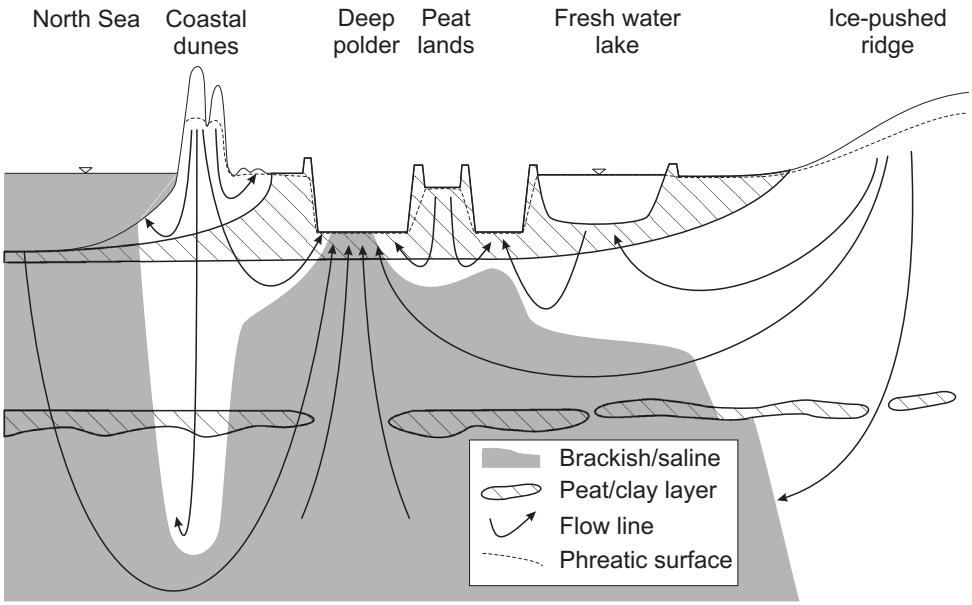

Figure 1.4: Schematic diagram of flow systems in the western part of the Netherlands (after Griffioen, 1994). The cross-section measures approximately 60 km in reality.

clays do not occur in the southern part of the area. All aquitards are heterogeneous both in their spatial distribution and hydraulic properties and many interconnections between the aquifers are present.

Groundwater levels are artificially controlled by a dense network of ditches and canals. Water levels in the polders are maintained by pumping excess rain and seepage water into canals and rivers that eventually discharge into the North Sea. Drainage density is smaller and groundwater levels are higher in the coastal dunes and the elevated Pleistocene terrain in the east. Groundwater flow patterns are mainly controlled by differences in surface water level between polders, lakes, canals and rivers, resulting in a complex system of local to regional groundwater flow systems (figure 1.4).

Precipitation in the western part of the Netherlands (averaged over the period 1971 to 2000) ranges from 725 mm/y to 900 mm/y. Average evapotranspiration (expressed as Makkink reference evaporation) varies from 555 mm/y to 615 mm/y. Precipitation excess (precipitation − evapotranspiration) ranges from 120 to 320 mm/y (Heijboer and Nellestijn, 2002).

1.3 Measurements

In the coastal area of the Netherlands, thousands of groundwater observation wells have been drilled and in many the chemical composition has been determined. The abundance of the isotopes of the elements C, H and O has been measured in hundreds of water samples. Geo-electrical soundings have been carried out systematically to map the salinity distribution at a regional scale (Van Dam, 1976). Also, many resistivity logs from boreholes are available that provide information on the Cl concentration of the groundwater (Van Dongen and Boswinkel, 1982). The isotope measurements are discussed separately in chapter 2. In the present study, Cl concentrations in observation wells have been used to map the spatial salinity distribution and borehole resistivity logs were used to study salinity variations within clay layers.

Chloride analyses from groundwater samples in observation wells were collected from the archives of the Netherlands Institute of Applied Geoscience TNO - National Geological Survey and the province of Noord-Holland. A three-dimensional version of Hardy's Multi Quadric Biharmonic interpolation method (Geenen, 1993; Van der Meij and Minnema, 1999) was employed to visualize the spatial distribution of Cl concentrations. Water samples taken prior to 1970 were excluded from the data set to avoid interference from temporal variations; if duplicate analyses were available, the most recent sample was included. The interpolation function to calculate the unknown Cl concentrations in a grid with a horizontal node spacing of 1 km and a vertical node spacing of 10 m was based on 3868 chloride analyses.

Information on the salinity of clay layers can solely be inferred from borehole resistivity logs as well screens have been installed in permeable layers only. For this purpose, a compilation of borehole measurements in the Netherlands by Van Dongen and Boswinkel (1982) was used. These authors used resistivity logs and groundwater samples to reconstruct the Cl concentrations vs. depth in 51 boreholes.

In this thesis, m_{Cl} denotes the Cl concentration. Based on their chlorinity, samples are subdivided into fresh water that has $m_{\mathrm{Cl}} \leq 8.4$ mmol/l (300 mg/l), brackish water with $8.4 < m_{\mathrm{Cl}} \leq 282$ mmol/l (300 – 10 000 mg/l) and saline water with $282 < m_{\mathrm{Cl}} \leq 564$ mmol/l (10 000 – 20 000 mg/l).

1.4 Results

The interpolated spatial distribution of chloride in groundwater is shown in figure 1.5. Since the interpolation method is sensitive to variations in the density of data points, these maps serve only to indicate regional trends in chlorinity. Actual measurement points have been plotted to indicate the reliability. The maps show that major occurrences of brackish to saline groundwater at shallow depth (< 20 m below mean sea level) are found in the province of Zeeland and the southwestern part of the province of Zuid-Holland, the northern part of the province of Noord-Holland and the IJsselmeer area. Furthermore, upconing of brackish groundwater is observed

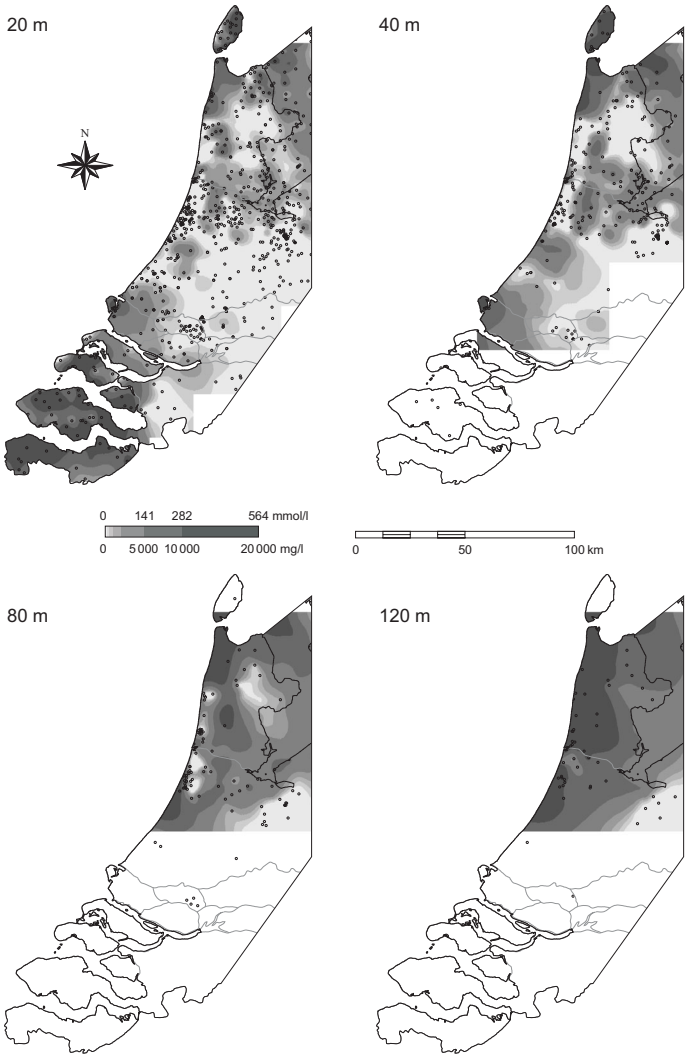

Figure 1.5: Maps showing the spatial distribution of Cl concentrations at 20, 40, 80 and 120 m below mean sea level. Dots indicate the location of observation wells within 5 m above or below the shown depth interval. No contours are shown in areas with too little observations. Based on data from the province of Noord-Holland, Netherlands Institute of Applied Geoscience TNO - National Geological Survey and Ouwerkerk (1993).

beneath deep polder areas in the provinces of Noord-Holland and Zuid-Holland. The most landward extension of brackish groundwater largely coincides with the landward extension of the Holocene transgressions (compare figures 1.2 and 1.5).

Fresh groundwater up to depths of 100 m below sea level or more is found below the coastal dunes, below the ice-pushed ridges and in the area of West-Friesland. Other occurrences of fresh groundwater are in the province of Utrecht and the eastern part of the province of Zuid-Holland and the southernmost part of the Zeeuws-Vlaanderen area (not all shown in figure 1.5). Locally, such as south of Amsterdam, individual pockets of fresh groundwater occur up to 80 m below the surface.

At depths greater than 100 m a seaward gradient is present, with Cl concentrations decreasing from seawater values near the coastline towards lower values more inland. Chloride and resistivity profiles measured in boreholes that penetrate Pliocene to Early-Pleistocene marine deposits, generally show an inversion (i.e., a decrease of the salinity with depth) that coincides with the occurrence of low-permeability clay layers in these strata (figure 1.6). The occurrence of these inversions is ubiquitous in the area that has been affected by the Holocene transgressions (figure 1.7, cf. figure 1.2). Inversions are also found within the upper part of the Pleistocene sequence, where they are mainly related to the occurrence of Early-Pleistocene fluvial clays, Saalian glacial deposits or Eemian and Holocene marine clays. The more saline water is found above or in these low-permeability layers, the fresher water below (Pomper, 1981; Gieske, 1991; Stuyfzand, 1993).

1.5 Discussion

The spatial distribution of the Cl concentrations (figure 1.5) is not easily explained. The vicinity of the North Sea and former transgressions will have played an important role, but other factors that influence the Cl concentrations in groundwater cannot be ruled out a priori. Table 1.1 lists the sources and processes responsible for high-salinity waters in coastal areas in general (cf. Stuyfzand and Stuurman, 1994). Before discussing the role of transgressions and connate seawater, the relevance of the remaining entries from table 1.1 as a source of the brackish and saline groundwater in the Pleistocene aquifers will be addressed.

1.5.1 Modern seawater

Land subsidence and over-exploitation of groundwater resources results in subsurface encroachment of modern seawater in many coastal areas around the world, which is commonly referred to as seawater intrusion (De Breuck, 1991). For the western part of the Netherlands, basic hydrological calculations and hydrochemical data indicate that the inland presence of intruded-contemporary North Sea water is limited to a region of about 2 to 6 km from the coastline (Stuyfzand, 1993). Therefore, modern seawater cannot be the source of the brackish groundwater that is found up to tens of kilometers inland.

1.5.2 Aerosols

Chloride aerosols mainly derive from sea spray (Vermeulen, 1977). The Cl concentration in bulk (dry + wet) precipitation near the coastline amounts to approximately 2 mmol/l and decreases exponentially inland to a background level of about 50 µmol/l (Stuyfzand, 1991). Of this value, 10 to 45 % is due to dry deposition of chloride aerosols on the rain gauge (Ridder et al., 1984; Stuyfzand, 1993). The total amount of atmospheric deposition on land surfaces can be 10 % higher than on bulk collectors if bare or scarcely vegetated, or 200 to 400 % higher if covered by shrubs or trees (Stuyfzand, 1993). The low concentrations of chloride in precipitation that result from aerosols make them a minor source of Cl concentrations > 10 mmol/l in groundwater.

1.5.3 Evaporites

Zechstein salt layers are found in the eastern and northeastern part of the coastal area and Cl concentrations of over 2 mol/l have been reported in Eocene aquifers at approximately 550 m below the surface (Glasbergen, 1981). There is some evidence that shallow groundwater (within 100 m below the surface) overlying salt domes (found at 200 m below the surface) might also be affected by rock salt dissolution (chapter 2, Glasbergen and Mook, 1982). Rock salt does not occur in the western part of the Dutch coastal area and can be ruled out as a source of dissolved solids here.

1.5.4 Anthropogenic pollution

Little is known about the contribution of anthropogenic sources to the Cl concentration of groundwater in the western Netherlands. Locally, contributions can be

Table 1.1: Sources and processes responsible for high-salinity groundwater in coastal areas and associated chlorinity.

Source or process	Approximate chlorinity [mmol/l]	Remarks
modern seawater	566	Can be lower due to fluvial input
transgressions, floods	566	Can be lower due to fluvial input or mixing with fresh groundwater
connate seawater	566	Can be lower due to fluvial input or mixing with fresh groundwater
aerosols	2	Bulk precipitation along the coast
salt formations	2 000	Reported by Glasbergen (1981)
anthropogenic pollution[a]	< 10	
evapo(trans)piration	< 10	evaporated rain water
ultrafiltration	< 100	dependent on original composition
freezing		dependent on original composition

[a] = waste sites, road salt, salt disposal.

expected from road salt (Werkgroep Midden West-Nederland, 1976), pollution by chlorinated solvents and waste disposal sites (Van Duijvenbooden and Kooper, 1981). An anthropogenic source that affects Cl concentrations on a regional scale is agriculture, where chloride is introduced to the environment through the application of fertilizers and manure. Studies in agricultural areas in the southern parts of the Netherlands, however, have shown that the highest Cl concentration of the groundwater beneath agricultural land is approximately 1.5 mmol/l (Broers and Griffioen, 1992). Agricultural activities in the coastal area are not more intensive than these investigated areas, so only a minor contribution to the total volume of brackish and saline groundwater is to be expected.

1.5.5 Evapotranspiration

Strong evaporation sometimes leads to extreme salt concentrations in groundwater in arid areas. In the Netherlands, evapotranspiration amounts on average to two-thirds of precipitation (Dufour, 1998), which will increase concentrations by a factor of 3. Locally, stronger evapotranspiration occurs depending on the vegetation. For example, concentration factors as high as 5.8 have been found in the coastal dunes below pine trees (Stuyfzand, 1993). The highest Cl concentrations in recharge waters are in the order of 10 mmol/l in areas with high atmospheric deposition and strong evapotranspiration. Higher concentrations are to be attributed to other sources of chloride. Evapotranspiration of seawater, however, did contribute to the salinity of groundwater in the coastal area as explained in chapter 4.

1.5.6 Ultrafiltration

Ultrafiltration (or reverse osmosis) occurs when groundwater flow due to a hydraulic head gradient occurs across a clay layer that acts as a semi-permeable membrane. Clay layers can act as natural membranes owing to their negative surface charge. Since they prevent the passage of charged solutes such as chloride ions, groundwater salinity on the inflow side of the clay layer will increase. Osmotic effects have been recognized in a harbour sludge depot directly overlying a brackish-water aquifer (Keijzer, 2000). To what extent this process plays a role in the coastal area of the Netherlands remains unclear. Since the osmotic efficiency of natural membranes rapidly decreases with salinity, however, it is assumed that ultrafiltration is ineffective at seawater concentrations (chapter 4).

1.5.7 Freezing

It is known that freezing of groundwater causes migration of solutes and the role of this process has been recognized in the formation of saline groundwater and brines (e.g. Bottomley et al., 1999; Bein and Arad, 1992; Herut et al., 1990). Permafrost conditions occurred in the coastal area during the glacial stages of the Pleistocene.

Therefore, this mechanism must have influenced the salinity distribution at least to some extent, as was previously proposed by Pomper (1978). In the present study, there are no data that support the conclusion that freezing has contributed to the salinity of groundwater (cf. chapter 4).

1.5.8 Transgressions

From the foregoing discussion, it follows that salinization of the Pleistocene aquifers in the coastal area of the Netherlands must be due to either former transgressions or the presence of connate seawater in the subsoil. A distinction between the two is relevant here: salinization during a transgression refers to the introduction of solutes in a fresh-water aquifer directly from the overlying or adjacent seawater, whereas salinization by connate seawater refers to the introduction of dissolved salts from marine sediments (deposited during a transgression) that still contain saline interstitial water.

The Netherlands has experienced several transgressions during the Cenozoic. The landward borders of the ones relevant here are depicted in figure 1.2. Marine sediments from the Pliocene to Early-Pleistocene, Eemian and Holocene transgressions still contain connate seawater (e.g. Van Dongen and Boswinkel, 1982; Van Rossum, 1998) and their potential contribution to the salinization of the Pleistocene aquifers will be discussed first. Then, salinization during the Holocene transgression will be elaborated in detail.

1.5.9 Salinization from marine deposits

The oldest marine deposits containing connate seawater that could act as a source of dissolved salts are the fine-grained sands and clays dating from the Pliocene and Early-Pleistocene. Upward diffusive salt transport from these marine layers did undoubtedly cause salinization of the Pleistocene fluvial sands that contained fresh water when they were deposited. It is unlikely, however, that they constitute the source of the bulk of brackish to saline groundwater that is found in the aquifers today as suggested by Meinardi (1991), since measurements in boreholes and observation wells show a chloride inversion at or below the boundary between Pliocene and Early-Pleistocene marine strata and Pleistocene fluvial deposits. An example is given by well 31E-0176 (figure 1.6, see figure 1.7 for its location). If the connate seawater is the source of the brackish groundwater in the Pleistocene fluvial aquifer and upward transport of dissolved solutes by diffusion occurs, an opposite gradient would be observed. The reverse is indicated: the marine strata have been freshened after deposition and dissolved salts from the overlying fluvial deposits migrate downward. Similar findings were reported by Appelo and Geirnaert (1991), based on the geochemical characteristics of sediment samples. Carbon-14 data further show that the brackish groundwater above the salinity inversion is of Holocene age and that the relic seawater below the inversion is much older (figure 1.6, chapter 2).

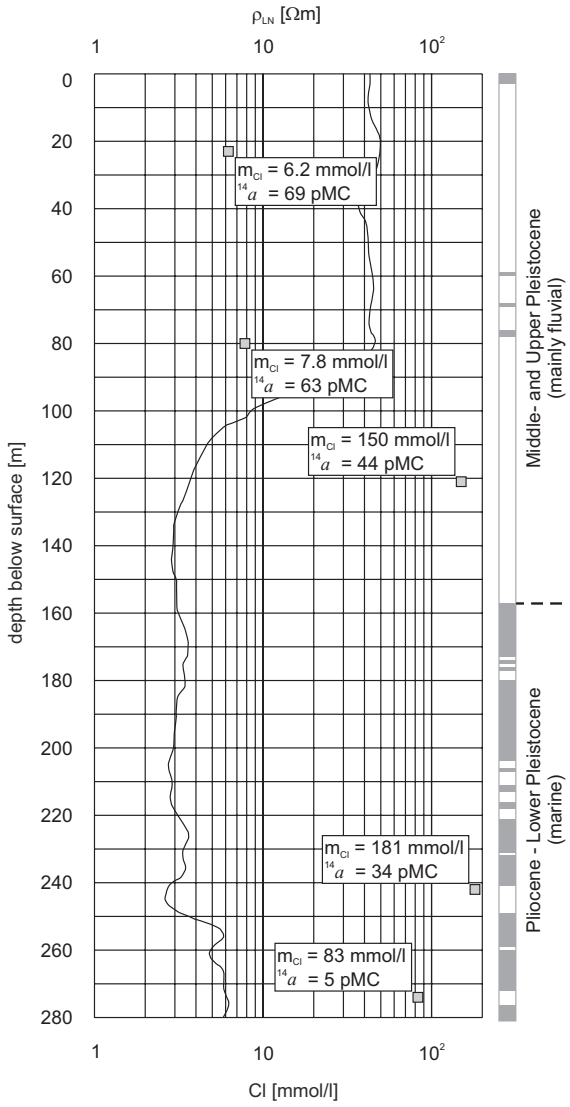

Figure 1.6: Graph of the Cl concentration (square markers) and long-normal resistivity (ρ_{LN}, solid line) vs. depth in well 31E-0176 (location shown in figure 1.7). Column on righthand side indicates sand (white) and clay layers (shaded). The top of the Early-Pleistocene marine strata is found here at a depth of $\sim$ 160 m. The decrease of the Cl concentration below 245 m is very pronounced. Carbon-14 data by courtesy of R. Boekelman.

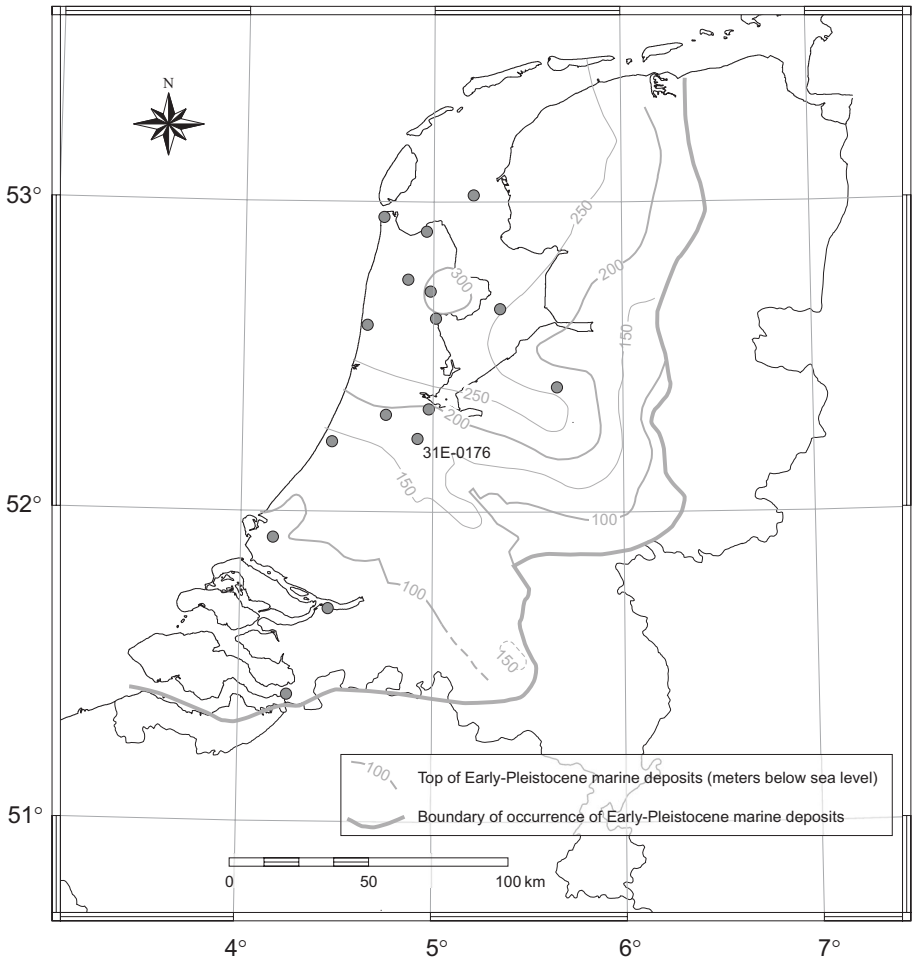

Figure 1.7: Map of the Netherlands showing known occurrences of salinity inversions within Pliocene to Early-Pleistocene marine deposits, compiled from data by Meinardi (1974), Pomper (1981), Van Dongen and Boswinkel (1982), Van Wieringen and Willemsen (1982), Boswinkel and Ritsema (1984), Gieske (1991), Hobma et al. (1993) and from the archives of the province of Noord-Holland. Contour lines represent the depth of the top of the Early-Pleistocene marine deposits below mean sea level (after Zagwijn and Van Staalduinen, 1975).

The large number of boreholes in which this inversion is observed and their distribution across the coastal area (figure 1.7) shows that this is a general phenomenon. This suggests that the occurrence of relic Pliocene and Early-Pleistocene seawater in the Pleistocene fluvial aquifers is an exceptional condition.

Although its contribution to the present volume of saline groundwater is small, large amounts of dissolved salt are likely to have entered the Pleistocene fluvial sediments over the past 1.6 My by diffusion and also compaction-driven flow. The latter results from natural compression of clastic sediments in response to sediment loading, leading to an upward flux of expelled pore water in the order of 10^{-4} m/y (Kooi and De Vries, 1998). The combined salt flux due to diffusion and compaction-driven flow is small compared to the average horizontal advective flux in the Pleistocene aquifers owing to topography-driven flow that is likely to have prevailed during the Pleistocene and hence most of this salt water has probably been removed.

There is little evidence of any large-scale contribution of connate seawater from Eemian marine deposits. The occurrence of Eemian-brackish groundwater has been documented in the northern part of the Netherlands, probably related to stagnant flow conditions in the Pleistocene aquifer (Hoogendoorn, 1985). Although similar occurrences in the western part of the Netherlands cannot be ruled out, they are to be considered of local significance only as can be inferred from the fact that the majority of brackish and saline groundwater samples have a ^{14}C signature that points towards a Holocene origin (chapter 2). Following the Eemian transgression, a 100 ky period of fresh water circulation occurred during the Weichselian glacial stage. Despite uncertainties about the characteristics of the flow regime, such as reduced infiltration owing to permafrost (Bath et al., 1978; Walraevens et al., 2001), low precipitation rates (Vaikmäe et al., 2001) and increased groundwater velocities during glacial periods (Van Weert et al., 1997), significant flushing of the Eemian deposits is to be expected.

1.5.10 Salinization during the Holocene transgression

The North Sea gradually inundated the westward sloping Pleistocene surface as global sea level began to rise at the beginning of the Holocene. Saline water was carried on top of the fresh groundwater in the Pleistocene aquifers upon inundation. Owing to its higher density, the saline water will sink into the fresh groundwater, provided that the permeability of the underlying sediments is sufficiently high. In this process, referred to as free convection, a boundary layer develops as dissolved salts enter the aquifer by diffusion until it reaches a critical thickness at which it becomes unstable and breaks up into salt plumes that descend to the aquifer bottom. Fresh water is expelled by rising plumes. Whether or not free convection will occur is controlled by the nondimensional aquifer Rayleigh number (Holzbecher, 1998):

$$Ra = \frac{\Delta\rho g k H}{\mu D_M} \tag{1.1}$$

where $\Delta\rho$ is the density contrast [kg/m^3], g is gravitational acceleration [m/s^2], k is intrinsic permeability [m^2], H is the height of the aquifer [m], μ is dynamic viscosity [kg/m/s] and D_M is the molecular diffusion coefficient [m^2/s] including both tortuosity and porosity. Typical Rayleigh numbers for the sandy aquifers in the coastal area are in the order of 10^5 – 10^6. This indicates that salinization by free convection is likely to have occurred as these values exceed the critical value of $Ra \approx 40$ by far. Associated vertical groundwater flow velocities are in the order of meters per year and the corresponding time span for the salinization of an aquifer with a depth of about 200 m is a few to tens of decades (chapters 5 and 6, Van der Molen, 1989; Gieske, 1991).

These numbers hold for highly-permeable aquifer sediments. Low-permeability strata will have greatly hindered free convection by (1) preventing the entry of saline water at the top of the aquifer system and (2) by obstructing the (vertical) passage of saline water as it moves through the aquifer. Both aspects will be discussed in more detail below.

Many studies have shown that clay layers can protect underlying fresh water aquifers from salinization for many thousands of years (e.g. Volker, 1961; Groen et al., 2000b, chapters 3 and 6) as dissolved salts, without water flow, need to pass primarily via diffusion. When the sea invaded the western part of the Netherlands some 7.5 ka BP, peat covered large parts of the sandy Pleistocene surface, protecting the underlying aquifer. In tidal inlets, however, erosion removed the peat layers, so that the permeable aquifer sediments came in direct contact with the overlying seawater and became prone to rapid salinization by free convection. A complication arises from the fact that deposition of fine-grained material occurred on the "seafloor" during inundation, so that a hydraulic resistance was built up and the salinization process was retarded (chapter 6).

Gieske (1991) proposed that, in the southern part of the IJsselmeer area, salinization during the Calais transgression was followed by freshening during the formation of the Holland Peat and that clay and peat deposits from these periods protected the fresh groundwater from salinization during the subsequent Duinkerke transgression. This suggests that the main phase of salinization must have occurred during the early parts of the Calais transgression as during later stages free convection was hindered or even impeded due to the presence of clay and peat. In the northern part of the IJsselmeer area, however, marine conditions were absent until 1 ka BP when the sea invaded the area and eroded the peat, resulting in favourable conditions for free convection. Strong erosion since the Middle Ages also removed large parts of the Holocene confining layers in the northwestern and southwestern parts of the coastal area (Zagwijn, 1986). In the central part of the coastal area, widespread marine conditions have not occurred following the closure of tidal channels since 5.5 ka BP (except for marine incursions along the inlets of the river Rhine and the Oer-IJ estuary), which means that in this area salinization mainly occurred during the Calais transgression.

Low-permeability layers have a retarding effect on salinization by free convec-

tion irrespective of the depth at which they occur. Observations often show that Cl concentrations decrease significantly over clay layers (Pomper, 1981; Gieske, 1991) or that they contain relatively-fresh water (Van Dongen and Boswinkel, 1982). At the same time, vast amounts of Holocene brackish to saline waters are present below many other clay layers. This implies that (1) these layers are laterally-discontinuous so that the saline water can flow around them and/or that (2) the permeability of these layers locally is high enough to permit the passage of saline water. Although clay layers have retarded the salinization process, they apparently have not always been able to prevent salt water from entering the underlying sediments. Aforementioned effects are quantified in chapter 6 with numerical models.

1.5.11 Freshening of the aquifer system

At present, flushing of the saline groundwater takes place as fresh water infiltrates due to natural and man-made hydraulic gradients.

The first stage of freshening began with the closure of barriers and final sedimentation of back-barrier areas around 5.5 ka BP. Fresh water was introduced to the former marine areas by riverine input and precipitation (Zagwijn, 1986). Hydraulic gradients were small as only minor elevation differences existed in the coastal zone (e.g. former barrier islands and levees) and significant freshening of the subsoil during that stage is not expected. Elevation differences of several meters were created upon formation of extensive peat bogs during the following 4 ka. Studies of modern undisturbed peat bogs have shown that vertical seepage losses to the underlying aquifer range between 10 and 30 mm/y (Van der Schaaf, 1998). Freshening of the aquifers up to tens of meters is therefore likely under favourable conditions. Significant freshening occurred below the coastal dunes that developed since the Middle Ages. Fresh groundwater is found here up to a depth of 120 m (figure 1.5).

The original peat bog topography has been almost completely transformed into a man-made topography (polder landscape). As elevation differences of several meters exist between individual polders and between polders and nearby surface waters (lakes, rivers, drainage canals), groundwater flow systems developed that extend up to tens of meters below the surface (e.g. Engelen and De Ruiter-Peltzer, 1986; Schot and Molenaar, 1992). Infiltration from surface water and elevated areas such as inverted tidal channels or peat remnants displaces the saline groundwater that subsequently discharges in the deepest polder areas (figure 1.4). Lateral fresh water inflow is also from the coastal dunes (Stuyfzand, 1993) and the Pleistocene sand district (Schot and Molenaar, 1992). The presence of brackish water in Holocene marine deposits (e.g. Van Rossum, 1998) shows that recharge of the Pleistocene aquifer by precipitation mainly occurs via preferential flow paths in zones where the Holocene confining deposits are relatively permeable or thin or where they are dissected by tidal channels (De Louw et al., 2000; Post et al., 2002).

1.6 Conclusions

The salinity distribution of groundwater in the Pleistocene aquifers in the coastal area of the Netherlands shows a complicated pattern, especially in the upper 50 m of the subsurface. The complexity of the observed pattern is mainly the result of Holocene marine influence as well as superimposed variations that are the result of local flow systems associated with man-made topography. At depths greater than 100 m, groundwater with the salinity of seawater is found near the coastline and concentrations decrease landward.

The origin of brackish and saline groundwater is linked to the Holocene transgression which can be concluded from: (1) indirect demonstration (the inability of other processes that increase groundwater salinity to explain the observed concentration patterns), (2) the occurrence of salinity inversions near the boundary between Early-Pleistocene marine and fluvial strata that exclude connate, Pliocene to Early-Pleistocene seawater as a source of brackish and saline groundwater in the Pleistocene fluvial deposits. Moreover, as will be discussed in detail in chapter 2, ^{14}C analyses indicate that most groundwater samples have a conventional age less than 10 ka.

Rayleigh numbers of the high-permeability Pleistocene sediments exceed the critical value by far. This suggests that salinization occurred primarily through free convection. Although especially Early-Pleistocene and Saalian clay layers have protected the underlying aquifers from salinization, the lateral continuity and/or resistance to groundwater flow of most aquitards was insufficient to counteract the vertical intrusion of saline water.

Freshening of the aquifers occurred after the sea retreated. Except in the coastal dunes and the elevated Pleistocene outcrops in the eastern part of the area, natural hydraulic head gradients were relatively small compared to the gradients created by human activities. This means that, although freshening also took place under natural conditions, the main phase of groundwater flow did not occur until man started to significantly alter the topography. Infiltration of meteoric water through the Holocene confining deposits is along preferential flow paths.

Chapter 2

Hydrological processes and timing of salinization inferred from natural isotope variations

Abstract

This study is the first comprehensive review of natural isotope measurements of groundwater in the coastal lowlands of the Netherlands. From ^{2}H, ^{18}O and Cl analyses it is inferred that a large part of the fresh groundwater underwent evaporation prior to infiltration. Many samples have a high salinity that can be attributed to mixing of modern precipitation or Rhine water and seawater. Correcting for the seawater contribution shows that fresh water end members of saline groundwater have more depleted $\delta^{18}O$ values than the overlying (i.e., younger) fresh groundwater. This implies that infiltration of evaporated meteoric water did not become significant until after the Holocene marine incursions. Radiocarbon dating proves impossible in the study area due to the large spatial variability of the ^{14}C activity of sedimentary-carbon sources. The effect hereof is quantified. Carbon-14 still proves useful for discrimination between old (Pliocene to Early-Pleistocene) and modern (Holocene) seawater contributions to groundwater salinity. Newly-collected Sr isotope measurements corroborate that salinization of aquifers occurred during the Holocene and show that dissolution of Pliocene marine shells occurs in the deeper parts of the aquifer system.

2.1 Introduction

Groundwater in coastal aquifers typically derives from different sources such as precipitation, river water and seawater, which all have distinct chemical and isotopic

This chapter is based on the paper: Post, V.E.A., Van der Plicht, H., Meijer, H.A.J., submitted to Journal of Hydrology. Use of natural isotope variations in groundwater to reconstruct paleohydrological processes: the coastal aquifers of the Netherlands.

characteristics. Superimposed variations result from physical, chemical and biological processes (Yurtsever, 1997). Therefore, changes in environmental conditions (e.g. climate, land use) are likely to be reflected by the isotopic composition of the groundwater and its solutes.

Numerous studies report on the use of natural isotopes in coastal areas. Applications include identification of salinization sources (e.g. Jørgensen and Holm, 1994; Hiscock et al., 1996; Oetting et al., 1996), reconstruction of hydrological processes (e.g. Barker et al., 1998; Barbecot et al., 2000; Edmunds et al., 2001; Walraevens et al., 2001), estimation of water budgets (e.g. Burnett et al., 2001) and groundwater age dating (e.g. Edmunds and Smedley, 2000; Van der Kemp et al., 2000; Loosli et al., 2001; Plummer and Sprinkle, 2001).

Over the past decades, hundreds of isotope analyses have been collected in the coastal lowlands of the Netherlands within several individual campaigns, but there have been no systematic attempts to integrate these data. This contribution is the first to present a comprehensive overview of the environmental isotope variations in groundwater of the Dutch coastal area. The analysis is complemented by a study of strontium isotope ratios, which was undertaken to test their feasibility for discerning between different sources of intruded seawater.

Geological environments in the study area during the Quaternary varied in space and time and included estuaries, tidal flats, lagoons, salt marshes, peat bogs and rivers. Furthermore, the landscape and hydrology changed dramatically during the last 1 000 y as a result of human activities related to land reclamation, de-watering and groundwater abstraction. Hydrological boundary conditions have thus changed continuously throughout geological time, with alternating periods of marine and terrestrial conditions. The primary objective of this study was to identify the prime hydrological processes that influenced the composition of the groundwater.

Particular interest was paid to timing of episodes of aquifer salinization. Radiocarbon measurements were available for several samples with a high salinity, but radiocarbon dating suffers from some well-known complications (e.g. Geyh, 2000). These mainly arise from mixing of water types with different ages and chemical reactions between groundwater and carbon-bearing aquifer material. Inverse-modelling techniques (Wigley et al., 1978) allow to correct for mixing effects and geochemical reactions to improve age estimates. Today, computer codes are readily available to carry out such calculations (Plummer et al., 1994; Parkhurst and Appelo, 1999). The difficulties associated with application of this approach in a geological setting such as the Dutch coastal area will be discussed.

2.2 Measurements

The data presented here were compiled from several regional groundwater surveys and have been retrieved from the archives of the Center for Isotope Research (CIO) and published reports. The water samples were taken from observation wells (figure

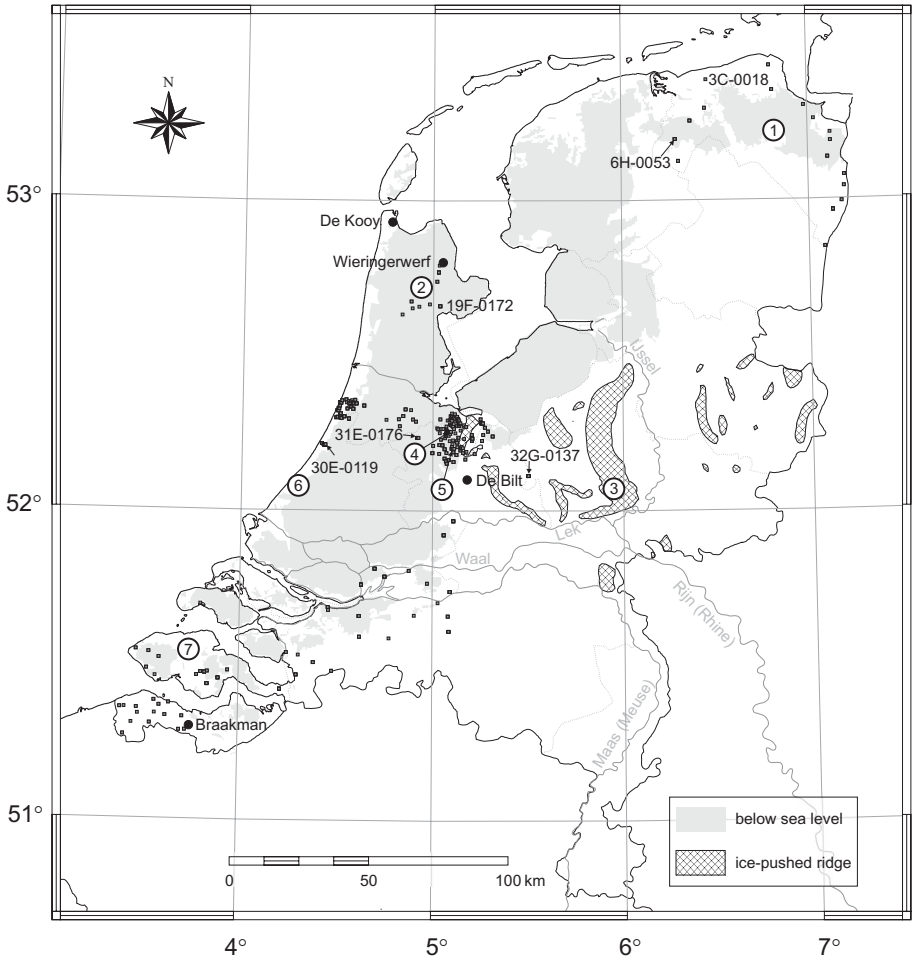

Figure 2.1: Map of the Netherlands showing the area below mean sea level, ice-pushed ridges and locations of the groundwater samples (squares) and GNIP stations (black circles). Numbers in circles refer to geographical names used in the text: 1 = province of Groningen, 2 = West-Friesland area, 3 = Veluwe, 4 = Horstermeer polder area, 5 = Loosdrechtse plassen area, 6 = city of Leiden and 7 = province of Zeeland.

2.1) that were mostly positioned in the Pleistocene fluvial aquifers and analysed at the CIO for ^{2}H, ^{3}H and ^{18}O of water and ^{13}C and ^{14}C of dissolved inorganic carbon (DIC). In many cases, chemical analyses were also available (table 2.1). For a number of samples, information on the location and depth of the observation well was missing.

Isotopic abundances are reported in δ notation relative to V-SMOW (Vienna Standard Mean Ocean Water) for ^{2}H and ^{18}O or V-PDB (Vienna Pee Dee Belemnite) for ^{13}C. Carbon-14 activity is expressed as percent modern carbon (pMC).

Inverse modelling calculations were carried out only for brackish or saline samples of which all major ions were analysed and electro neutrality was less than 5 % off. The quality of the chemical analyses was further checked following the criteria for saturation indices as proposed by Griffioen et al. (2002).

The ^{2}H and ^{18}O contents of mean precipitation and the local meteoric water line (LMWL) were determined from monthly precipitation measurements at the stations from the Global Network for Isotopes in Precipitation (GNIP) at Braakman, De Bilt, De Kooy and Wieringerwerf (figure 2.1). Samples were taken between 1981 and 1999 (IAEA/WMO, 2001).

Samples for Sr isotope analysis were obtained from well 31E-0176 (figure 2.1) in December of 2002. Two ml of filtered groundwater were evaporated in ultra-clean pfa teflon vials and converted to 100 ml 3N HNO_3 solutions that were loaded and eluted on 0.17 ml Sr-Spec columns in order to obtain a purified strontium fraction. This fraction was loaded onto a single zone-refined outgassed Re filament with the $TaCL_5$-H_3PO_4 sandwiching technique. $^{87}Sr/^{86}Sr$isotope ratios were determined by thermal ionization mass spectrometry using a Finnigan MAT 262 collecting 10 blocks of 10 ratios using a dynamic triple jump with 16 s integration time and 4 s stabilization time and a normalization of the $^{86}Sr/^{88}Sr$ to a preset value of 0.1194, resulting in a 2σ precision of 0.000006 to 0.000008. NBS-987 standard $[^{87}Sr/^{86}Sr = 0.710239 \pm 0.000008$ (n=13; $2\sigma)]$ was measured to monitor the long-term reproducibility of the measurements.

Table 2.1: Number of groundwater samples per isotope combination. For example, 701 samples were available in which $\delta^{18}O$ was measured and 551 samples were available in which both $\delta^{18}O$ and $\delta^{13}C$ were measured.

	^{2}H	^{18}O	^{13}C	^{14}C	^{3}H	Cl	Major ions
^{2}H	208	208	163	104	112	189	105
^{18}O		701	551	225	388	606	208
^{13}C			559	225	341	481	183
^{14}C				225	170	214	138
^{3}H					398	355	159
Cl						655	208
Major ions							208

2.3 Results

The local meteoric water line was determined from a least squares fit of the measured δ^2H and δ^{18}O values [%] at the GNIP stations Braakman, De Bilt, De Kooy and Wieringerwerf ($R^2 = 0.92$):

$$\delta^2\mathrm{H} = 7\delta^{18}\mathrm{O} + 2.66 \tag{2.1}$$

Mean precipitation (weighted by rainfall intensity) has $\delta^2\mathrm{H} = -47.02$ % and $\delta^{18}\mathrm{O} = -7.11$ % . Coastal stations show an enrichment of ^{18}O up to 0.5 % relative to inland (> 10 km from the coastline) stations (Stuyfzand, 1991).

The observed δ^2H and δ^{18}O values of the groundwater samples show a wide range: -62 % < δ^2H < -6.6 % and -10.01 % < δ^{18}O < -1.13 % (figure 2.2a). Chloride concentrations (m_{Cl}) range from 0.1 to 500 mmol/l (figure 2.2). The mixing lines of seawater ($m_{\mathrm{Cl}} = 566$ mmol/l, $\delta^{18}\mathrm{O} = 0$ %) and modern precipitation ($m_{\mathrm{Cl}} \approx 0.2$ mmol/l, $\delta^{18}\mathrm{O} = -7.11$ %) and pre-industrial Rhine water ($m_{\mathrm{Cl}} \approx 0.3$ mmol/l, $\delta^{18}\mathrm{O} \approx -9.4$ %) are also shown in figure 2.2a.

Fresh and brackish samples mainly plot above the mixing line of precipitation and seawater. Saline samples tend to cluster around the mixing lines of precipitation or Rhine water and seawater. Using the Cl concentration as a measure of the amount of seawater in the mixture, δ^{18}O (and δ^2H) of the fresh water end member was calculated according to (Mook, 2000):

$$\delta^{18}\mathrm{O}_f = \frac{\delta^{18}\mathrm{O}_m(m_{\mathrm{Cl},s} - m_{\mathrm{Cl},f}) - \delta^{18}\mathrm{O}_s(m_{\mathrm{Cl},m} - m_{\mathrm{Cl},f})}{(m_{\mathrm{Cl},s} - m_{\mathrm{Cl},m})} \tag{2.2}$$

where the subscripts f, m and s denote the fresh water end member, sample and seawater end member respectively and m_{Cl} is the Cl concentration [mmol/l]. Since $m_{\mathrm{Cl},f} \ll m_{\mathrm{Cl},s}$ (= 566 mmol/l) it was neglected. The second term in the numerator vanishes when it is assumed seawater equals standard mean ocean water so that $\delta^2\mathrm{H}_s = \delta^{18}\mathrm{O}_s = 0$ % .

Due to evaporation of ocean water, $\delta^2\mathrm{H}_s$ and $\delta^{18}\mathrm{O}_s$ can be increased by ~ 6 % and ~ 1 % respectively (Yurtsever, 1997), which can significantly affect the outcome of equation 2.2 when $m_{\mathrm{Cl},m} \rightarrow m_{\mathrm{Cl},s}$. The salinity of seawater ($m_{\mathrm{Cl},s}$) has also been shown to be affected by evapotranspiration in the Netherlands (chapter 4). Figure 2.3 shows the error that is possibly introduced due to erroneous assumptions about the composition of the seawater end member. The chart shows the calculated value of $\delta^{18}\mathrm{O}_f$ as a function of $m_{\mathrm{Cl},m}$ for two seawater end members that differ from ocean water. One end member has $\delta^{18}\mathrm{O}_s = -1$ % , $m_{\mathrm{Cl},s} = 509$ mmol/l, the other has $\delta^{18}\mathrm{O}_s = 1$ % , $m_{\mathrm{Cl},s} = 623$ mmol/l. When it is erroneously assumed that $\delta^{18}\mathrm{O}_s = 0$ % , $m_{\mathrm{Cl},s} = 566$ mmol/l, the calculated $\delta^{18}\mathrm{O}_f$ will deviate several per mil from the true $\delta^{18}\mathrm{O}_f$ at high $m_{\mathrm{Cl},m}$ (figure 2.3).

Calculated values of $\delta^2\mathrm{H}_f$ and $\delta^{18}\mathrm{O}_f$ of the groundwater samples are shown graphically in figure 2.4 along with the lines that represent evaporation of precipitation and Rhine water. The slopes of these lines are based on observations in shallow

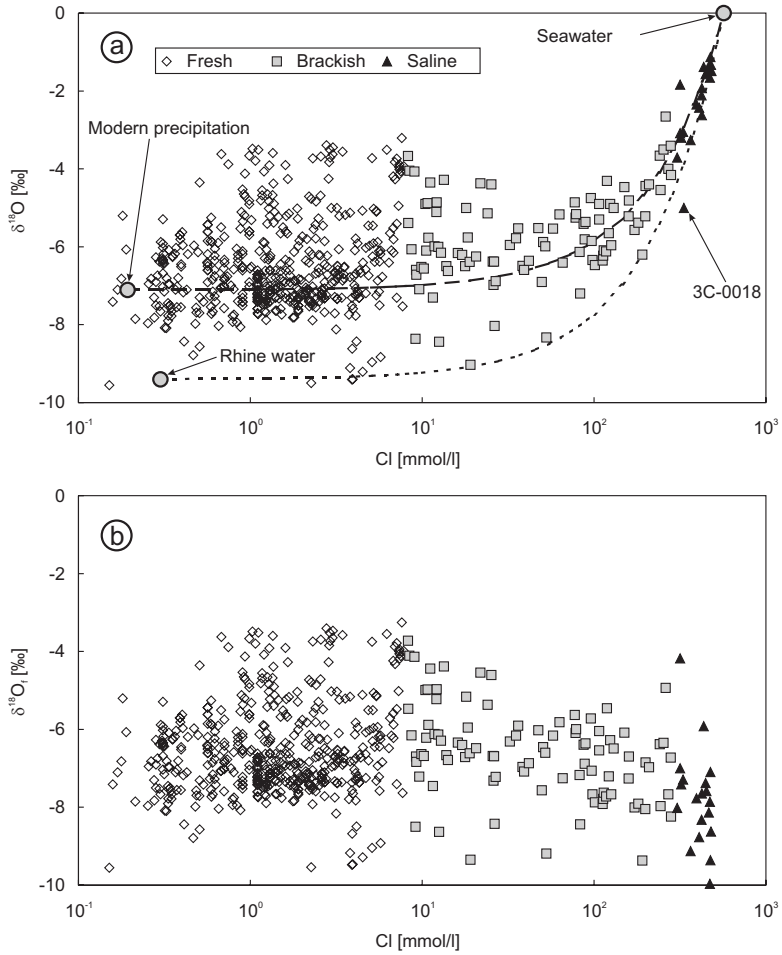

Figure 2.2: Graphs of (a) δ^{18}O and (b) fresh water end member δ^{18}O vs. Cl concentration of groundwater samples from the coastal area. Lines represent mixing of modern precipitation (dashed line) or Rhine water (dotted line) and seawater.

lakes in the Loosdrechtse Plassen area (figure 2.1) where δ^2H and δ^{18}O of surface waters plot along a line with a slope $\mathrm{d}\delta^2\mathrm{H}/\mathrm{d}\delta^{18}\mathrm{O} = 5.4$ (Hettling, 1985). Fresh and brackish samples are mostly banded by the LMWL and the evaporation line of Rhine water, with many data points scattered along the evaporation line of precipitation. Saline samples show quite some scatter, which is partly due to the larger error at high $m_{\mathrm{Cl},m}$ when correcting for seawater mixing (figure 2.3).

The data suggest that $\delta^{18}\mathrm{O}_f$ becomes progressively-less enriched with increasing m_{Cl} (figure 2.2b). The same trend is observed in many observation wells in which

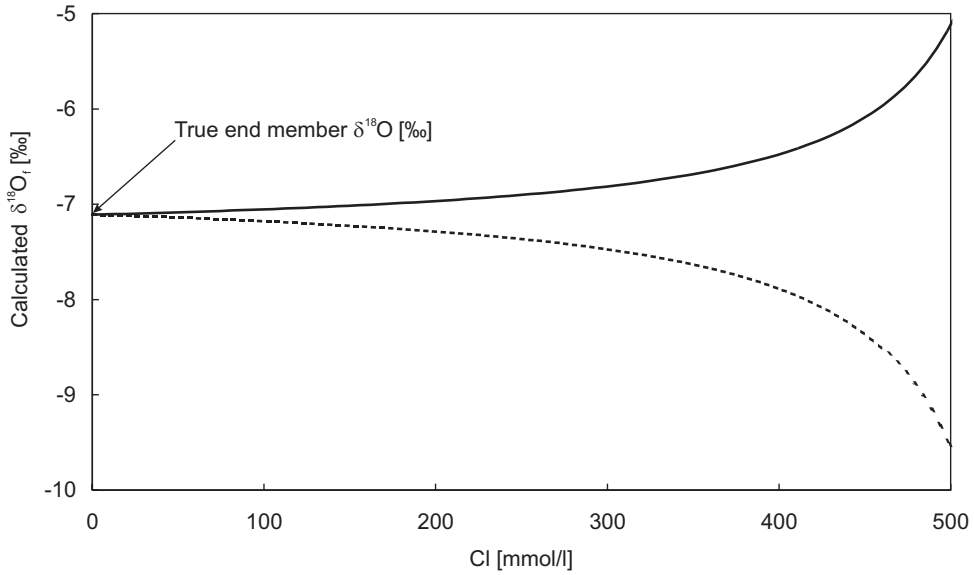

Figure 2.3: Graph of the calculated δ^{18}O of the fresh water end member in a seawater mixture vs. Cl concentration of the mixture. The chart shows the values that would be calculated when it is erroneously assumed that the seawater end member has $m_{\mathrm{Cl},s} =$ 566 mmol/l, $\delta^{18}\mathrm{O} = 0$ ‰ , whereas the true seawater end member has $m_{\mathrm{Cl},s} = 623$ mmol/l, $\delta^{18}\mathrm{O}_s = 1$ ‰ (solid line) or $m_{\mathrm{Cl},s} = 509$ mmol/l, $\delta^{18}\mathrm{O}_s = -1$ ‰ (dotted line). The true fresh water end member has $\delta^{18}\mathrm{O}_f = -7.11$ ‰ .

$\delta^{18}\mathrm{O}_f$ values decrease with salinity and with depth (figure 2.5).

Carbon-14 activity (^{14}a) in observation well 31E-0176 shows a sharp drop in the Pliocene to Early-Pleistocene marine strata that coincides with a marked decrease of groundwater salinity (figure 1.6). On the other hand, there appears to be no correlation between ^{14}a and the Cl concentration for samples from the Pleistocene aquifers (figure 2.6). A cumulative frequency plot of ^{14}a (figure 2.7) of samples from the Pleistocene aquifers shows that of the brackish and saline samples ($m_{\mathrm{Cl}} >$ 8.4 mmol/l), approximately 80 % have a conventional ^{14}C age < 10 ka.

Brackish and saline samples almost all have tritium contents below detection limits. Significant tritium activity is only measured in fresh groundwater samples.

The measured variation of $^{87}\mathrm{Sr}/^{86}\mathrm{Sr}$ of the three brackish samples in observation well 31E-0176 is small (0.709016 – 0.709063), but significant. Figure 2.9 shows the measured values and the mixing line of Rhine water ($m_{\mathrm{Sr}} \approx 6$ µmol/l, $^{87}\mathrm{Sr}/^{86}\mathrm{Sr} \approx$ 0.7084) and modern seawater ($m_{\mathrm{Sr}} \approx 89$ µmol/l, $^{87}\mathrm{Sr}/^{86}\mathrm{Sr} \approx 0.70918$). In the chart of figure 2.9a, $^{87}\mathrm{Sr}/^{86}\mathrm{Sr}$ is plotted against $1/m_{\mathrm{Sr}}$, yielding a straight mixing line (Faure, 1986). In the chart of figure 2.9b, m_{Sr} is plotted against m_{Cl}. In both figures, sample 1 (depth = 121 m below the surface) plots on the mixing line as opposed to

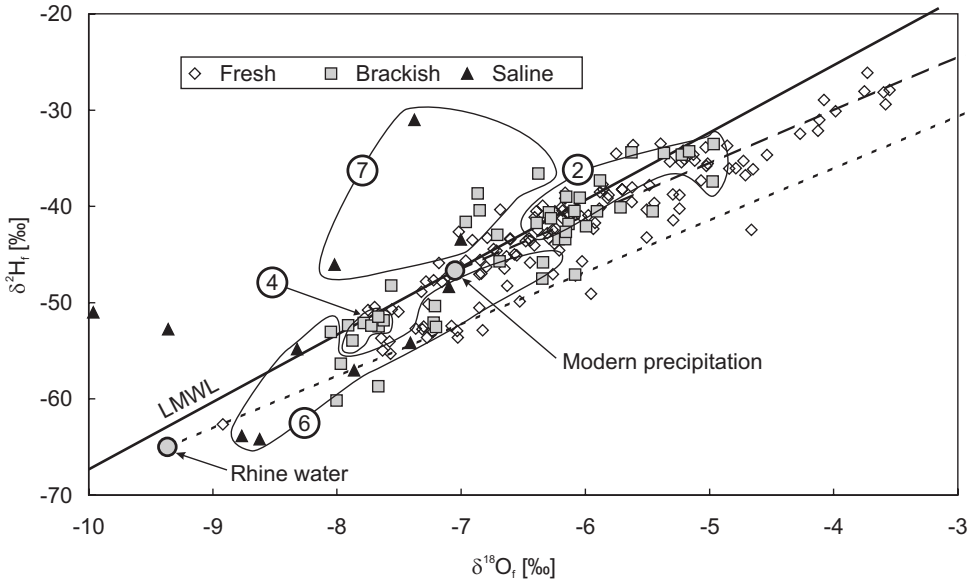

Figure 2.4: Graph of δ^2H vs. δ^{18}O of the fresh water end members of groundwater samples in the coastal area. Lines represent the local meteoric water line ($\delta^2\mathrm{H} = 7\delta^{18}\mathrm{O} + 2.66$, solid line), evaporation of precipitation (dashed line) and Rhine water (dotted line). Brackish and saline samples that are encircled belong to a specific geographical region with numbers in circles referring to the regions in figure 2.1.

samples 2 and 3 (depth = 242 m and 274 m below the surface, respectively).

2.4 Discussion

2.4.1 Water

The results presented in the previous section indicate that the two main processes that influence the groundwater composition in the Dutch coastal area are (1) evaporation and (2) mixing of fresh water and seawater. These two processes account for the range in δ^2H and δ^{18}O values that is observed in the samples.

Evaporation is recognized by the δ^2H and δ^{18}O enrichment of fresh and brackish samples compared to modern precipitation and Rhine water (figures 2.2 and 2.4). Especially the fresh samples plot along the evaporation line of modern precipitation. Groundwater $\delta^2\mathrm{H}_f$ and $\delta^{18}\mathrm{O}_f$ follow the same trend as lake waters, which suggests that aquifers receive a significant part of their recharge from surface water.

Mixing of seawater and fresh water is especially clear in samples that have $m_{\mathrm{Cl}} >$ 200 mmol/l and occurred in either (1) estuaries, tidal creeks, rivers, lakes and lagoons

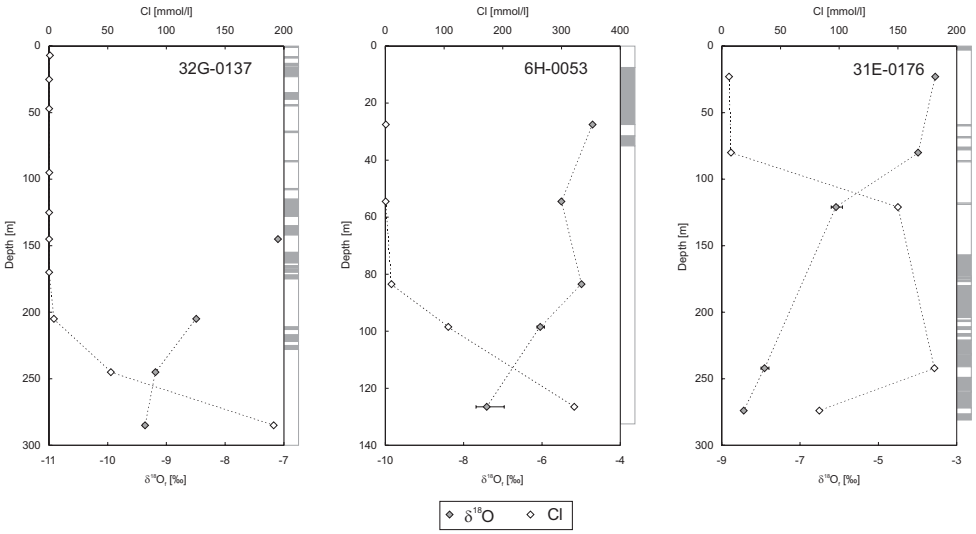

Figure 2.5: Graphs of the Cl concentration (open diamonds) and δ^{18}O of the fresh water end members (gray diamonds) vs. depth for wells 32G-0137, 6H-0053 and 31E-0176 (see figure 2.1 for their location). Bars indicate the associated errors according to figure 2.3. Shaded areas in the columns to the right of the charts indicate low-permeability sediments (mainly clay), white areas represent sand layers. Data from Meinardi (1975), Glasbergen and Mook (1982) and by courtesy of R. Boekelman

that existed during the Holocene or (2) the subsurface. Subsurface mixing, however, is less rapid than surface water mixing as it occurs by diffusion and dispersion.

The fresh water component may constitute river water, precipitation or ambient groundwater and vary in isotopic composition depending on its age (Weichselian vs. Holocene) or hydrological evolution (enrichment of heavier isotopes by evaporation).

The decrease of $\delta^{18}O_f$ with increasing m_{Cl} (figure 2.2b), implies that fresh water that mixed with seawater, experienced less evaporation than fresh groundwater that was not affected by mixing. In several observation wells, the relatively-enriched fresh groundwater overlies the more saline groundwater (figure 2.5). Cation exchange patterns show that the fresh water has displaced the more saline groundwater, which is concluded from the positive base exchange index (Stuyfzand, 1993) of the fresh samples as opposed to the negative or zero base exchange index of the more saline samples. This suggests that the fresh water is youngest, meaning that the increased contribution of evaporated water to groundwater recharge postdates the marine incursions, which corroborates findings by Gieske (1991) in the IJsselmeer area (cf. chapter 1).

Regional differences between the fresh water end members of the brackish and saline groundwater exist (figure 2.4). The brackish samples from the Horstermeer

polder area (figure 2.1 have δ^2H_f and $\delta^{18}O_f$ values that equal infiltrated meteoric water below the adjacent ice-pushed ridge (Hettling, 1985) and probably represent a mixture of seawater and fresh groundwater that discharges in this area. Saline and brackish samples from the coastal dunes near the city of Leiden have (evaporated) Rhine water as their fresh water end member. A tidal inlet was present here during the Holocene that was connected to a major discharge channel of the river Rhine (Beets et al., 1992). Here Rhine water mixed with encroaching seawater and subsequently entered the aquifers. Fresh water end members from the West-Friesland area plot on the LMWL and show an enrichment compared to modern precipitation by as much as ~ 10 ‰ for ^2H and ~ 2 ‰ for ^{18}O. In the province of Zeeland, the fresh water end members plot well above the LWML, although this may partly be due to uncertainty about the exact composition of the seawater end member (figure 2.3).

Beekman (1991) explained the values from the West-Friesland area by assuming that recharge occurs mainly during summer when precipitation is enriched in the heavy isotopes. This seems unlikely, however, given the upper limit in monthly averaged δ^2H (~ 38.4 ‰) and $\delta^{18}O$ (~ 5.8 ‰) values in precipitation at the nearby GNIP station at Wieringerwerf and the precipitation deficit during this period (cf. figure 4.2). Observed groundwater values are well below the maximum δ^2H (~ 14.9 ‰) and $\delta^{18}O$ (~ 2.5 ‰) values of individual storms, but these values are associated with low-intensity rainfall when little recharge is expected. Therefore, the explanation for these numbers remains unclear.

The large range of δ^2H and $\delta^{18}O$ in groundwater from the coastal lowlands contrasts with groundwater from the Veluwe area, which has an isotopic composition close to mean precipitation (Mook, 1968; Gehrels, 1999). In this more elevated part of the Netherlands, there are no shallow occurrences of seawater and, because of the thick unsaturated zone and lack of surface water, direct evaporation is small.

A noteworthy observation is sample 3C-0018 (figure 2.1) that plots well below the mixing lines of seawater and precipitation or Rhine water (figure 2.2a). It is from a depth of ~ 70 m below the surface and located directly above the Pieterburen salt dome that protrudes through overlying Tertiary layers up to 218 m below the surface (Zagwijn et al., 1985). Possibly the rock salt constitutes the source for the observed additional salinity, but it is uncertain how the dissolved salt migrates upward. Perhaps groundwater ascends preferentially via faults as was suggested by Glasbergen and Mook (1982). Alternatively, the sample may represent diluted seawater that was subject to evapotranspiration in a salt marsh as explained in chapter 4.

2.4.2 Carbon-14

Radiocarbon measurements are useful for establishing the age of a groundwater sample. The problems with dating groundwater using ^{14}C are well-known and have been given considerable attention in the literature (for a recent overview see Geyh, 2000).

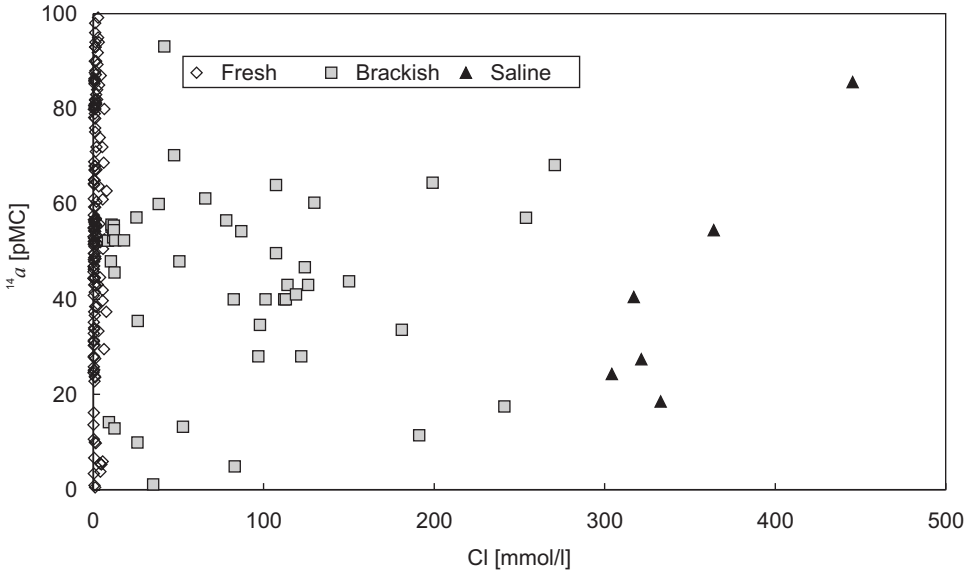

Figure 2.6: Graph of the ^{14}C activity (^{14}a) vs. Cl concentration of groundwater samples from the coastal area.

The measured ^{14}C activity must be corrected for alterations in the subsurface that interfere with the decreasing activity due to radioactive decay since the groundwater was isolated from the atmosphere. Even though the geochemical evolution of the groundwater samples could satisfactorily be reconstructed in this study, it proved impossible to obtain reliable ages owing to the presence of carbon sources with highly variable ages. The effect hereof will be quantified below to illustrate the limitations of radiocarbon dating in comparable geological settings.

There have been multiple phases of marine conditions in the coastal area during the Cenozoic. Therefore, the ^{14}C signal of brackish and saline groundwater may reflect either: (1) mixing of old (Eemian or Pliocene to Early-Pleistocene), ^{14}C-free seawater and Holocene fresh water or (2) intrusion of the water during the Holocene. The first step in the interpretation of ^{14}C data was thus to establish whether ^{14}C is indicative of a Holocene origin of brackish and saline samples.

For this purpose, ^{14}C activities measured at 5 different depths in observation well 31E-0176 (figure 1.6) were examined. As was elaborated in chapter 1, the lower salinity of the deepest sample compared to the overlying brackish groundwater implies that this sample represents relic Pliocene or Early-Pleistocene seawater. Having an age > 1.6 Ma, the deepest sample is expected to be ^{14}C-free but still has $^{14}a = 5$ pMC, which might be attributed to admixing of younger (< 25 ka) fresh water. It can not be excluded that the measured activity is due to pollution by drilling fluid or shortcut flow in the well. The ^{14}a of the brackish samples above the

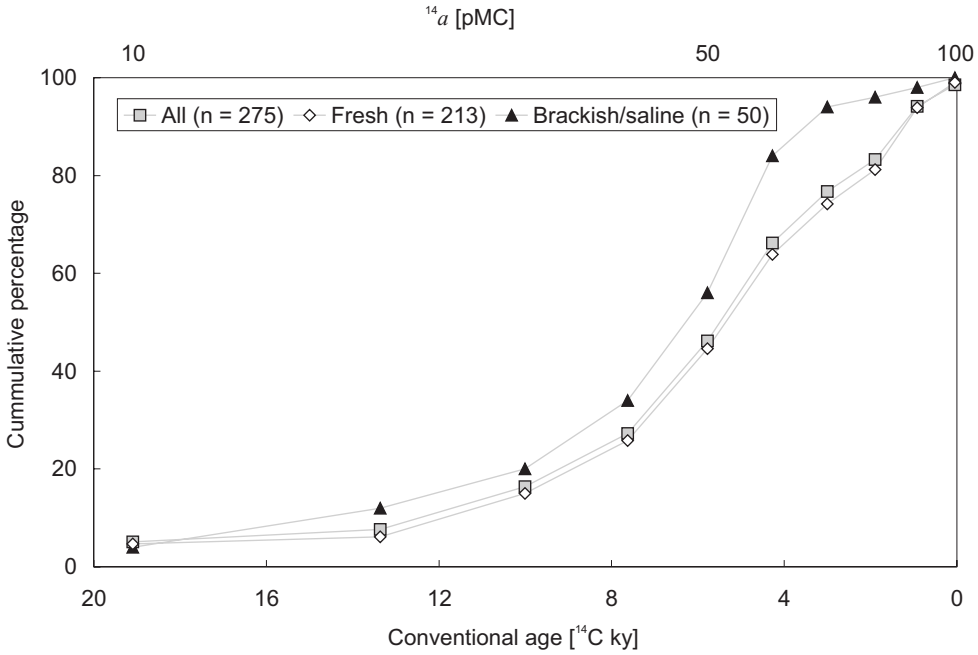

Figure 2.7: Cumulative frequency distribution of ^{14}C activities and corresponding conventional ages of groundwater samples in the coastal area. The conventional ^{14}C age is an estimate of the maximum groundwater age. It was calculated using equation 2.3 with $^{14}a_{nd} = 100$ pMC, which represents atmospheric ^{14}C activity in 1950.

chloride inversion is conspicuously higher (figure 1.6). As follows from their higher salinity, the ^{14}C signature of these samples can not be due to mixing of Holocene fresh water and Pliocene to Early-Pleistocene seawater, which means that the high ^{14}a is indicative of a Holocene seawater contribution.

Since the salinity inversion in well 31E-0176 is a general phenomenon (figure 1.7), high ^{14}C activities of brackish to saline samples from other parts of the coastal area are also considered to be representative for a Holocene origin. Moreover, if mixing of Holocene fresh water and Pliocene to Early-Pleistocene seawater would control ^{14}a of the brackish and saline groundwater in the Pleistocene fluvial aquifers, a decrease of ^{14}a with m_{Cl} along a mixing line would be observed as the seawater component is ^{14}C-free. Figure 2.6, in which ^{14}a is plotted vs. m_{Cl}, shows that no such trend exists.

Approximately ~ 80 % of all groundwater samples with $m_{\mathrm{Cl}} > 8.4$ mmol/l have a ^{14}C activity higher than 30 pMC (figure 2.7) and thus date from the Holocene. Samples with an activity below 30 pMC possibly represent older waters but correction for geochemical reactions is likely to prove them younger than their conventional

age.

Given the Holocene origin of the brackish and saline groundwater, the next step towards calculating its age was to derive a reaction scheme that led to its chemical composition in order to quantify the contribution of carbonate dissolution, sedimentary-organic carbon (SOC) mineralization and methanogenesis to DIC. The reaction scheme was calculated using the inverse-modelling option of the geochemical code PHREEQC (Parkhurst and Appelo, 1999). Given an initial water composition and the measured composition of the groundwater sample, the program calculates mole transfers of reacting phases. The reactions that were considered are listed in table 2.2. Carbon-13 was not used as a constraint because precipitation of calcite and siderite was anticipated, in which case isotopes whose fractionation factor is not unity cannot be used to constrain inverse-modelling calculations (Plummer et al., 1994). Moreover, $\delta^{13}C$ of the precipitated mineral phases is unknown.

Salinization during the Holocene is assumed to have occurred mainly by free convection. Fresh water and seawater mixed in large estuaries and tidal channels that cut into the Pleistocene aquifers (De Mulder and Bosch, 1982; Beets et al., 1992). This mixture subsequently sank into the underlying aquifer due to its higher density than the ambient-fresh groundwater (chapter 5). Assuming that subsurface mixing was only minor, the initial water composition for the inverse-modelling calculations can be represented by a mixture of seawater and a single fresh water end member. The fresh water end member was derived from the composition of pre-industrial Rhine water (table 2.3). The relative contribution of the end members was calculated for each sample from m_{Cl} of that sample.

Inverse-modelling calculations were carried out for 15 groundwater samples (table 2.3). The results indicate that oxidation of organic matter adds significantly to DIC and that, in general, calcite and siderite precipitate (table 2.4). The deficit of sulfate in the samples relative to sulfate in the initial water (i.e., the mixture of Rhine water and seawater, table 2.4) indicates that sulfate reduction is the predominant pathway

Table 2.2: Phase transfers considered in the inverse-modelling scheme.

Reaction
$Na^+ + X^- \leftrightarrow NaX$
$K^+ + X^- \leftrightarrow KX$
$NH_4^+ + X^- \leftrightarrow NH_4X$
$H^+ + X^- \leftrightarrow HX$
$Ca^{2+} + 2X^- \leftrightarrow CaX_2$
$Mg^{2+} + 2X^- \leftrightarrow MgX_2$
$Ca^{2+} + CO_3^{2-} \leftrightarrow CaCO_3$
$Fe^{2+} + CO_3^{2-} \leftrightarrow FeCO_3$
$FeOOH + 3H^+ \leftrightarrow Fe^{3+} + 2H_2O$
$SO_4^{2-} + 9H^+ + 8e^- \leftrightarrow HS^- + 4H_2O$
$FeS_2 + 2H^+ + 2e^- \leftrightarrow Fe^{2+} + 2HS^-$
$2CH_2O(NH_3)_{0.075} + 0.15H_2O \leftrightarrow 0.15HCO_3^- + 0.85CO_2 + 0.15NH_4^+ + CH_4$

Table 2.3: Composition of the samples used for inverse-modelling. The geographical location (Loc.) is indicated with numbers that refer to the numbers in figure 2.1. DIC was calculated with PHREEQC from pH and HCO_3.

	Well	Depth	Loc.	$\delta^{13}C$	^{14}a	pH	Concentration [mmol/l]									
		[m]		[‰]	[pMC]		Na	K	Mg	Ca	NH_4	Cl	HCO_3	SO_4	Fe	DIC
1	19F-0172[a]	109	2	−6.3	57	7.3	87	1.7	6.3	2.4	1.7	78	28.8	0.3	0.1	31.5
2	25H-0094[b]	38	4	−12.0	41	7.7	96	0.5	8.5	12.1	0.1	119	2.8	4.2	0.4	2.8
3	25H-0238[b]	100	4	−14.9	35	7.7	77	0.6	7.1	8.7	0.1	98	5.0	1.3	0.2	5.1
4	30E-0119[c]	56	6	−12.0	49	7.5	348	6.1	42.0	10.6	0.8	415	4.4	18.6	0.2	4.5
5	31F-0002[d]	11	4	−13.7	28	7.3	91	0.5	8.3	10.4	0.1	122	7.1	2.7	0.3	7.8
6	31F-B1[d]	3.9	4	−14.0	43	7.3	91	0.7	8.6	9.6	0.2	126	7.5	3.1	0.3	8.2
7	31F-B2[d]	3.6	4	−14.0	40	7.4	80	0.5	7.9	10.5	0.1	113	6.3	2.9	0.3	6.8
8	31F-B6[d]	4.0	4	−14.0	40	7.2	55	0.2	3.6	11.3	0.1	82	5.3	2.6	0.3	5.9
9	31F-L49[d]	8.0	4	−14.8	43	7.5	86	0.5	7.0	9.8	0.1	114	4.9	3.7	0.3	5.2
10	31F-L55[d]	11	4	−14.0	28	7.3	71	0.2	4.1	10.8	0.1	97	4.7	2.6	0.3	5.1
11	3G-0012[e]	26	1	−7.1	55	7.0	286	3.4	31.7	12.6	4.2	364	42.0	0.9	0.3	48.0
12	6H-0053[e]	99	1	−1.2	50	6.9	41	0.2	4.4	29.3	0.2	107	4.6	1.0	1.2	5.7
13	6H-0053[e]	127	1	−11.4	27	6.9	203	0.3	24.9	29.4	0.6	322	5.2	1.1	1.2	6.1
14	7C-0101[e]	49	1	−5.8	47	6.8	51	0.1	5.1	28.8	0.2	124	4.0	1.2	1.6	5.1
15	7C-0101[e]	62	1	−13.8	57	7.0	181	0.5	11.5	25.1	0.6	254	8.9	2.2	1.3	10.3
	Rhine[f]					7.7	0.2	0.1	0.4	1.3		0.3	2.6	0.4		2.7
	Sea[g]			1	95	8.2	485	10.6	55.1	10.6		566	2.4	29.3		2.4

a = Beekman (1991); b = P.P. Schot (unpublished data); c = R.I.D., National Institute for Water Supply (unpublished data); d = De Groot and Van der Linden (1987); e = Glasbergen and Mook (1982); f = Molt (1961), Van der Weijden and Middelburg (1989); g = Appelo and Postma (1994), Yurtsever (1997).

for organic matter mineralization. Methanogenesis is predicted for samples 1 and 11, which corroborates their relatively high δ^{13}C. On the other hand, samples 12 and 14 also have a high δ^{13}C but seem to have no contribution from methanogenesis. Their high δ^{13}C may be indicative for calcite dissolution due to protons released from organic matter and iron hydroxides, which was confirmed by calculations that included proton exchange (not shown here). Extending the number of reactions added to the non-uniqueness of the inverse-modelling problem, thereby increasing the already overwhelming complexity of radiocarbon dating.

With the mass transfers known, the age of a sample (T_m) can theoretically be calculated from:

$$T_m = -\frac{T_{1/2}}{\ln 2} \ln \frac{{}^{14}a_m}{{}^{14}a_{nd}} = -8267 \ln \frac{{}^{14}a_m}{{}^{14}a_{nd}} \tag{2.3}$$

where $T_{1/2}$ is the half life of ^{14}C [5 730 y], $^{14}a_m$ the measured ^{14}C activity of the sample [pMC] and $^{14}a_{nd}$ denotes the ^{14}C activity of the sample if no decay would have occurred [pMC], which is calculated according to:

$${}^{14}a_{nd} = \frac{{}^{14}a_f \;\; m_{\mathrm{DIC},f} \;\; (1-f_s) + {}^{14}a_s \;\; m_{\mathrm{DIC},s} \;\; f_s + {}^{14}a_c \;\; m_{\mathrm{DIC},c}}{m_{\mathrm{DIC},f} \;\; (1-f_s) + m_{\mathrm{DIC},s} \;\; f_s + m_{\mathrm{DIC},c}} \tag{2.4}$$

where the subscripts f, s and c denote the fresh water end member (Rhine water), seawater end member and reacted carbon phases respectively, m_{DIC} denotes the DIC concentration [mmol/l] of the fresh and seawater end members ($m_{\mathrm{DIC},f}$ and $m_{\mathrm{DIC},s}$,

Table 2.4: Initial DIC and SO_4 concentrations, phase transfers and calculated-conventional ages (i.e., $^{14}a_{nd} = 100$ pMC) of the groundwater samples in table 2.3. Initial water composition is the calculated mixture of Rhine water and seawater. Negative phase transfers indicate precipitation, positive numbers indicate dissolution.

	Initial conc. [mmol/l]		Phase transfers [mmol]				Age
	DIC	SO_4	Calcite	Siderite	SOC	Methane	[ky]
1	2.7	4.4	7.6	0.0	35.0	−13.6	4.7
2	2.7	6.5	−2.6	−2.0	4.8	0.0	7.4
3	2.7	5.4	−3.3	−2.6	8.3	0.0	8.8
4	2.5	21.6	−0.9	0.0	3.0	0.0	5.8
5	2.7	6.6	−2.1	0.0	7.3	0.0	10.5
6	2.6	6.8	−2.3	0.0	7.9	0.0	7.0
7	2.7	6.2	−1.7	0.0	5.8	0.0	7.6
8	2.7	4.6	−1.7	0.0	4.6	0.0	7.6
9	2.7	6.2	−1.2	0.0	3.9	0.0	7.0
10	2.7	5.3	−2.2	−0.8	5.4	0.0	10.5
11	2.5	19.0	0.0	0.0	59.0	−13.3	5.0
12	2.7	5.9	−5.4	−1.4	9.8	0.0	5.8
13	2.5	16.8	−16.8	−12.4	32.8	0.0	10.7
14	2.7	6.7	−6.8	−2.0	11.2	0.0	6.3
15	2.6	13.4	−10.1	−4.5	22.4	0.0	4.6

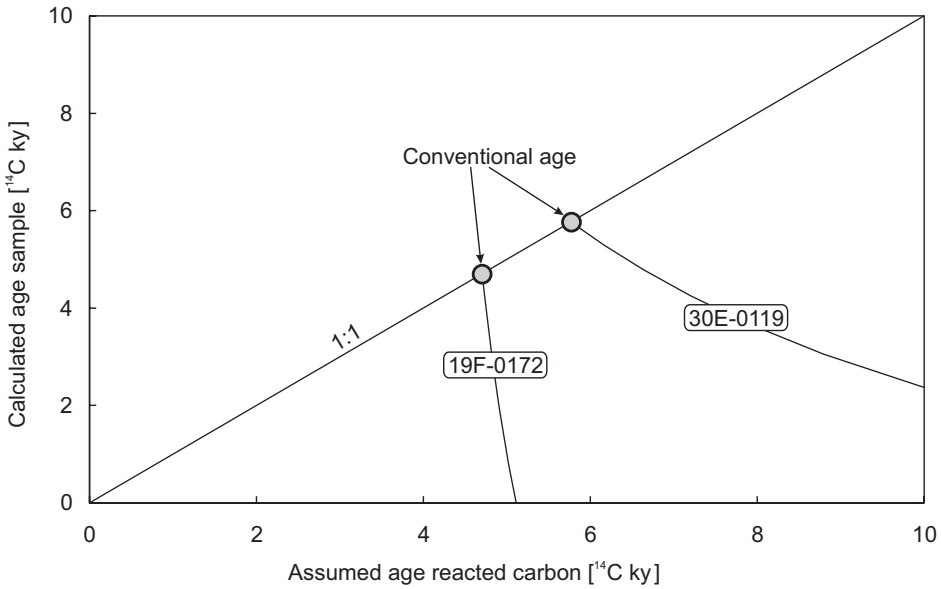

Figure 2.8: Graph of the calculated sample age vs. assumed age of the carbon sources adding to m_{DIC} for samples 19F-0172 and 30E-0119. Sample age decreases from the conventional age (i.e., ${}^{14}a_{nd} = 100$ pMC) towards lower values as the assumed age of the reacting carbon increases.

respectively) or contribution [mmol/l] from reacting carbon phases ($m_{\mathrm{DIC},c}$) and f_s is the fraction of seawater in the mixture [dimensionless]. Fractionation effects were not taken into account.

Since $m_{\mathrm{DIC},c}$ dominates over m_{DIC} in the initial water (table 2.4), T_m (equation 2.3) becomes very sensitive to the selected value of ${}^{14}a_c$. This effect is illustrated in figure 2.8 for samples 19F-0172 and 31E-0119 , which shows their calculated age (T_m) as a function of the assumed age of the reacting carbon phases. Sample 31E-0119 has a low contribution from $m_{\mathrm{DIC},c}$ and is relatively insensitive to the selected value of ${}^{14}a_c$, whereas sample 19F-0172 has a high contribution and displays an extreme sensitivity.

These results show that selection of the appropriate value for ${}^{14}a_c$ is crucial. However, there is no way of knowing the age of the contributing carbon sources. Within Holocene strata, ${}^{14}a_c$ varies both laterally and with depth. Due to reworking of clastic sediments, different phases within a single layer sometimes have completely different ages. For example, shells and organic matter from the same unit below the coastal dunes have ${}^{14}a = 43$ pMC and ${}^{14}a = 83$ pMC, respectively (H.J. Streurman, unpublished data). Also, one needs to know ${}^{14}a_c$ at the onset of reaction that adds to m_{DIC}, which depends on the unknown age of the sample. Moreover, the rel-

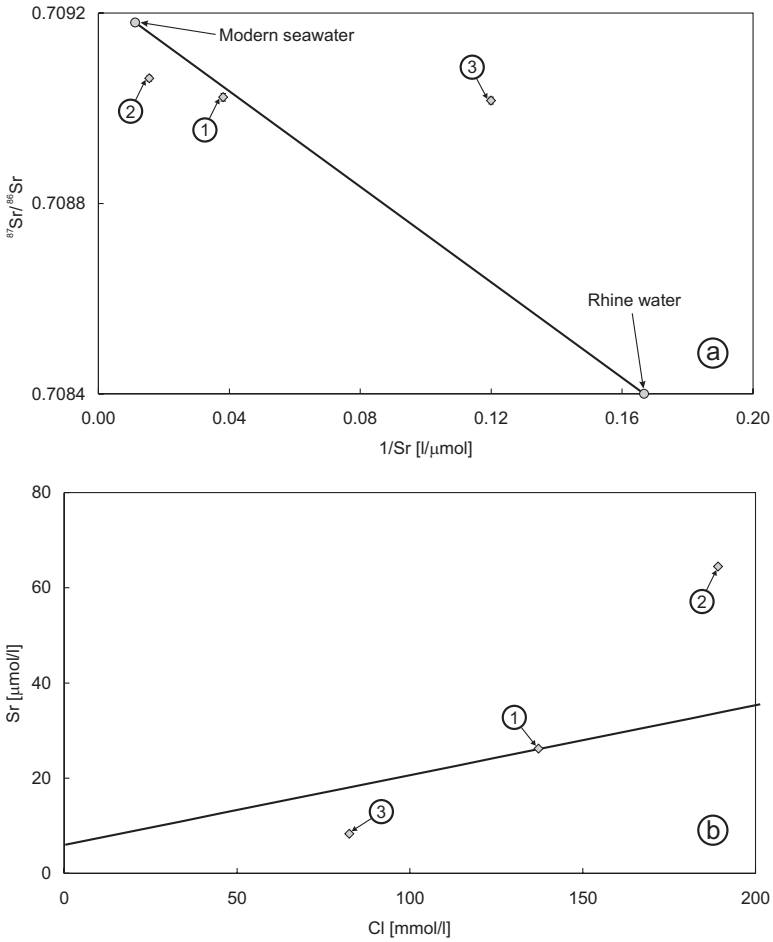

Figure 2.9: Graphs of (a) $^{87}Sr/^{86}Sr$ vs. 1/Sr and (b) the Sr concentration vs. Cl concentration of groundwater samples from well 31E-0176. Lines represent mixing of modern seawater and Rhine water. Numbers refer to samples from different depths below the surface: 1 = 121 m, 2 = 242 m and 3 = 274 m. Composition of modern seawater ($m_{Sr} \approx 89$ µmol/l, $^{87}Sr/^{86}Sr \approx 0.70918$) and Rhine water ($m_{Sr} \approx 6$ µmol/l, $^{87}Sr/^{86}Sr \approx 0.7084$) end members after C.J. Beets (personal communication).

atively high conventional ages of some samples compared to the onset of seawater incursions (i.e., > 7.5 ka, table 2.4) suggests dilution by 'dead' carbon ($^{14}a_c = 0$ pMC) from Pleistocene deposits, which contain small amounts of reactive organic matter (Hartog et al., 2002), as well as carbonates such as shells.

2.4.3 Strontium

The deepest sample in observation well 31E-0176 (sample 3, depth = 274 m below the surface) has a $^{87}Sr/^{86}Sr = 0.709016$ (figure 2.9a). This value supports the presumed Pliocene origin of this water as discussed above since shells from this period have comparable $^{87}Sr/^{86}Sr$ values (Beets, 1992).

The sample from 121 m below the surface (sample 1) has an almost similar $^{87}Sr/^{86}Sr = 0.709023$ but, following from its high ^{14}a, must have a Holocene origin. A Holocene origin is also attributed to the sample from 242 m below the surface (sample 2), which has a higher $^{87}Sr/^{86}Sr = 0.709063$. The measured Sr isotope ratios of these samples can be explained by mixing and, for sample 2, dissolution of Sr-bearing carbonates.

In both figures 2.9a and 2.9b, sample 1 plots on the mixing line, indicating that Sr in this water is influenced only by mixing of modern seawater and Rhine water. The position of sample 2 above the mixing line in figure 2.9b, however, indicates that additional Sr has dissolved. As can be seen from the position of the sample below the mixing line in figure 2.9a, the $^{87}Sr/^{86}Sr$ of the contributing Sr-bearing mineral has to be lower than the $^{87}Sr/^{86}Sr$ of the mixture. Therefore, the shells in the Pliocene marine strata are believed to be the source of the additional Sr. Sample 1 originates from fluvial deposits devoid of any Pliocene shell material (cf. figure 1.6), which explains why it has been influenced by mixing only.

Dissolution of Pliocene shells has implications for the interpretation of the radiocarbon activities, confirming the suspected dilution of some samples by 'dead' carbon.

The selection of Rhine water as the fresh water end member for the calculation of the mixing line is justified for sample 1 by its δ^2H_f and $\delta^{18}O_f$ values. Sample 2, however, has δ^2H_f and $\delta^{18}O_f$ values that suggest a local, meteoric origin. Modern meteoric water in this area is likely to have $^{87}Sr/^{86}Sr$ ratios resembling that of modern seawater (cf. Jørgensen and Holm, 1994), but the fresh water component may well date from the Weichselian (its δ^2H_f and $\delta^{18}O_f$ are slightly depleted with respect to modern precipitation). In that case, the $^{87}Sr/^{86}Sr$ could have been different owing to the more distant location of the shoreline. In any case, the sample will plot below the mixing line in figure 2.9a and the interpretation presented above remains valid.

Three samples were analysed in this study and the findings presented here need verification by sampling additional observation wells.

2.5 Conclusions

Natural isotope measurements of water and its solutes (^2H, ^{18}O, ^{13}C, ^{14}C and $^{87}Sr/^{86}Sr$) proved useful in the interpretation of the hydrological processes that determine the groundwater composition in the coastal area of the Netherlands. Evaporation and mixing of seawater and fresh water are the prime processes that account

for the range in observed values. Locally, in the province of Groningen, dissolution of rock salt may add to groundwater salinity.

Given that the fresh water end member of the brackish groundwater samples does not show signs of evaporation whereas the overlying fresh groundwater often does, the contribution of evaporated-meteoric water to groundwater recharge appears to have postdated salinization of the aquifers.

Due to the large contribution of sedimentary carbon sources to groundwater DIC and the heterogeneous age distribution of carbon-bearing materials in the subsurface, accurate radiocarbon dating of the brackish and saline groundwater proved impossible. Carbon-14, however, could be used to distinguish a Holocene from a Pliocene to Early-Pleistocene seawater contribution. Strontium isotopes also appeared useful in this respect.

Part II: studies of the pore water composition in confining units

Chapter 3

Evidence for ongoing salinization of fresh paleogroundwater below the southern North Sea

Abstract

The occurrence of relic, meteoric groundwater below continental shelves up to tens of kilometers offshore from the present coastline is believed to be a worldwide phenomenon. Chemical and isotopic analyses of pore waters in three low-permeability seafloor beds are used to demonstrate the presumed presence of such offshore fresh water below the southern North Sea. Two of the three pore water profiles yield inconclusive results. The third shows a marked decrease in salinity to less than 50 % of seawater at 6 m below the seafloor. Modelling shows that diffusion is the prime mode of transport. Model-optimized diffusion coefficients of Cl and ^{18}O, as well as laboratory-determined values, show that the charged Cl ion moves at a slower rate than H_2O. This discrepancy is attributed to anion-exclusion effects or extremely small pores, which may be related to the dehydration of the clay during the Weichselian. The diffusion coefficient of Cl is up to 1 order of magnitude smaller than for comparable lithologies reported in the literature. The clay layer thus forms an effective barrier against salinization of meteoric water in the underlying sand.

3.1 Introduction

During the past decades, an increasing number of studies (Kohout et al., 1977; Hathaway et al., 1979; Wang, 1994; Maathuis et al., 1996; Hinsby et al., 2001; Groen, 2002) have reported on the occurrence of fresh ($m_{Cl} < 8.5$ mmol/l, where m_{Cl} is the Cl concentration) and brackish ($8.5 < m_{Cl} < 282$ mmol/l) groundwater in offshore

This chapter is based on the paper: Post, V.E.A., Hooijboer, A.E.J., Groen, J., Gieske, J.M.J., Kooi, H., submitted to Earth and Planetary Science Letters. Evidence for ongoing salinization of fresh paleogroundwater below the southern North Sea.

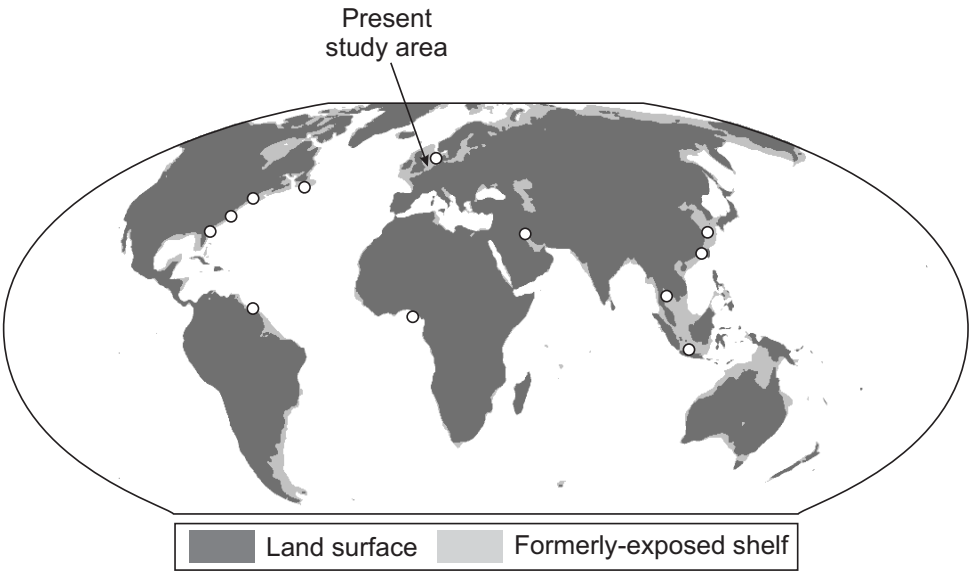

Figure 3.1: World map showing known occurrences of offshore fresh to brackish groundwater (modified from Groen, 2002) and continental shelf areas that were exposed during the last glacial maximum (25 – 15 ka BP).

sediments up to 100 km from the present coastline (figure 3.1) . These occurrences are not connected to active flow systems and should be considered as relics of former flow systems that existed during the last glacial period (Weichselian, 110 – 10 ka BP) when sea level was low and large parts of the continental shelves were exposed (figure 3.1).

Conditions that favour the preservation of these bodies of relatively-fresh groundwater include rapid coastline migration and the presence of low-permeability deposits such as clays, tills and shales at the seafloor (Kooi et al., 2000). If such conditions are met, diffusive transport is the dominant mode of salinization. Because this is a slow process, the pore water composition of the low-permeability deposits often retains signals of the hydrologic conditions prior to inundation for periods of up to thousands of years. A classical example is provided by the pore water Cl concentrations in Kau Bay, Indonesia (Eggenkamp et al., 1994), a former fresh water lake that became saline after the last glaciation.

The southern North Sea experienced a similar geological history. The area was partially exposed during the Weichselian glacial stage and inundated during the Holocene sea level rise (figure 3.2). Regionally, clay layers are present in which pore waters are likely to reflect these paleogeographical changes. This chapter reports on the Cl concentration and isotopic composition (δ^2H, δ^{18}O, δ^{37}Cl) of the pore waters from three low-permeability layers below the seafloor in the southern North

Sea. These data were collected in order to establish whether diffusive concentration profiles are also present in these units. If so, these can be considered indicative of fresh to brackish water in the underlying, more permeable strata.

The study of offshore pore water profiles has traditionally been the realm of marine geochemistry and focuses primarily on early diagenesis (e.g. Berner, 1980; Schulz and Zabel, 2000). Few publications deal with offshore water quality observations from a hydrogeological perspective although they were used by some authors to quantify vertical-submarine groundwater discharge rates (Volker and Van der Molen, 1991; Piekarek-Jankowska, 1996) and rates of sediment deposition (Beekman, 1991). Studies onshore, however, have demonstrated that pore water profiles of aquitards are excellent targets for identification of hydrological processes and quantification of hydraulic parameters. Topics studied include diffusive transport due to periodic sea level changes (Sjöberg et al., 1984; Groen et al., 2000b; Manzano et al., 2001), disposal of radioactive waste (Boisson et al., 2001; Gautschi, 2001; Degueldre et al., 2003), solute concentration by evaporation (Ortega-Guerrero et al., 1996, chapter 4) and quantification of transport by diffusion and advection (Desaulniers et al., 1981; Remenda et al., 1996; Hendry and Wassenaar, 1999, 2000; Hendry et al., 2000). Therefore, besides establishing the presence of brackish water below the North Sea, the present study aimed to identify the processes that control the distribution of solutes within the confining units and determine the rate of salinization.

3.2 Physical setting

The southern North Sea has experienced alternating periods of marine and continental conditions during the Pleistocene. During the last glacial period the present seafloor was exposed. The earliest brackish water incursion as a result of the Holocene transgression may have occurred as early as 10 ka BP but fully-marine conditions only became established widely after 7 ka BP (Cameron et al., 1993).

Clay cores were obtained from three sites (figure 3.2), each with a different lithology: (1) Dogger Bank Formation, (2) Bolders Bank Formation and (3) Brown Bank Formation.

The Dogger Bank Formation was deposited in a glaciolacustrine environment during the Late Weichselian. Its thickness ranges from 4 to 20 m (Laban, 1995). The cored sediment consists of stiff clay with silt laminae with a varve-like structure. The Bolders Bank Formation constitutes a Late Weichselian till with a thickness between 2 and 6 m. The sampled material consists of extremely stiff, sandy clay with intercalated pebbles. Pollen-analytical investigation showed that the Brown Bank Formation consists of Early Weichselian lacustrine clay (W.Z. Hoek, unpublished data). At the sampling site, the clay has a thickness of 5 m and was encountered below 1 m of Holocene sand. Especially the upper 2 m of the clay are very stiff, which is attributed to dehydration during permafrost conditions (Laban, 1995). In the upper 20 cm, small cracks filled with sand and shell fragments are present. Fine

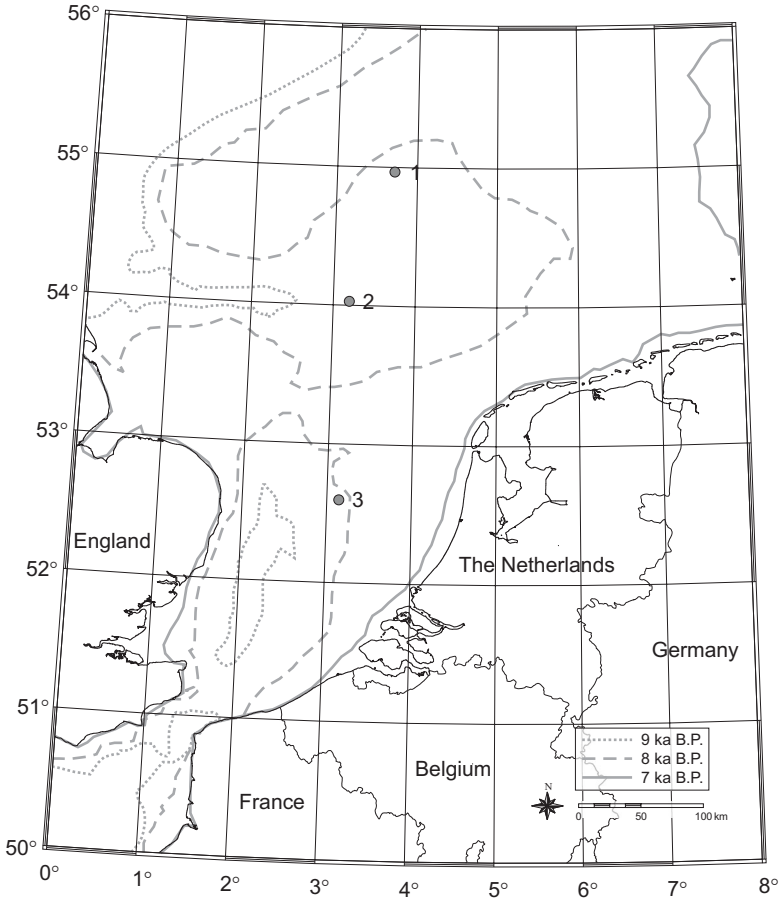

Figure 3.2: Map of the southern North Sea showing locations of sampling sites and coastline configurations at 9, 8 and 7 ka BP (after Shennan et al., 2000).

marine sand containing shell fragments underlies the clay, at least to a depth of 12 m below the seafloor.

3.3 Measurements

3.3.1 Methods

The clay samples were obtained during two drilling campaigns. During the first campaign (July 1998), three undisturbed sediment cores were obtained using a vibrocorer in 100 mm PVC tubes at the three different sites in the North Sea (figure

3.2). Owing to the stiffness of the clays, only the upper 2 to 3 m could be cored. The cores were cut in 1 m sections and their ends were sealed with a paraffin layer of at least 25 mm thick and a plastic cover that was taped airtight. They were then stored in a refrigerator until further processing. Pore water samples were obtained in the laboratory in Amsterdam at 30 cm intervals by squeezing a 7 cm slab of clay at a pressure of 0.4 10^6 – 1 10^6 Pa in a glove box filled with gaseous nitrogen ($O_2 < 1$ ppm). These samples were analysed for major ion chemistry.

During the second campaign (February 1999) a clay core was obtained from the Brown Bank Formation using a counterflush technique (Geodoff method) at the same location as during the first campaign (site 3, figure 3.2). This method was applied to reach a greater depth than could be achieved with the vibrocorer. Intact pieces of clay were obtained, but drawbacks of this method are (1) deformation of the samples (elongation due to different diameters of tubes in the drilling system) and (2) contact of the sample with seawater and the atmosphere. The entire, 5 m thick clay section was sampled. The samples were wrapped in cellophane foil and sealed in plastic to prevent evaporation from the clay and stored in a refrigerator during transport to the laboratory. Clay samples were squeezed at intervals of 25 cm and their pore waters were analysed for major ions. Selected samples were analysed for the isotopes ^{2}H, ^{18}O and ^{37}Cl. The accuracy of the δ^2H and δ^{18}O measurements (expressed relative to V-SMOW, Vienna Standard Mean Ocean Water) amounts to 2 ‰ and 0.1 ‰ respectively. δ^{37}Cl (expressed relative to SMOC, Standard Mean Ocean Chloride) was measured following the procedures described by Eggenkamp (1994). The reproducibility of the analyses is better than 0.1 ‰ .

The radial diffusion method (Van der Kamp et al., 1996; Novakowski and Van der Kamp, 1996) was used on four undisturbed clay samples to determine the effective porosities and diffusion coefficients of both Cl and ^{18}O. Porosity was also quantified gravimetrically.

3.3.2 Results

Figure 3.3 shows the Cl concentration vs. depth at the three sites that were sampled during the first campaign (vibrocores). At site 1, the Cl concentrations in the upper part of the clay exceed that of ocean water (566 mmol/l) and abruptly decrease between 2.2 and 2.5 m. Except for one outlier, the Cl concentrations at site 2 show a slight decrease with depth, but the sampled depth interval is too small to show any significant change. The most obvious decrease in Cl concentration is found in the clay at site 3 (figure 3.3).

Figure 3.4 displays the Cl concentrations at site 3. It includes both the points from the first campaign (vibrocore) and the second campaign (counterflush). The Cl concentrations show a decrease from 562 mmol/l at the top to 253 mmol/l at the bottom of the clay layer. Pore water concentrations from the vibrocore samples show excellent agreement with the concentrations from the counterflush samples. This also holds for the other ions (not shown here), which implies that the results

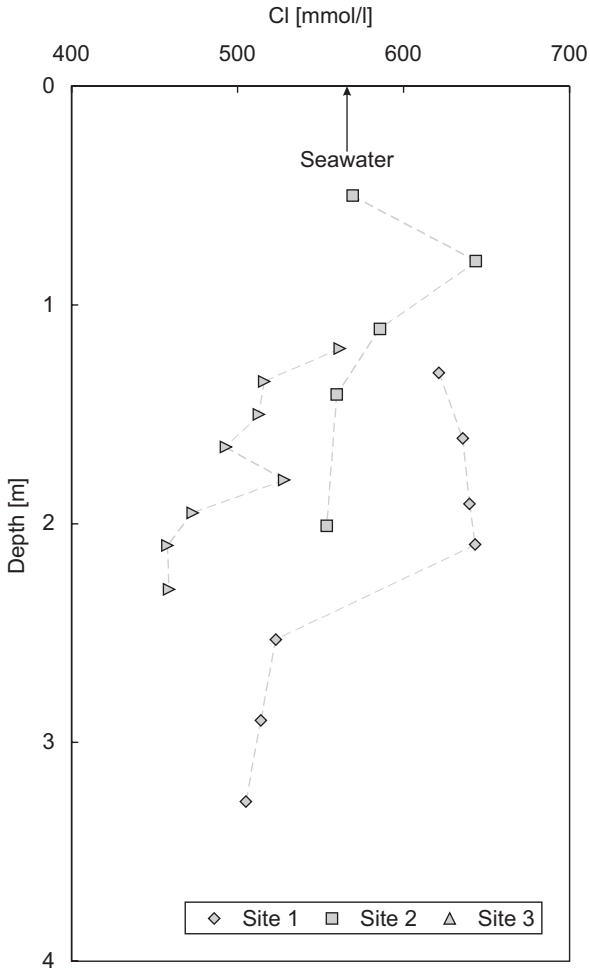

Figure 3.3: Graph of the observed Cl concentration vs. depth below the seafloor at the three sampling sites.

obtained with the counterflush technique are reliable.

The heavy isotopes (^{2}H, ^{18}O and ^{37}Cl) all become progressively depleted with depth (figures 3.4 and 3.5). A linear relation exists between δ^{18}O and Cl ($R^2 = 0.99$) and δ^{2}H and Cl (figure 3.6, $R^2 = 0.98$, one outlier excluded).

The radial diffusion experiments show that the effective porosity of Cl is lower than that of ^{18}O (table 3.1). The porosity of ^{18}O as determined with the radial diffusion method is higher than the porosity that was measured gravimetrically. This is consistent with other reports from the literature (G. van der Kamp, personal

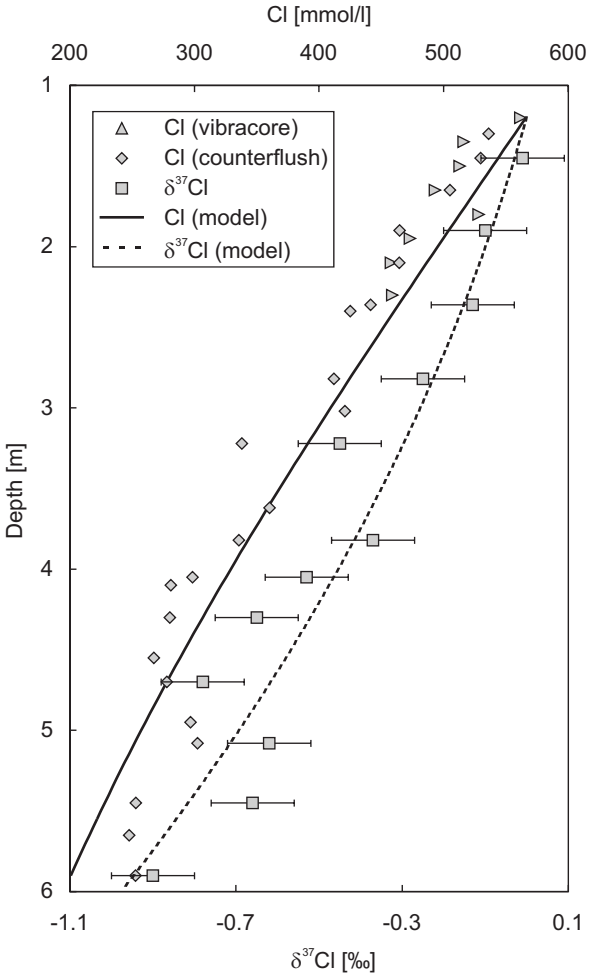

Figure 3.4: Graph of the observed and modelled Cl concentration and δ^{37}Cl vs. depth below the seafloor at site 3.

communication; Hendry and Wassenaar, 1999). The diffusion coefficient of ^{18}O is up to a factor of 2 higher than that of Cl (table 3.1).

3.4 Analysis

At sites 1 and 2, Cl concentrations were measured that exceed that of seawater. It is unclear what process is responsible for this enrichment. Possibly, evapotranspiration

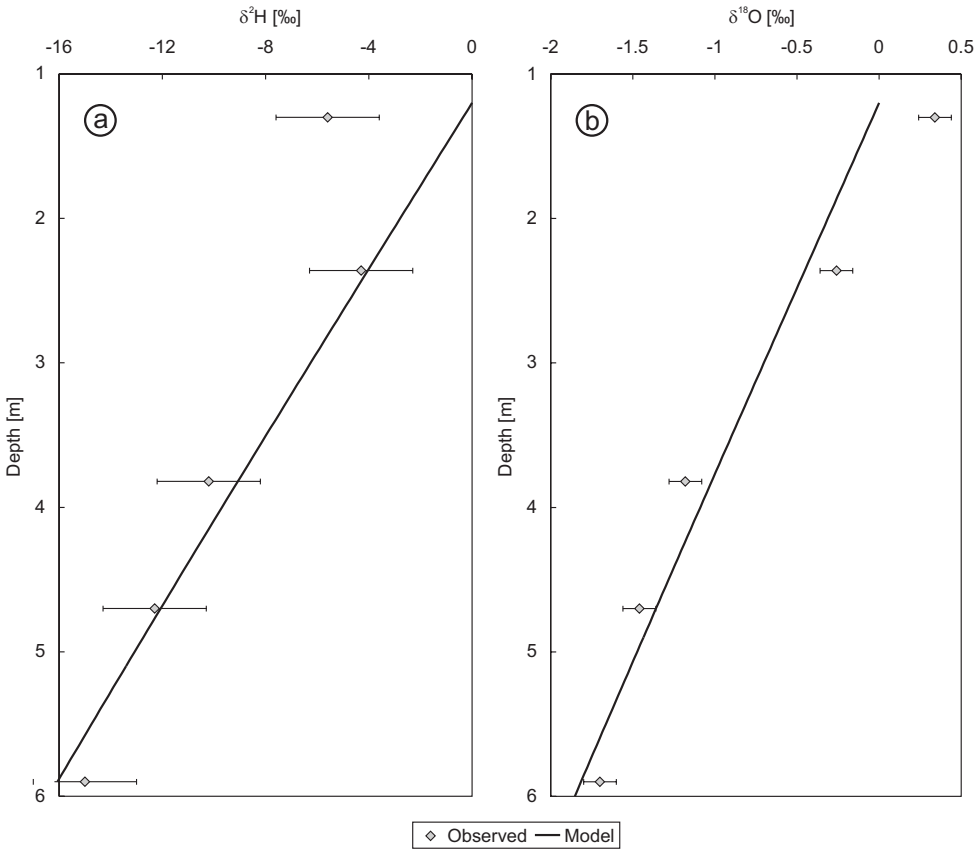

Figure 3.5: Graphs of the observed and modelled (a) δ^2H and (b) δ^{18}O vs. depth at site 3.

played a role prior to inundation. This mechanism most-likely exerted important influence on the salinity of groundwater onshore as elaborated in chapter 4. At both sites, the highest Cl concentrations occur in the upper part of the profile. The gradual decrease that is observed at site 2 may point to downward-diffusive transport. The more abrupt change observed at site 1 is difficult to interpret.

The decrease of Cl, δ^2H and δ^{18}O with depth observed at site 3 (figures 3.4 and 3.5) indicates that salinization of fresh-meteoric water takes place. The negative δ^{37}Cl values (figure 3.4) are indicative for diffusive transport of saline water into fresh water (Desaulniers et al., 1986).

In order to evaluate the salinization processes that are responsible for the observed pore water chemistry patterns, a simple diffusion model was applied. The partial differential equation that describes the transport due to diffusion derives from

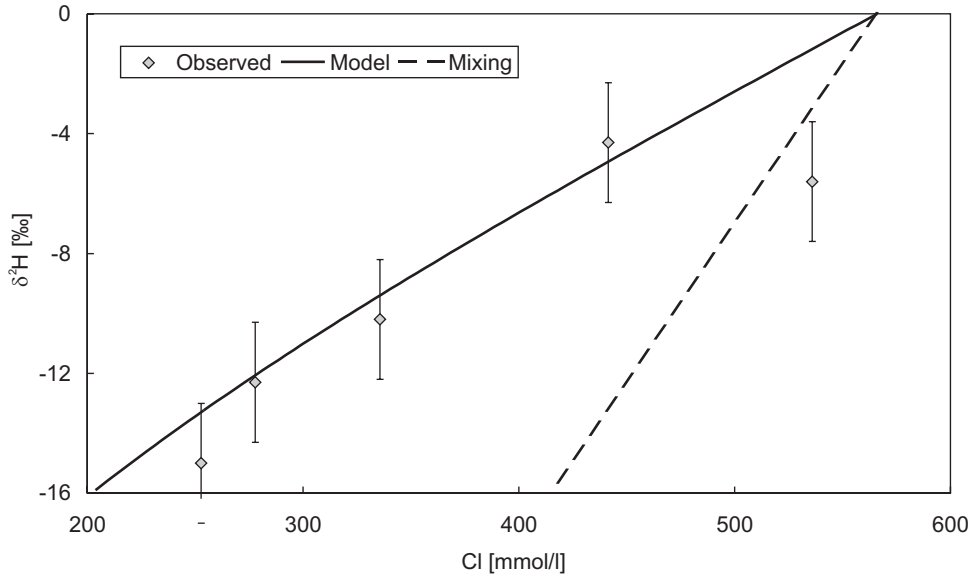

Figure 3.6: Graph of δ^2H vs. Cl concentration showing the observed and modelled values at site 3. Dashed line indicates the relation that would follow from simple mixing (i.e., equal diffusion coefficients).

Fick's law and the conservation of mass:

$$\frac{\partial m_{\mathrm{Cl}}}{\partial t} = D_e \frac{\partial^2 m_{\mathrm{Cl}}}{\partial z^2} \tag{3.1}$$

where m_{Cl} denotes the Cl concentration [mmol/l], t is time since inundation [s], D_e the spatially-uniform, effective diffusion coefficient that includes the effects of tortuosity but not porosity [m^2/s] and z the depth below the top of the clay layer [m]. The solution of equation 3.1 subject to the initial and boundary conditions in

Table 3.1: Gravimetric (oven-dried) porosity, effective porosity and effective diffusion coefficients of Cl and ^{18}O obtained from radial diffusion testing of Brown Bank sediments.

Sample	Depth [m]	Porosity [dimensionless]			D_e [m^2/s] 10^{10}	
		grav.	Cl	^{18}O	Cl	^{18}O
1	1.23 - 1.32	0.51	0.41	0.56	4	5
2	1.38 - 1.47	0.46	0.43	0.64	4	8
3	1.53 - 1.62	0.46	0.45	0.56	6	8
4	2.13 - 2.21	0.47	0.41	0.53	5	9

table 3.2 is:

$$m_{\mathrm{Cl}}(z,t) = m_{\mathrm{Cl},i} + (m_{\mathrm{Cl},s} - m_{\mathrm{Cl},i})\mathrm{erfc}\left(\frac{z}{\sqrt{4D_e t}}\right) \tag{3.2}$$

where the subscripts i and s refer to the pristine pore water (prior to inundation) and seawater, respectively.

For ^{2}H, ^{18}O and ^{37}Cl equation 3.2 was used with the concentrations expressed for the respective species. Owing to its greater mass, ^{37}Cl has a slightly lower diffusion coefficient than ^{35}Cl (Eggenkamp, 1994):

$$\alpha = \frac{^{35}D_e}{^{37}D_e} > 1 \tag{3.3}$$

Because ^{35}Cl is more mobile than ^{37}Cl, the salinized pore water becomes depleted with respect to the heavy isotope (even if initially no δ^{37}Cl gradient existed) as evidenced by the negative δ^{37}Cl values (figure 3.4).

The assumptions contained in this model require some further attention. First, it is assumed that the initial concentration distribution was uniform with depth. For Cl this seems reasonable since freshening occurred for many tens of thousands of years during the Weichselian. However, δ^{2}H and δ^{18}O may not necessarily have been constant since they are affected by the temperature of the recharge water. No information is available on their distribution prior to inundation and therefore it was assumed that their initial values were (1) constant with depth and (2) depleted relative to modern meteoric water (table 3.2, Rozanski, 1985). Second, it is presumed that the boundary condition at the top of the clay layer changed in a stepwise fashion upon inundation. That is, the concentrations instantly changed from fresh water values to seawater values whereas in reality a more gradual transition may be expected.

Flooding of this site during the Holocene transgression occurred around 8 ka BP (Shennan et al., 2000), which constrains t in equation 3.2.

The effective diffusion coefficients of Cl, ^{2}H and ^{18}O and α were optimized to match observations using the non-linear parameter estimation program PEST (Doherty, 2002). Modelled curves for all parameters show good agreement with measured values (figures 3.4 and 3.5).

The optimized values of D_e are listed in table 3.3. Parameter covariances and correlation coefficients are listed in table 3.4. Table 3.3 also lists diffusion coefficients

Table 3.2: Initial and boundary conditions for the transport model at site 3. Initial values for δ^{2}H and δ^{18}O from Rozanski (1985).

Species	$z \geq 0,\ t = 0$	$z = 0,\ t > 0$	$z = \infty,\ t > 0$
m_{Cl} [mmol/l]	0	566	0
δ^{37}Cl [‰]	0	0	0
δ^{2}H [‰]	−60	0	−60
δ^{18}O [‰]	−9	0	−9

in seawater (D_s). Direct comparison between D_e and D_s is not possible since the effective diffusion coefficients include the effects of tortuosity θ (but not porosity) as well as other effects and processes not included in the diffusion model. If tortuosity were the sole cause for the difference between D_e and D_s then its value would follow from the ratio

$$\theta^2 = \frac{D_s}{D_e} \tag{3.4}$$

and, assuming that the difference in effective porosity does not affect θ, should be equal for both Cl and H_2O. The ratio for H_2O (table 3.3) is well within the range of tortuosity values reported in the literature (Boudreau, 1997). The ratio for Cl, however, is higher. Evidently, this ion moves at a slower rate than would be expected from diffusion alone. This is also demonstrated by the slope of the observed-linear relation between δ^2H and Cl (figure 3.6), which is lower than the slope that would result from simple mixing (i.e., equal diffusion coefficients). A similar relation (not shown) exists for δ^{18}O vs. Cl. Moreover, the radial diffusion experiments showed that Cl has a lower effective porosity and diffusion coefficient than ^{18}O. The mobility of Cl and to a lesser extent ^{18}O, however, appears to be higher in the radial diffusion cells than in the field.

The cause for this discrepancy is unclear. Using the high, experimentally-found values of D_e for Cl (table 3.1) in equation 3.2 would require t to be set to $\sim$ 1 ka or $m_{\mathrm{Cl},i}$ to a negative value, which is highly unrealistic. Therefore, it is believed that the model assumptions are valid and that the difference between field- and experimentally-determined values of the diffusion coefficients must be attributed to experimental conditions that do not compare to the field conditions. Possible causes include cracking of the core due to desiccation during storage or the low pressure at which the test was conducted ($\sim 10^5$ Pa) compared to the in situ pressure below the seafloor ($\sim 5\ 10^5$ Pa). Furthermore, anisotropy could play a role as the field data yield a diffusion coefficient in the vertical direction, whereas diffusion in the radial diffusion cells was predominantly horizontal. Studies have shown that diffusion parallel to bedding planes can be up to 6 times faster (L. van Loon, personal communication), but no material was available to quantify this effect for the Brown

Table 3.3: Optimized effective diffusion coefficients of Cl, ^{2}H and ^{18}O for Brown Bank sediments and diffusion coefficients in free solution. Right column shows the ratio between the two.

Parameter	D_e	95 % confidence limits		D_s [m^2/s]	D_s/D_e
	[m^2/s]	Lower	Upper		
Cl	$5.1\ 10^{-11}$	$4.6\ 10^{-11}$	$5.6\ 10^{-11}$	$1.3\ 10^{-9a}$	25.5
^{2}H	$3.7\ 10^{-10}$	$-1.0\ 10^{-9}$	$1.8\ 10^{-9}$	$1.6\ 10^{-9b}$	4.3
^{18}O	$6.7\ 10^{-10}$	$-2.2\ 10^{-8}$	$2.4\ 10^{-8}$	$1.8 - 2.4\ 10^{-9c}$	3.1

a = Value in seawater at 10 °C (Schulz and Zabel, 2000); b = value in distilled water (Wang et al., 1953); c = range for distilled water to Dead Sea brine at 22 °C (Yechieli and Ronen, 1996).

Bank clay.

Comparison of values of D_e for Brown Bank sediments (table 3.3) with various low-permeability deposits reported in the literature (table 3.5) shows that D_e of Cl from the present study is extremely low. The optimized value of $\alpha = 1.0012 \pm 0.0268$ is on the lower end of the range of values reported in the literature (1.0012 - 1.0030, Groen, 2002).

The relative immobility of Cl is not easily explained. Effects of upward flow or erosion can be discarded since these would affect D_e of both H_2O and Cl to the same degree. Further, only a minor effect of anion exclusion is expected. With this process, the negatively-charged Cl ion is unable to pass the pores when the negative potentials that extend from the charged surface of clay particles into the adjacent pore water overlap, whereas the uncharged H_2O remains unaffected. The process becomes ineffective at seawater concentrations, however, because the distance over which the negative potential extends into the pores rapidly decreases with ionic strength. This seems to be confirmed by measurements of the effective porosity of Cl (table 3.1), which is only slightly lower than gravimetric (i.e. total) porosity, indicating that the larger part of the pore space is accessible to Cl. Alternatively, pore geometry could limit transport of Cl when the pore radii approach the hydrated radius of the Cl ion (Halamickova et al., 1995). It may be speculated that strong weathering, which caused dehydration and gave the clay its stiffness (Laban, 1995), is responsible for the low diffusion coefficient of Cl.

3.5 Discussion and conclusions

The observed decrease of salinity with depth in the pore waters of the Brown Bank formation in the southern North Sea indicates that brackish water occurrences have

Table 3.4: Parameter covariance and correlation matrices for optimized effective diffusion coefficients of Cl (D_e), ^{2}H (^2D_e) and ^{18}O ($^{18}D_e$) and α.

Parameter	Covariance			
	D_e	^2D_e	$^{18}D_e$	α
D_e	$6.7\ 10^{-24}$	$1.3\ 10^{-16}$	$1.0\ 10^{-37}$	$1.7\ 10^{-35}$
^2D_e	$1.3\ 10^{-16}$	$1.8\ 10^{-4}$	$6.9\ 10^{-31}$	$3.6\ 10^{-28}$
$^{18}D_e$	$1.0\ 10^{-37}$	$6.9\ 10^{-31}$	$4.9\ 10^{-19}$	$2.2\ 10^{-34}$
α	$1.7\ 10^{-35}$	$3.6\ 10^{-28}$	$2.2\ 10^{-34}$	$1.3\ 10^{-16}$
	Correlation coefficient			
	D_e	^2D_e	$^{18}D_e$	α
D_e	1	$3.7\ 10^{-3}$	$5.6\ 10^{-17}$	$5.7\ 10^{-16}$
^2D_e	$3.7\ 10^{-3}$	1	$7.4\ 10^{-20}$	$2.4\ 10^{-18}$
$^{18}D_e$	$5.6\ 10^{-17}$	$7.4\ 10^{-20}$	1	$2.7\ 10^{-17}$
α	$5.7\ 10^{-16}$	$2.4\ 10^{-18}$	$2.7\ 10^{-17}$	1

potentially been preserved below this formerly-exposed area. The pore water composition still reflects the presence of meteoric water dating from the Weichselian glacial stage. No samples could be obtained from the permeable sand layer below the clay. From the shape of the salinity profile within the clay, however, it is expected that these also contains brackish water. The lateral extent of such a brackish water occurrence is likely limited by the extent of the overlying clay deposits.

The dominant transport process in the clay is diffusion. Modelling of this process satisfactorily describes the overall distribution of solutes and isotopic species, but superimposed deviations from the idealized profile remain, which are difficult to explain.

Both field data and radial diffusion experiments show that Cl is less mobile compared to H_2O. The optimized effective diffusion coefficient of ^2H and ^{18}O includes the effect of tortuosity whereas the optimized effective diffusion coefficient of Cl includes additional effects, possibly related to extremely small pore sizes. The observed discrepancy between diffusion coefficients based on field observations and those obtained from radial-diffusion experiments is attributed to deviation of the experimental conditions from field conditions.

This study shows the potential of pore water analyses for the reconstruction of former hydrologic conditions and transport properties of clay materials. Offshore locations are especially suitable because of the relatively-simple geologic history and absence of unknown man-made disturbances (e.g. groundwater abstraction, controlled water levels).

Table 3.5: Overview of effective diffusion coefficients reported in the literature. Listed values include effects of tortuosity but not porosity and are not normalized with respect to temperature.

Study	D_e [m^2/s] 10^{10}		Lithology
	Cl	H_2O	
Beekman, 1991	4.2		clay, silt, peat
Boisson et al., 2001		1.4^a	marl, argillite
Degueldre et al., 2003	2.6	5.2^b	clay
Desaulniers et al., 1981	3	3^b	clay, till
Desaulniers et al., 1986	6		till
Eggenkamp et al., 1994	13		
Groen et al., 2000b	7		clay
Hendry and Wassenaar, 1999; Hendry et al., 2000	1.5 – 2.1	1.7^c	clay, till
Johnson et al., 1989	4 – 6		till
Ortega-Guerrero et al., 1996	3 – 13		
Sjöberg et al., 1984	5		clay
Volker and Van der Molen, 1991	4.6 – 5.7		clay, silt, peat
Present study	0.51	$3.7 – 6.7^b$	dehydrated clay

$a = {}^3H$; $b = {}^2H$ and ^{18}O; $c = {}^2H$.

Chapter 4

Origin of hypersaline shallow groundwater

Abstract

Groundwater with a salinity exceeding that of seawater by as much as 50 % is found in the Dutch coastal plain up to a depth of 112 m below the surface. The isotopic composition (^{2}H, ^{18}O and ^{37}Cl) of this groundwater is studied to investigate the processes that led to its formation. Direct evaporation and transpiration of seawater by halophytes in a salt marsh are identified as the most likely mechanisms. Dissolution of salt crystals, salt secretion by plants and dry deposition may also play a role. These results show that evaporative concentration of seawater and the formation of hypersaline groundwater is not exclusively associated with arid climates. Freshening presumably started when the area was reclaimed from the sea. Modelling vertical transport of chlorine (^{35}Cl, ^{37}Cl), ^{2}H and ^{18}O in a shallow clay layer is used to estimate the original salinity. Diffusion is the dominant transport mechanism in the clay but best agreement with field data is only obtained by simulating a small downward flow rate. Especially chlorine isotope ratios prove to be sensitive to the magnitude of this rate.

4.1 Introduction

The coastal area of the Netherlands is a low-lying area that experienced several periods of inundation by seawater during the Holocene (Beets et al., 2003). Seawater entered the underlying aquifers and mixed with pristine fresh groundwater as a result of which large volumes of brackish ($8.5 < m_{\mathrm{Cl}} < 282$ mmol/l, where m_{Cl} is the Cl concentration) to saline ($282 < m_{\mathrm{Cl}} < 564$ mmol/l) groundwater are still encountered today (chapter 1).

Intrusion of seawater alone is not enough to explain, however, several accounts of Cl concentrations in groundwater that exceed that of seawater (figure 4.1). Such

This chapter is based on the paper: Post, V.E.A., Kooi, H., submitted to Water Resources Research. Origin of hypersaline shallow groundwater in the coastal area of the Netherlands.

hypersaline conditions ($m_{Cl} > 564$ mmol/l) have been encountered below the island of Texel (up to 672 mmol/l, L. Reiniers, personal communication), the island of Ameland (770 mmol/l, Csonka and Otte, 1985), near the city of Leiden ($m_{Cl} = 839$ mmol/l, De Ruiter, 1988) and below the province of Zeeland (up to 626 mmol/l, Ouwerkerk, 1993). The deepest occurrence is near the city of Leiden where a sample with $m_{Cl} = 578$ mmol/l was found at a depth of 112 m below mean sea level (Van Dongen and Boswinkel, 1982).

Rock salts that might dissolve do not occur in these areas. A contribution from anthropogenic sources (e.g. road salt Howard and Beck, 1993; Fabricius and Olofson, 1996) is not anticipated as the wells are located in areas where human activities are minimal or absent. Therefore, a different mechanism must have increased the salinity of the groundwater.

This chapter focuses on identification of the responsible process. Several potential mechanisms have been described in the literature. Reverse osmosis, or ultrafiltration, is the process whereby the salinity of groundwater increases upgradient of a clay or shale layer that acts a semi-permeable membrane. It has been put forward as an explanation of the origin of subsurface brines (Berry, 1967; Fleischer et al., 1977; Graf, 1982) and has been suggested to operate in aquifers (Phillips et al., 1986). Freezing of saline groundwater leads to an increase of the salt concentration in the unfrozen parts and could explain brine formation, in particular in areas of permafrost (Herut et al., 1990; Bein and Arad, 1992; Bottomley et al., 1999). In semi-arid areas, evaporation often leads to high salt concentrations in surface waters (Ortega-Guerrero et al., 1996; Drever, 1997), which results in salinization of underlying aquifers by diffusion or convective flow (e.g. Fan et al., 1997; Wooding et al., 1997a). During the present study, Jørgensen (2002) presented a case of shallow (< 3 m below the surface) groundwater in Denmark that is up to five times more concentrated than seawater. The elevated salinity was attributed to transpiration of seawater by halophytic plants. Finally, groundwater salinity can be increased by washing down of salts deposited at the surface, such as aerosols (Stuyfzand, 1993).

Here the results are presented of a detailed study of the composition of hypersaline groundwater below the island of Texel. Both chemical (chloride) and isotopic (^{2}H, ^{18}O, ^{37}Cl) data are used to evaluate the potential of each of the aforementioned processes in explaining observed salinities.

4.2 Physical setting

The island of Texel in the northwestern part of the Netherlands is bordered by the North Sea and the Wadden Sea. It has a surface area of 160 km^2 and consists of three morphological units: (1) a remnant of a moraine near the village of Den Burg (elevation $\sim$ 15 m above mean sea level), (2) a 2 km wide strip of dunes along the northwestern coastline (elevation up to 25 m above mean sea level) and (3) a polder area (elevation down to -1 m above mean sea level), which covers the larger part of

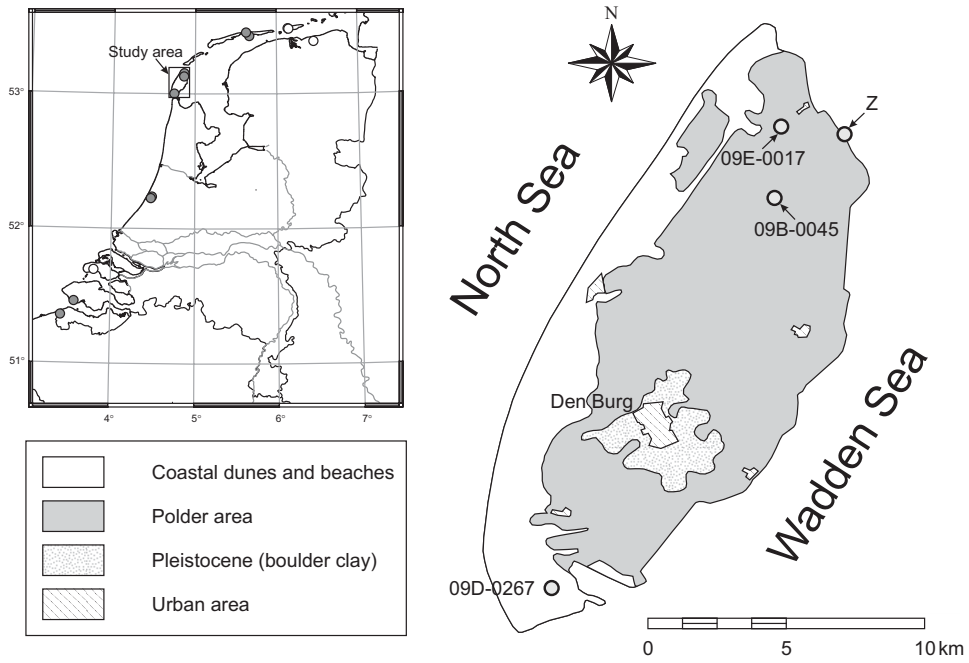

Figure 4.1: Map of Texel showing three main morphological units and sampled observations wells. Numbers are indicated for wells with hypersaline groundwater. Inset shows a map of the Netherlands with known (gray circles) and inferred (from isotopes, white circles) occurrences of hypersaline groundwater.

the island (figure 4.1).

The stratigraphic sequence in the upper 300 m of the subsurface consists mainly of Pleistocene fluvial sand and clay, underlain by fine-grained marine strata. The top of a heavy, lacustrine clay (locally known as 'Pot-clay') is found at depths of 40 to 80 m below sea level. These sediments locally reach a thickness of over 30 m in former subglacial valleys dating from the Elsterian glacial stage (380 – 360 ka BP). Boulder clay that formed during the Saalian glacial (180 – 130 ka BP) outcrops in the aforementioned relic moraine. In other parts of the island, the top of these deposits is found up to 50 m below sea level. Holocene sediments are found at the surface and consist mainly of lagoonal sand or clay and peat.

When sea level rose during the Holocene, only the northwestern part of the island was flooded around 5.3 ka BP (Zagwijn, 1986). Marine influence decreased again when a barrier island developed and peat could start to grow. The southern part of the island remained relatively high above sea level at that time so that peat growth was hampered here. Renewed marine incursions occurred on the northern

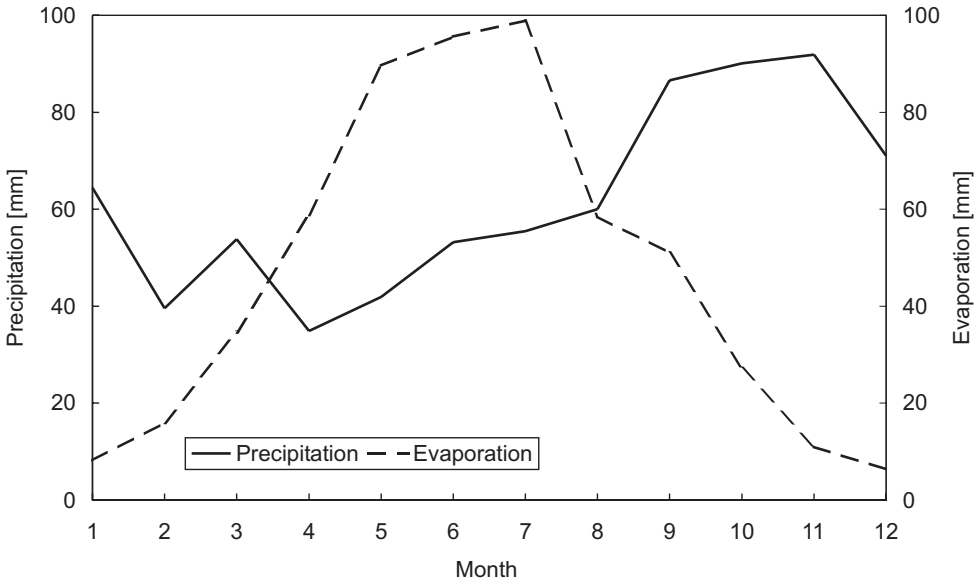

Figure 4.2: Monthly sums of precipitation and evaporation (average 1971 - 2000) at De Kooy, 6 km south of Texel.

part of the island and from 3 ka BP onward tidal flats were established. Peat bogs were then also present at the southern tip of the island but were flooded by the sea around 1.5 ka BP and the landscape turned into a salt marsh environment. Only the relic moraine near Den Burg remained above sea level throughout the entire Holocene. Around 0.4 ka BP, two small islands were present, which were separated by tidal flats and channels. Gradually, man reclaimed the salt marshes bordering these islands, giving the island its present form.

The highest groundwater levels are found in the coastal dunes and the remnant of the moraine near Den Burg. Groundwater levels are generally below sea level in the polder area. The demand for drinking water is covered by supply from the mainland through a pipeline. The only major use of groundwater resources is near Den Burg (figure 4.1) where approximately-equal volumes are abstracted and injected below the boulder clay at a depth of 20 to 25 m below mean sea level. Groundwater abstraction from the coastal dunes on the southern tip of the island started in 1956 but was discontinued in 1991.

The average amount of precipitation varies from 740 to 800 mm/y between the three measuring stations at Texel. Evaporation is measured at De Kooy on the mainland 6 km south of Texel and amounts to 592 mm/y (average over 1971 – 2000, expressed as Makkink reference evaporation). During summer months, evaporation exceeds precipitation (figure 4.2).

4.3 Measurements

4.3.1 Methods

In February 2002, 22 groundwater samples were taken from observation wells (figure 4.1). A seawater sample was taken as well. All wells consisted of PVC pipes with a diameter of 2.54 cm and a 1 m screen at the lower end. Prior to sampling, a volume of groundwater equal to three times the volume of the well was abstracted using a centrifugal pump. The actual sample was taken using a peristaltic pump. Samples were stored in PE bottles (100 ml non-acidified, 50 ml acidified with 65 % HNO_3) for major ion chemistry and glass bottles (30 ml) with a polypropylene cap for isotope (^{2}H, ^{18}O, ^{37}Cl) analyses. Electrical conductivity (EC), temperature, pH and alkalinity were measured in the field.

Fifty meters north of well 09B-0045, a 5.2 m sequence of Holocene sediments was cored using a manual rig. The lower 3.9 m of the core consisted of clay that was cut into pieces of 20 cm and stored in airtight PE bags. In the laboratory, these clay samples were centrifuged at 4 000 rpm for 1 h the next day to extract the pore water that was stored in glass bottles. The amount of pore water obtained varied between 1 and 13 % of the weight of the soil sample. The pore water samples were analysed for Cl and 8 samples were analysed for the isotopes ^{2}H, ^{18}O, ^{37}Cl.

The accuracy of the δ^2H and δ^{18}O measurements (expressed relative to V-SMOW, Vienna Standard Mean Ocean Water) amounts to 2 ‰ and 0.1 ‰ respectively. δ^{37}Cl (expressed relative to SMOC, Standard Mean Ocean Chloride) was measured following the procedures described by Eggenkamp (1994). The repro-

Table 4.1: Chloride concentrations measured in observation wells 09E-0017, 09B-0045 and 09D-0267 during previous years and the present study. Old data by courtesy of L. Reiniers, Province of Noord-Holland.

Well	Depth [m]	Cl [mmol/l]	
		06-09-1989	04-03-2002
09B-0045	6.8	439	407
	18.8	672	625
	29.8	560	527
	50.8	571	544
09D-0267	9.7	448[a]	
	25.2	491[a]	424
	38.7	615[a]	607
	56.7	581[a]	522
	67.7	592[a]	560
09E-0017	3.5	600	
	21.6	485	406
	28.1	435	491

a = Sampling date 7-12-1993.

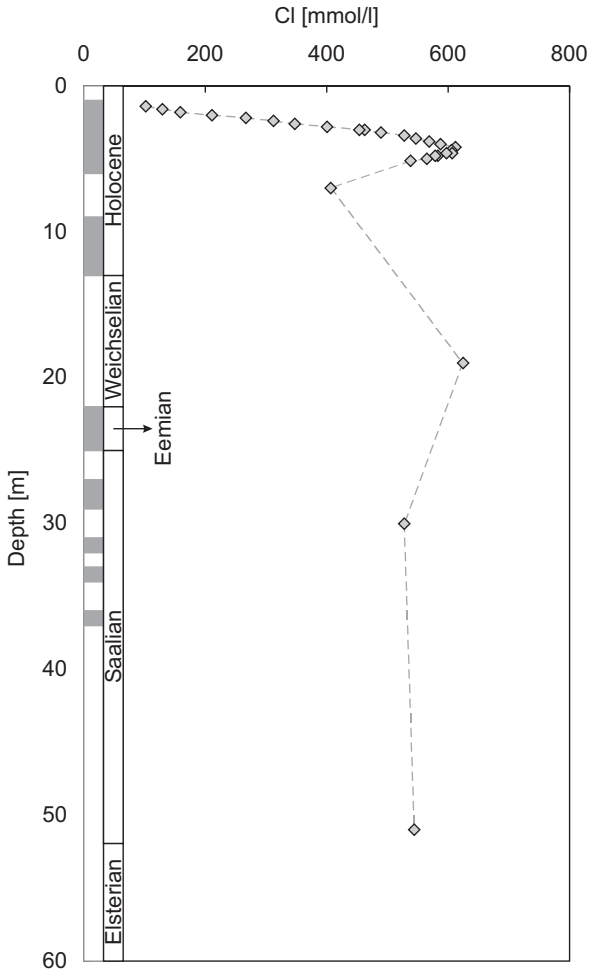

Figure 4.3: Graph of the observed Cl concentration vs. depth in well 09B-0045. Shaded areas in the left column indicate low-permeability sediments (mainly clay), white areas represent sand. Right column shows chronostratigraphy.

ducibility of the analyses was generally better than 0.1 % , although some samples could only be determined within 0.2 % accuracy due to analytical difficulties.

4.3.2 Results

In table 4.1 the Cl concentrations are presented for wells 09B-0045, 09D-0267 and 09E-0017. The highest Cl concentrations that have been encountered in the present

study ($m_{Cl} = 625$ mmol/l) are 50 % higher than seawater presently found near the coast ($m_{Cl} = 413$ mmol/l). The Cl concentrations that were measured in wells 09B-0045 and 09D-0267 are somewhat lower than in previous years. No sample was taken from the uppermost screen of well 09E-0017 because EC continued to increase during pumping. Apparently, the well screen is positioned near the interface between fresh and saline groundwater that has presumably moved downward since the well was sampled in 1989.

The stratigraphy of well 09B-0045 is depicted in figure 4.3. The layer from which the pore water samples were taken is found between 1.3 to 5.2 m below the surface and consists of gray, calcite-rich clay with a very low silt content. Fine sand is found above the clay layer, the underlying sequence consists of an alternation of sand and clay layers. Up to a depth of 13 m, sediments are of Holocene age (TNO-NITG, unpublished data).

The vertical distribution of Cl in the pore water samples from the clay layer shows that hypersaline water occurs in the lower part of the clay layer, between 3.8 and 4.8 m below the surface (figure 4.4). Cl concentrations steadily decrease from the maximum value ($m_{Cl} = 612$ mmol/l) at 4.2 m towards $m_{Cl} = 100$ mmol/l at the top and $m_{Cl} = 538$ mmol/l at the bottom of the clay layer. Similar patterns are observed for δ^2H, δ^{18}O, and δ^{37}Cl (cf. figure 4.4). In the aquifers below the clay layer, hypersaline water is found between Holocene and Eemian marine clay (figure 4.3).

The pore water samples plot along a straight line in a δ^2H vs. Cl or δ^{18}O vs. Cl plot (figure 4.5). The intercept with the vertical axis ($m_{Cl} = 0$ mmol/l) is found at $\delta^2\text{H} = -40.2$ ‰ and at $\delta^{18}\text{O} = -6.37$ ‰ (table 4.2). This is close to the mean isotopic composition of precipitation at De Kooy that has $\delta^{18}\text{O} = -7.24$ ‰ and $\delta^2\text{H} = -47.32$ ‰ (IAEA/WMO, 2001).

Groundwater samples plot between the mixing line of meteoric and seawater ($m_{Cl} = 566$ mmol/l, $\delta^2\text{H} = \delta^{18}\text{O} = 0$ ‰) and the regression line based on the pore water data in the δ^2H vs. Cl and δ^{18}O vs. Cl plots (figure 4.5). In the δ^2H vs. δ^{18}O plot (figure 4.6), both the pore water and the groundwater samples lie below the local meteoric water line (LWML). Statistically, the slopes of the regression lines

Table 4.2: Slopes and intercepts of the regression lines in figures 4.5 and 4.6.

Regression line	n	R^2	95 % confidence limits			
			Slope		Intercept	
			Lower	Upper	Lower	Upper
$\delta^{18}\text{O} = 0.0062 m_{Cl} - 6.37$	7	1.00	0.0058	0.0065	−6.53	−6.20
$\delta^2\text{H} = 0.0313 m_{Cl} - 40.2$	6	0.97	0.0243	0.0383	−43.1	−37.2
$\delta^2\text{H} = 5.18\delta^{18}\text{O} - 7.4^a$	6	0.98	4.26	6.09	−11.3	3.5
$\delta^2\text{H} = 6.34\delta^{18}\text{O} - 5.7^b$	12	0.83	4.35	8.34	−9.9	−1.6

a = pore water samples; b groundwater samples.

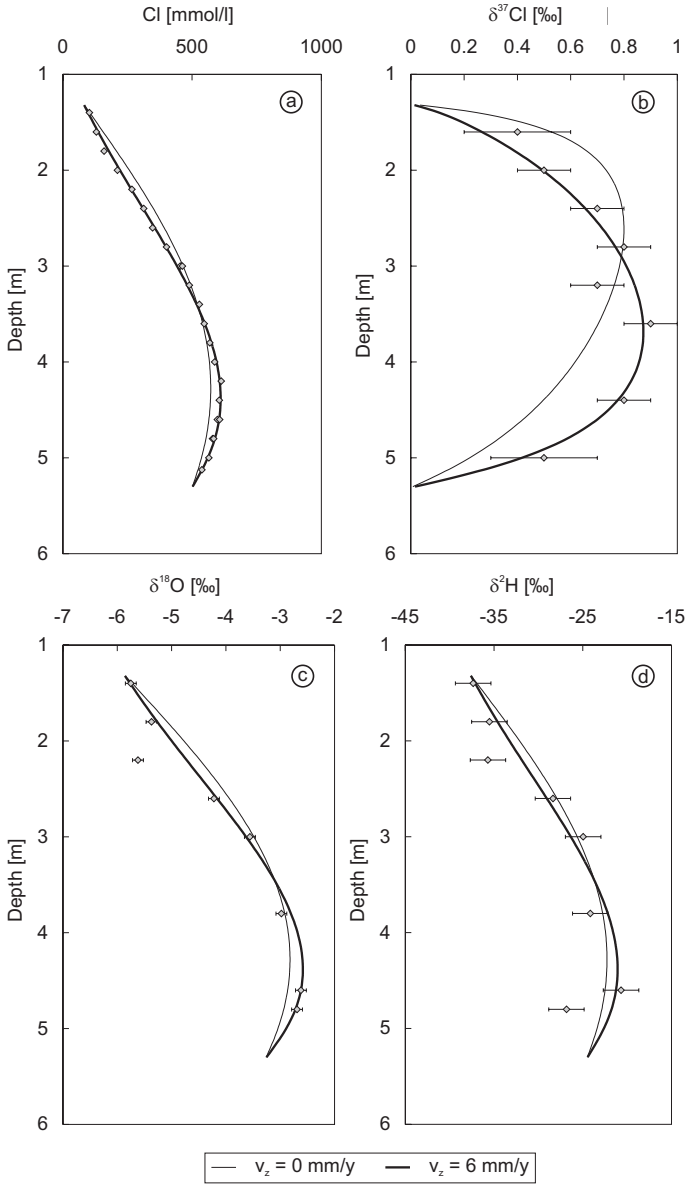

Figure 4.4: Graphs of the observed (diamond symbols) and modelled (a) Cl concentration, (b) δ^{37}Cl, (c) δ^{18}O and (d) δ^{2}H vs. depth in the clay layer near well 09B-0045. The model scenario for $D_e = 4.2\ \ 10^{-10}$ m^2/s without vertical flow (thin line) and with vertical flow (thick line) are shown.

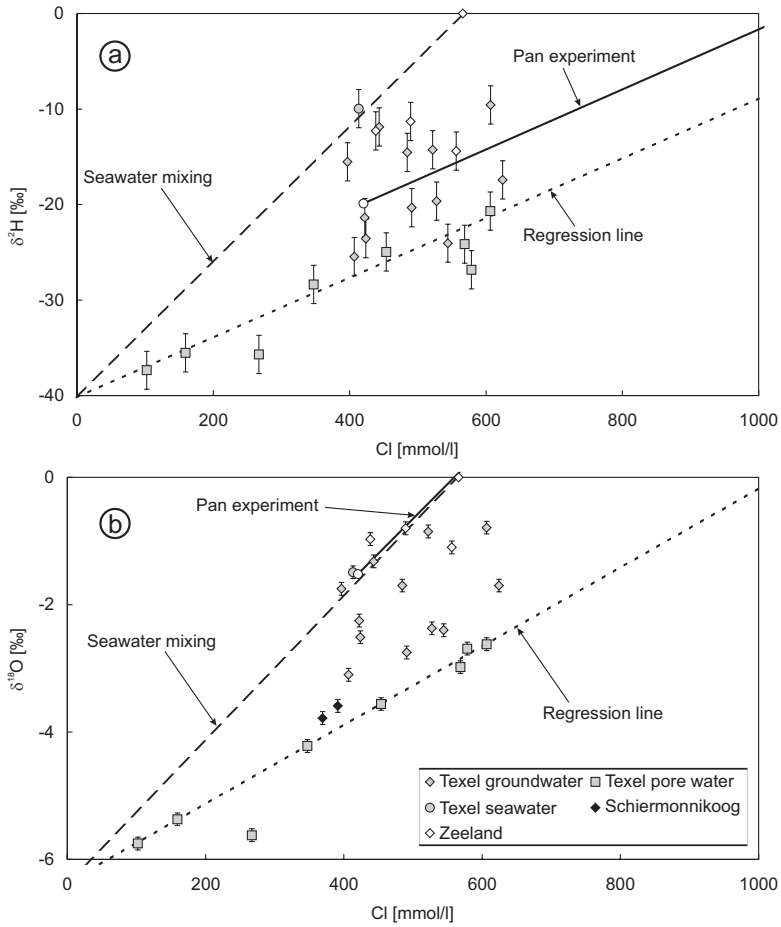

Figure 4.5: Graphs of (a) δ^2H vs. Cl concentration of water samples from Texel and Zeeland and (b) δ^{18}O vs. Cl concentration of water samples from Texel, Schiermonnikoog and Zeeland. Dashed line represent mixing of seawater ($m_{\mathrm{Cl}} = 566$ mmol/l, $\delta^{18}\mathrm{O} = \delta^2\mathrm{H} = 0$ %) and local meteoric water ($\delta^{18}\mathrm{O} = -6.37$ % , $\delta^2\mathrm{H} = -40.2$ %), dotted line is the regression line based on pore water samples (table 4.2).

through the pore water samples and groundwater samples do not differ significantly (table 4.2).

For comparison, data from the island of Schiermonnikoog (CIO, unpublished data) and Zeeland have been plotted as well (figure 4.5). The two saline samples from Schiermonnikoog and one sample from Zeeland have the same characteristics as the Texel data, which possibly indicates that they underwent the same evolution.

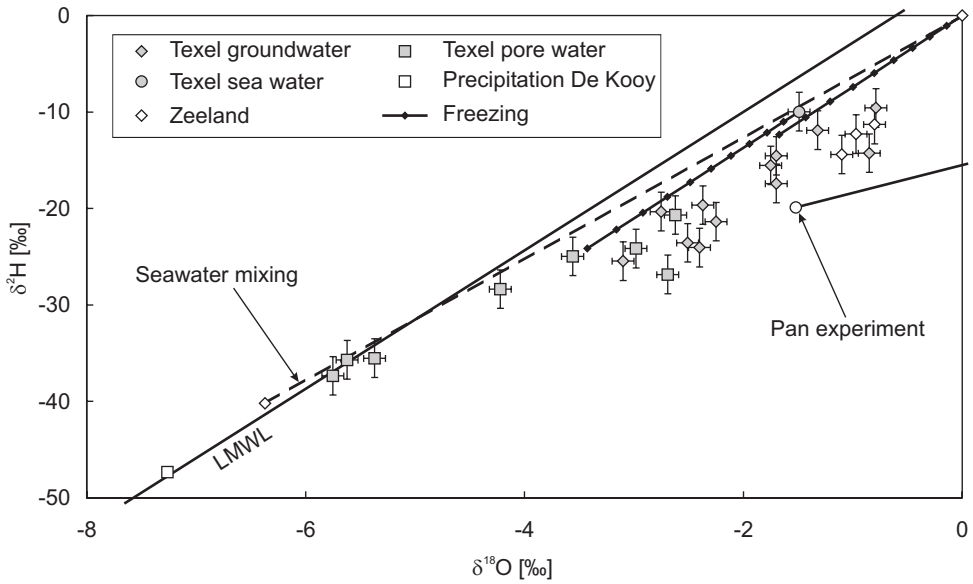

Figure 4.6: Graph of δ^2H vs. δ^{18}O of water samples from Texel and Zeeland. Dashed line represent mixing of seawater ($\delta^{18}\mathrm{O} = \delta^2\mathrm{H} = 0$ ‰) and local meteoric water ($\delta^{18}\mathrm{O} = -6.37$ ‰ , $\delta^2\mathrm{H} = -40.2$ ‰). Solid lines with diamond symbols indicate theoretical change in composition due to seawater freezing for an initial seawater isotopic composition of $\delta^{18}\mathrm{O} = -1.49$ ‰ , $\delta^2\mathrm{H} = -10.0$ ‰ (measured) and $\delta^{18}\mathrm{O} = \delta^2\mathrm{H} = 0$ ‰ (standard mean ocean water), where the diamond markers indicate the fraction of frozen seawater with an interval of 0.05. The direction into which the isotopic composition of seawater would evolve due to direct evaporation is also indicated (pan experiment by Jørgensen, 2002).

4.4 Analysis

4.4.1 Concentration of solutes

Ultrafiltration

Groundwater flow across a clay layer that acts as semi-permeable membrane causes enrichment of dissolved salts on the inflow side, a process often referred to as ultrafiltration or reverse osmosis. The osmotic efficiency of the clay layer is expressed by the reflection coefficient (σ) which varies between 1 for ideal membranes and 0 for clay having no membrane properties. The difference between the concentration at the upgradient interface of the membrane (m_0) and in the aquifer some distance away (m_i), causes a diffusive flux that opposes the advective flux of solute towards the clay layer (figure 4.7). It follows from mass balance considerations that, in a steady-state system, the concentration of the water exiting the clay layer at the

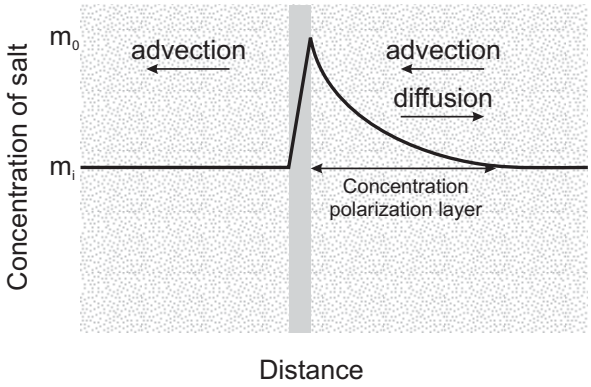

Figure 4.7: Schematic diagram of salt concentrations across a semi-permeable membrane (modified from Fritz and Marine, 1983). Arrows indicate the direction of the advective and diffusive fluxes.

downgradient side equals m_{i}. In such a system, the reflection coefficient can be shown to be a function of m_0 and m_{i} (Fritz and Marine, 1983; Kooi et al., 2003):

$$\sigma = \frac{m_0 - m_{\mathrm{i}}}{m_0 + m_{\mathrm{i}}} \tag{4.1}$$

The activity of water at the more concentrated (upgradient) side is lower than at the more dilute (downgradient) side, due to which a pressure $\Delta\Pi$ develops that opposes the hydraulic pressure. Advective transport only occurs across the clay layer when:

$$\Delta P > \sigma \Delta\Pi \tag{4.2}$$

where ΔP and $\Delta\Pi$ denote the hydraulic and osmotic pressure [Pa], respectively (Fritz and Marine, 1983). The latter is calculated from:

$$\Delta\Pi = vRT(m_0 - m_{\mathrm{i}}) \tag{4.3}$$

where $v = 2$ for NaCl solution (Fritz and Marine, 1983), R is the gas constant [8.314 10^{-3} kJ/mol/K] and T is the absolute temperature [K]. Equation 4.1 was used to calculate the reflection coefficient a clay layer must possess to raise the salinity from seawater ($m_{\mathrm{i}} = 413$ mmol Cl/l) to the maximum salinity observed in the field ($m_0 = 625$ mmol Cl/l). The reflection coefficient obtained this way can be inserted into equation 4.2, which, combined with equation 4.3, yields an estimate of the hydraulic pressure that is needed to force the seawater through the clay. Using $m_0 = 625$ mmol Cl/l yields conservative numbers as concentrations measured during previous studies were higher (672 mmol Cl/l). It follows that a reflection coefficient of $\sigma = 0.2$ is needed to raise the Cl concentration from 413 to 625 mmol/l

and a hydraulic head difference of about 20 m is required to overcome osmotic pressure. The latter condition can certainly not be met in the field. Furthermore, the calculated $\sigma = 0.2$ is about 2 orders of magnitude greater than maximum values reported for natural membranes at similar ionic strength (Keijzer, 2000). Using $m_{\mathrm{i}} = 566$ mmol Cl/l (i.e., representative of an open marine environment) would require a head difference of 1.4 m but the calculated σ is lowered by merely a factor of 4. Therefore, it is concluded that the dissolved salt enrichment of the hypersaline groundwater was not caused by ultrafiltration.

Freezing

The changing isotopic composition of seawater due to freezing can be calculated by treating the process as a form of Rayleigh distillation. The ice that is formed has a higher ^{2}H and ^{18}O content and the remaining seawater becomes progressively depleted in the heavy isotopes (Yaqing et al., 2000). The equation that describes the isotopic composition of the remaining seawater is:

$$\delta_r = (1 + \delta_s) f^{(\alpha_{i/w} - 1)} - 1 \tag{4.4}$$

where δ_r is δ^2H or δ^{18}O of the remaining seawater, δ_s is δ^2H or δ^{18}O of the original seawater and $\alpha_{i/w}$ is the fractionation factor between water and ice. The latter was set to 1.0208 for ^{2}H and 1.0028 for ^{18}O (Suzuoki and Kumura, 1973).

Besides the present seawater composition, standard mean ocean water ($\delta^{18}\mathrm{O} = \delta^2\mathrm{H} = 0$ ‰) was considered as initial seawater composition to account for the higher salinity of the Wadden Sea in the past compared to that today (Van der Hoeven, 1982). Application of equation 4.4 shows that the shift in isotopic composition of the remaining seawater is approximately parallel to the mixing line between meteoric water and seawater (figure 4.6). The data points plot below the mixing line, however, so freezing of seawater does not appear to be a feasible mechanism to explain the occurrence of hypersaline groundwater.

Moreover, the hypersaline groundwater dates from the Holocene. Under the climatic conditions that prevailed during this period, freezing to some depth may have occurred in winter but thawing would follow in summer. It is unlikely that an ever-increasing part of the intruded seawater froze so that salinity could rise.

Evapotranspiration in a salt marsh environment

Hypersaline groundwater on the island of Texel is encountered in areas where salt marshes existed between 1.5 ka BP and the onset of large-scale land reclamation in the nineteenth century. Strong evapotranspiration in these settings during summer months (figure 4.2) leads to increased salt concentrations in soil water. Formation of salt crystals at the surface has been reported by Den Hartog (1958) in the Balgzand salt marsh, directly south of Texel. De Vries (1935) reported Cl concentrations of up to 808 mmol/l in the upper 10 cm of the soil along the shore of the mainland

south of Texel. Measurements were carried out in October, which shows that these high concentrations can persist even during months in which precipitation exceeds evaporation.

Jørgensen (2002) described a salt marsh environment on a small island in Denmark where hypersaline groundwater with Cl concentrations up to 2.1 mol/l occurs in a shallow aquifer. He postulated that formation of this hypersaline groundwater is via transpiration of seawater by halophytic plants after flooding events. Transpiration causes an increase in salinity without isotope fractionation (Clark and Fritz, 1997). Jørgensen (2002) further presented the results of a pan experiment in which local seawater was subject to direct evaporation. The result shows that formation of hypersaline groundwater by means of direct evaporation would result in a saline end member with enriched δ^2H and δ^{18}O values that plots below the local meteoric water line (figure 4.6). The outcome of this experiment can be considered representative for the island of Texel as its climatic conditions are comparable to those of Denmark.

The data presented here are in support of both direct evaporation and transpiration by plants.

In figure 4.6, groundwater and pore water samples with a high Cl concentration plot below the local meteoric water line and the mixing line of meteoric water ($\delta^{18}\mathrm{O} = -6.37$ ‰ , $\delta^2\mathrm{H} = -40.2$ ‰) and seawater ($\delta^{18}\mathrm{O} = \delta^2\mathrm{H} = 0$ ‰), which is indicative for direct evaporation as indicated by the results of the pan experiment by Jørgensen (2002). Direct evaporation is likely to occur in local depressions were seawater ponds after a flooding event (Van Huissteden and Van de Plassche, 1998).

If, however, direct evaporation were the sole mechanism that led to the formation of hypersaline groundwater, the regression lines in figure 4.5 and the lines that represent direct evaporation would intersect at some point. This is not the case and the hypersaline end member (that must be located on the regression line in figure 4.5), appears to have a higher Cl concentration than would follow from direct evaporation alone. This means that an additional increase of Cl has occurred that was not accompanied by isotopic fractionation (i.e., a shift parallel to the x-axis in figure 4.5).

As suggested by Jørgensen (2002), this might be the result of transpiration by halophytic plants. Furthermore, formation of salt crystals has been observed (Den Hartog, 1958) that could have been washed down after flooding events, which would also lead to a higher salinity without isotopic fractionation. This also holds for salt secretion by plants (Jørgensen, 2002) and dry deposition of sea salts (Stuyfzand, 1993). The data do not allow for quantification of the relative contribution of each individual process.

Like the island of Texel, the study area of Jørgensen (2002) has excess precipitation over evaporation, but flushing of the hypersaline groundwater by meteoric water is prevented because, due to its high density, the hypersaline water sits in depressions in the slightly-undulating aquifer base. The study by Jørgensen (2002) shows that seawater can become concentrated up to five times. Even the highest

concentrations encountered in the Netherlands ($m_{\mathrm{Cl}} = 839$ mmol/l, De Ruiter, 1988) can therefore be attributed to evaporative concentration. Higher concentrations are likely to have occurred in the Dutch coastal lowlands but have diminished due to redistribution and dilution.

4.4.2 Redistribution of solutes

Figures 4.3 and 4.4 show that the hypersaline pore water in the clay layer near well 09B-0045 underwent freshening as the concentrations decrease both towards the top and the bottom of the layer. Diluted hypersaline water is also present in the subjacent aquifers (inferred from the isotopic composition of the samples). The degree of flushing is highest in the sand layer directly below the clay. Apparently, infiltration of meteoric water takes place along preferential flow paths since otherwise, concentrations in the overlying clay layer could not have remained high. Freshening started 170 y ago when the area was reclaimed from the sea. As soon as inundations by seawater ceased, a fresh water lens presumably developed in the overlying sand layer.

One-dimensional transport of ^{35}Cl, ^{37}Cl, ^{2}H and ^{18}O in the clay layer was modelled numerically. The purpose was to estimate the original salinity of the clay before freshening started ($m_{\mathrm{Cl},i}$). A 4 m section of clay was considered. Transport was described by:

$$\frac{\partial m_{\mathrm{Cl}}}{\partial t} = -v_z \frac{\partial m_{\mathrm{Cl}}}{\partial z} + D \frac{\partial^2 m_{\mathrm{Cl}}}{\partial z^2} \tag{4.5}$$

where m_{Cl} is the Cl concentration in the pore water [mmol/l], t is time [s], v_z is the vertical seepage rate [m/s], z is depth below the surface [m] and D the effective dispersion coefficient [m^2/s]. Velocity-dependent dispersion was neglected since flow velocities are extremely low, as will be shown below, so that $D = D_e$, where D_e is the effective molecular diffusion coefficient that includes the effect of tortuosity but not porosity. Equation 4.5 was also used to describe transport of ^{2}H, ^{18}O and ^{37}Cl and was solved numerically using the mixing cell approach described by Appelo and Postma (1994) with a cell size of 0.02 m, subject to the boundary conditions in table 4.3.

Table 4.3: Boundary conditions for transport model of the clay layer near well 09B-0045. Values at $z = 5.3$ m varied linearly for $0 < t < 170$ y between the values at $t = 0$ and $t = 170$ y. Values of δ^2H and δ^{18}O based on regression lines based on pore water data (table 4.2).

Species	$z = 1.3$ m, $t \geq 0$	$z = 5.3$ m, $t = 170$ y
m_{Cl} [mmol/l]	80	500
δ^{37}Cl [‰]	0	0
δ^{2}H [‰]	−37.7	−24.5
δ^{18}O [‰]	−5.87	−3.27

Time was fixed at $t = 170$ y. Concentrations were specified both at the top and the bottom of the model. The concentration at the top was held constant during the entire simulation whereas the concentration at the bottom decreased linearly with time. This was done to account for the decreasing concentration in the underlying sand layer in which horizontal groundwater flow is assumed. Higher concentrations were used at the sand-clay interface than those observed further away in the adjacent sand layers in order to match the concentration at the bottom and top of the clay layer. Apparently horizontal flow above and below the clay layer is so small that the diffusive profile does not end abruptly at the boundaries of the clay layer but extends some distance into the adjacent sand units.

Due to its greater mass, ^{37}Cl has a slightly lower diffusion coefficient than ^{35}Cl (Eggenkamp, 1994):

$$\alpha = \frac{^{35}D_e}{^{37}D_e} > 1 \tag{4.6}$$

Because ^{35}Cl moves faster than does ^{37}Cl, the source zone becomes enriched with respect to the heavy isotope, which is clearly visible in the field data (positive δ^{37}Cl values, figure 4.4). The value of $^{35}D_e$ was varied from 4.2 10^{-10} m^2/s to 5.7 10^{-10} m^2/s, which represents the range for this type of Holocene sediment (Beekman, 1991; Volker and Van der Molen, 1991). It was assumed that ^{2}H and ^{18}O have the same diffusion coefficient as Cl.

The values of α and the Cl concentration of the pore water before freshening started ($m_{\mathrm{Cl},i}$) were optimized using the non-linear parameter estimation program PEST (Doherty, 2002). Both a scenario without vertical flow ($v_z = 0$ mm/y) and a scenario in which vertical flow was optimized were considered.

Figure 4.4 shows the modelled and observed isotopic composition and Cl concentration vs. depth in the clay layer for the simulation with $D_e = 4.2$ 10^{-10} m^2/s. A poor fit between modelled and observed values is observed for the model with diffusion only, especially for δ^{37}Cl. To obtain a fit with field data, a downward seepage velocity $v_z = 6$ mm/y is required. The sensitivity of the shape of the calculated δ^{37}Cl curve to the magnitude of the seepage velocity makes it a useful tracer for detecting such small flow rates.

The optimized parameter values for the model with $D_e = 4.2$ 10^{-10} m^2/s and vertical flow are listed in table 4.4. Parameter covariances and correlation coefficients

Table 4.4: Optimized values of v_z, $m_{\mathrm{Cl},i}$ and α for transport model of the clay layer near well 09B-0045 with $D_e = 4.2$ 10^{-10} m^2/s.

Parameter	Optimized	95 % confidence limits	
	value	*Lower*	*Upper*
v_z [mm/y]	6.0	5.5	6.4
$m_{\mathrm{Cl},i}$ [mmol/l]	1047	1023	1071
α [dimensionless]	1.0015	0.9925	1.0104

are listed in table 4.5. The optimized value of $m_{\mathrm{Cl},i}$ amount to $m_{\mathrm{Cl},i} = 1\,047$ mmol/l and $m_{\mathrm{Cl},i} = 1\,338$ mmol/l for the models with $D_e = 4.2\ 10^{-10}$ m^2/s and $D_e = 5.7\ 10^{-10}$ m^2/s, respectively. These outcomes suggest that seawater could have been concentrated up to a factor of three.

The isotopic composition of the sample from 51 m below sea level in well 09B-0045 ($m_{\mathrm{Cl}} = 544$ mmol/l) shows that it represents 'diluted hypersaline water', which means that evaporated seawater of late Holocene age was transported into the Pleistocene aquifer to at least this depth. Transport almost certainly occurred by free convection, a mechanism that has been advocated to be responsible for rapid salinization of Pleistocene aquifers elsewhere in the Netherlands during the Holocene transgressions (Van der Molen, 1989; Gieske, 1991, chapter 5).

4.5 Discussion and conclusions

Hypersaline groundwater occurs at several locations along the Dutch coast in the upper 112 m of the subsurface. Based on stable isotope and Cl concentrations of pore waters and groundwater on the island of Texel, direct evaporation and transpiration by halophytic plants in a former salt marsh is advocated as a likely means for the formation of this hypersaline groundwater. Dissolution of salt crystals, salt secretion by plants and dry deposition probably also contribute but the data do not allow for estimation of the relative contribution of each. The results presented here resemble those by Jørgensen (2002) in a contemporary salt marsh in Denmark. The difference with the case presented here is that the study by Jørgensen (2002) is for an active system, whereas on the island of Texel, the salt marshes have disappeared and redistribution and dilution of the hypersaline groundwater has taken place.

High salinities in groundwater due to evapotranspiration are usually associated with arid environments (e.g. sabkhas) but this study shows that they can also occur in more humid climates. As salt marshes were ubiquitous in many coastal zones during the Holocene, such as for example in the Netherlands (Zagwijn, 1986), it may be expected that evapotranspiration has contributed to the salinity of groundwater in many of such environments. Recognition of this process is often difficult, however, as dilution or mixing of the evaporated water with one or more other water types (precipitation, river water, seawater) blurs the original chemical and isotopic

Table 4.5: Parameter covariance and correlation matrices for optimized parameter values in table 4.4.

Parameter	Covariance			Correlation coefficient		
	v_z	$m_{\mathrm{Cl},i}$	α	v_z	$m_{\mathrm{Cl},i}$	α
v_z	$5.0\ 10^{-2}$	2.414	$1.9\ 10^{-6}$	1	0.9332	0.0019
$m_{\mathrm{Cl},i}$	2.414	135.6	$7.5\ 10^{-5}$	0.9332	1	0.0015
α	$1.9\ 10^{-6}$	$7.5\ 10^{-5}$	$2.0\ 10^{-5}$	0.0019	0.0015	1

fingerprint.

Modelling vertical transport of ^{35}Cl, ^{37}Cl, ^{2}H and ^{18}O in the Holocene clay layer near well 09B-0045 suggest that the hypersaline groundwater had a Cl concentration between approximately 1 and 1.4 mol/l before freshening started approximately 170 y ago. This implies that concentration by evapotranspiration resulted in a salinity increase up to a factor of three.

The observed vertical distribution of Cl in the clay layer and the subjacent sand also provides useful insight in the hydraulic properties of the Holocene deposits. It particularly highlights the importance of preferential flow, which contrasts with the often-applied assumption in modelling studies that the Holocene deposits form a single, homogeneous unit. The sensitivity of modelled $\delta^{37}Cl$ to the magnitude of the seepage velocity makes it a useful tracer for quantification of small flow rates.

Part III: numerical modelling

Chapter 5

Rates of salinization by free convection in high-permeability sediments

Abstract

Numerical modelling and dimensional analysis is used to study the salinization of thick, high-permeability aquifers by free convection from a salt source at the surface. Current understanding of this process mainly concerns the initial stages of salinization only (boundary layer development, break-up into fingers and initial phase of finger descent). In the modelling, special attention is paid to the role of two processes in the long-term salinization rate: (1) the progressive loss of dissolved salt from fingers by lateral diffusion and (2) the coalescence of fingers during their descent.

From the numerical simulations a relationship is derived that describes the development of the horizontally-averaged salinity with depth and time as a function of permeability and initial-density contrast for aquifer Rayleigh numbers up to $Ra = 6\,000$. This relationship is consistent with and provides an extension to previous generalized relationships of the rate of finger descent. Its applicability to real-world aquifers ($Ra > 10^5$) that include complexities due to anisotropy, heterogeneity, and mechanical dispersion is discussed. Application to the Pleistocene coastal aquifer of the Netherlands (thickness ~ 200 m, permeability $\sim 10^{-11}$ m^2) suggests that salinization of the aquifer during historic episodes of inundation by seawater occurred within decades.

5.1 Introduction

Many coastal areas around the world have experienced shifts in their coastline as a result of sea level changes on a geological timescale. Transgression (landward migration of the coastline in response to a relative sea level rise) can carry seawater

This chapter is based on the paper: Post, V.E.A., Kooi, H., accepted for publication in Hydrogeology Journal. Rates of salinization by free convection in high-permeability sediments: insights from numerical modelling and application to the Dutch coastal area.

on top of fresh groundwater, thereby producing an unstable density stratification, which can cause vertical seawater intrusion. In low-permeability strata, transport of dissolved salts proceeds slowly, primarily by diffusion, thus protecting the underlying fresh water from salinization for centuries to millennia (chapter 3). In the absence of such confining deposits, the unstable density stratification may give rise to free convection (fingering) whereby advective flow driven by density gradients results in a much more rapid salinization than in the case of diffusion.

Unstable fluid-density stratifications occur in many natural settings (Schincariol and Schwartz, 1990) and numerous studies have dealt with this subject (table 5.1). Research has mainly focused on laboratory experiments and numerical modelling. These studies have shown that initially a boundary layer develops by diffusion that becomes unstable when it reaches a certain critical thickness and then breaks up into fingers that descend to the aquifer bottom. Aspects that have been studied include the stability of the boundary layer (Wooding, 1962; Elder, 1968; Schincariol et al., 1994; Wooding et al., 1997a), the phase of finger descent (Wooding, 1969; Wooding et al., 1997b), and the coalescence of individual fingers (Bachmat and Elrick, 1970; Wooding et al., 1997b). Numerical models of free convection have been applied extensively for small-scale problems (e.g. Elder, 1967, 1968; Schincariol et al., 1994; Wooding et al., 1997a,b; Kolditz et al., 1998; Simmons et al., 1999; Ackerer et al., 2000; Oswald and Kinzelbach, 2000) but application to the aquifer scale (tens to hundreds of meters) is limited owing to the strict discretization requirements that apply (Kooi et al., 2000), in particular for high-permeability sediments.

Some valuable relationships have been obtained that can be used to predict aquifer salinization, such as for example the rate of descent of the individual salt fingers. Little is known, however, about the long-term salinization rates at the depth scale of coastal aquifers. Moreover, it is not a priori evident that rates for these initial stages are also applicable for long-term salinization. For example, expressions

Table 5.1: Aquifer Rayleigh numbers for simulations of free convection published in the literature.

Studies	*Ra*	Convection type	Remarks
Elder, 1967; Voss and Souza, 1987; Kolditz et al., 1998;			
Ackerer et al., 2000	400	free	Elder problem
Elder, 1968	1 600	free	
Koch, 1994		free	$\alpha_L = 1$ m, $\alpha_T = 0.1$ m
Schincariol et al., 1994, 1997		free/forced	$\alpha_L = 3\ \ 10^{-4}$ m
Simmons and Narayan, 1997		free/forced	$\alpha_L = 50$ m, $\alpha_T = 5$ m
Wooding et al., 1997b;			
Simmons et al., 1999	4 870	free/forced	Salt lake problem
Present study	6 000	free	
Wooding, 1969	$0.2 - 3.6\ \ 10^5$	free	Hele-Shaw cells
Oswald and Kinzelbach, 2000	$\sim 10^3$	free	Container experiment

for the rate of descent of salt fingers employ a constant density contrast between the plume and the ambient water, whereas during descent, the density contrast diminishes as a result of diffusion. It is to be expected that this progressive decrease in density contrast affects the long-term salinization rate. Also, coalescence of individual fingers has been observed in laboratory experiments (Bachmat and Elrick, 1970) and numerical simulations (Wooding et al., 1997b). The importance of this process for salinization rates is little understood.

This chapter reports on an attempt to gain more insight into the significance of diffusive mass loss and coalescence for long-term, large-scale salinization by free convection in high-permeability sediments. This was done by numerical modelling. Interest is not so much in the salinity patterns and salinization rate at the scale of individual fingers, but rather in spatially-averaged salinities and salinization rates, representative of large parts of the aquifer.

The model simulations reported here were carried out for a macroscopic Rayleigh number (Ra) of 6 000 , where the Ra is defined by:

$$Ra = \frac{\Delta\rho g k H}{\mu D} \tag{5.1}$$

where $\Delta\rho$ is the density contrast [kg/m^3], g is gravitational acceleration [m/s^2], k is intrinsic permeability [m^2], H is the height of the aquifer or model domain [m], μ is dynamic viscosity [kg/m/s] and D is a scalar measure of dispersion [m^2/s]. This value is still low compared to the laboratory experiments by Wooding (1969) but high compared to the classical Elder problem (table 5.1). Several numerical studies have worked with rather large values of H, but also incorporated large hydrodynamic dispersion, thereby maintaining relatively-low effective macroscopic Rayleigh numbers. The present numerical study does not include effects of hydrodynamic dispersion because (1) the theory of free convection in porous media has only been fully developed for homogeneous and isotropic dispersion and (2) it allows comparison with results from studies with Hele-Shaw cells. However, the role of hydrodynamic dispersion will be addressed in the discussion section at the end of this chapter.

5.2 Methodology

The numerical simulations were conducted using the 2D (vertical section) version of METROPOL-3, a finite-element, variable-density flow and transport code that solves two coupled non-linear partial differential equations for pressure and salt mass fraction (Sauter et al., 1993). The following mass-balance equations for liquid and solute were solved:

$$\frac{\partial(n\rho)}{\partial t} + \nabla\ (\rho q) = 0 \tag{5.2}$$

$$\frac{\partial(n\omega\rho)}{\partial t} + \nabla\ (\rho\omega q) + \nabla\ J = 0 \tag{5.3}$$

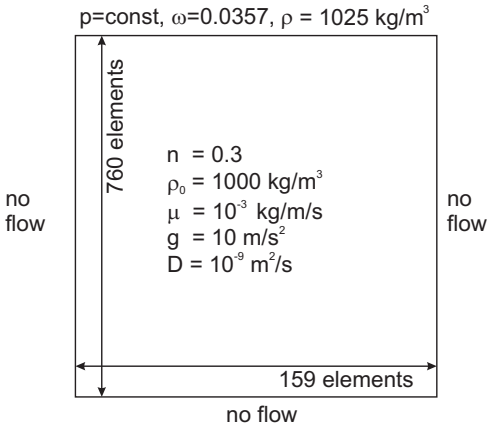

Figure 5.1: Geometry and boundary conditions for the numerical simulations. Parameter values that were constant for all simulations are also listed.

where n is porosity [dimensionless], ρ is the fluid density [kg/m^3], q is the Darcy velocity [m/s], ω is the salt mass fraction [dimensionless] and J is the diffusive flux [kg/s/m^2]. The Darcy velocity is written as:

$$q = -\frac{k}{\mu} \ (\nabla p + \rho g) \tag{5.4}$$

where k is the intrinsic permeability tensor [m^2], μ is the dynamic viscosity [kg/m/s], p is the fluid pressure [Pa] and g is the gravitational acceleration [m/s^2]. The diffusive flux is written as:

$$J = -\rho D_M \ \nabla\omega \tag{5.5}$$

where D_M is the molecular-diffusion coefficient [m^2/s].

The equations are non-linear because the fluid density ρ and dynamic viscosity μ depend on ω and coupling of the equations is through ρ and q. Here, μ was assumed constant and ρ dependent on salt mass fraction according to $\rho = \rho_0 e^{0.69\omega}$ (Leijnse, 1992). Fluid and pore compressibility were assumed negligible. METROPOL-3 uses the Galerkin weighted residual finite-element method to numerically solve the equations using fully-implicit time stepping with automatic time step control based on convergence criteria. For the non-linear pressure equations, this criterion is:

$$|\Delta p_{max}| \leq 10^{-5} + 10^{-5}|p| \tag{5.6}$$

where Δp_{max} is the largest change of p over two successive iterations. The same criterion is used for ω.

Figure 5.1 depicts the geometry and boundary conditions for the simulations. The left, bottom, and right sides were assigned a no-flow and a no-dispersive flux

boundary condition. The upper boundary was assigned a prescribed pressure and prescribed salt mass fraction, representative for a well-mixed body of overlying seawater. Initially, the entire model domain was filled with fresh water.

METROPOL-3 uses an Eulerian discretization method, so the mesh-Peclet condition restricts the element size to avoid spurious oscillations in the solute distribution:

$$\Delta z \leq \frac{2D_M}{|v_z n|} \tag{5.7}$$

where v_z is the vertical component of flow velocity [m/s], the dominant flow component in the free convection experiments.

Analysis of the physical properties that determine the characteristic velocity of the descending salt fingers in a porous medium shows that $v_z \sim \Delta\rho g k/\mu n$ (e.g. Gebhart et al., 1988, p. 822). Wooding (1969) carried out experiments using Hele-Shaw cells and an analysis of the suitably-weighted, horizontally-averaged transport equations and found the velocity to be approximately:

$$v_z = \frac{\Delta\rho g k}{4\mu n} \tag{5.8}$$

The same rate approximately applies to the ascending fresh water fingers. Equations 5.7 and 5.8 can be combined to obtain an initial estimate of the maximum element height.

In addition to the mesh-Peclet condition, the element size of models to simulate free convection is restricted by the critical thickness (δ_{cr}) of the boundary layer (the moment it becomes unstable) and the wavelength (λ_{cr}) of the fingers that develop (Kooi et al., 2000):

$$\Delta z < \left(\delta_{cr} = \frac{Ra^{\delta}_{cr}\mu D}{\Delta\rho g k}\right) \tag{5.9}$$

$$\Delta x < \left(1/8\lambda_{cr} = 2\delta_{cr} = \frac{2Ra^{\delta}_{cr}\mu D}{\Delta\rho g k}\right) \tag{5.10}$$

where Ra^{δ}_{cr} is the critical boundary layer Rayleigh number. The boundary layer Rayleigh number is defined as:

$$Ra^{\delta} = \frac{\Delta\rho g k \delta}{\mu D} \tag{5.11}$$

where δ is the thickness of the boundary layer at the seafloor, which grows with time due to diffusion. It can be seen from equations 5.9 and 5.10 and the combination of equations 5.7 and 5.8 that the size of the elements is inversely proportional to the permeability. For example, at a permeability of 10^{-11} m^2 (or a conductivity of approximately 10 m/d) and otherwise appropriate parameters for the case of seawater intrusion, the maximum element dimensions become in the order of millimeters. It then becomes immediately clear that even modelling a very small section

of a real-world aquifer requires an enormous computational effort that is practically impossible.

Since modelling free convection in real-world situations at high permeabilities is not feasible, the following approach was adopted in the present study. A series of numerical simulations were done for permeabilities that range from 1.16 10^{-16} to 1.16 10^{-11} m^2. For each simulation, corresponding to one permeability value, the mesh size (model domain) was chosen as large as the computational restrictions allowed. Subsequently, from the simulations, a general relationship was sought that describes how the salinization rate of the aquifer depends on permeability. Since the main focus was to study the progression of average salinity with depth, the problem was reduced to 1D by horizontally averaging the salt mass fractions of the 2D simulations:

$$\omega(z,t)_{avg} = \frac{\int_{x_0}^{x_{max}} \omega(x,z,t)dx}{x_{max} - x_0} \tag{5.12}$$

where integration is across the width of the model domain. By subsequently selecting a salt mass fraction, a "salinity front" can be defined. In this study the salinity front was defined as a certain fraction of seawater:

$$f_s = \frac{\omega_{front}}{\omega_{sea}} \tag{5.13}$$

That is, $f_s = 0.1$ means 10 % seawater. From the results of the simulations, the relationship between salinization rate and permeability was investigated as a function of f_s.

All models have a macroscopic Rayleigh number of 6 000 . Element size and hence the size of the model domain varied depending on permeability for the reasons explained above. The element height was determined using equations 5.7 and 5.8 to have a mesh-Peclet number of 2 (at the same time equation 5.9 is also satisfied); element width was set to twice the element height, following from equation 5.10. The number of elements was set to 159 in the horizontal direction to ensure the simulation of approximately 10 salt fingers and 760 in the vertical direction (figure 5.1).

To ensure that equations 5.7 to 5.10 warrant a proper resolution of the boundary layer and salt fingers, grid convergence was tested for the experiment with the highest permeability ($k = 1.16\ \ 10^{-11}$ m^2). A uniform mesh with Δz and Δx following from these equations was refined 2, 3, and 4 times. Additional runs were performed with Δz halved in the (1) 10 and (2) 20 topmost rows. The number of salt fingers varied non-systematically between 9 and 18 among these 12 test runs, which is attributed to random fluctuations in the numerical round off errors that trigger the initial instabilities. The finest mesh did not yield the highest number of salt fingers. Numerical dispersion must therefore be negligible. If it were not, its effect would decrease with decreasing element size and result in a larger number of fingers according to equation 5.10. Salinization rates are hardly affected. These results indicate that the applied discretization suffices.

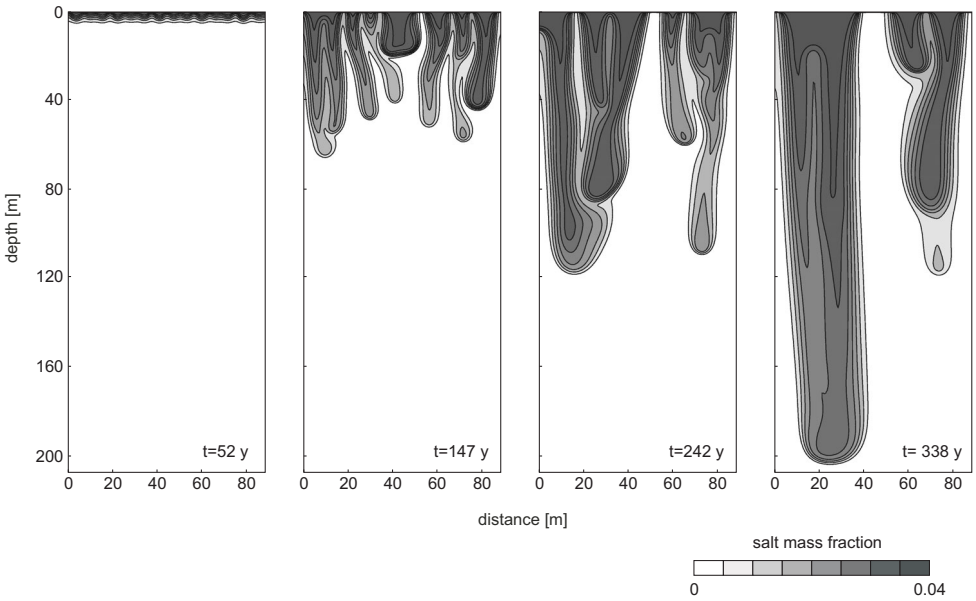

Figure 5.2: Salinization concentration patterns for simulation number 5 after 52, 147, 242, and 338 y.

The simulation time was chosen such that the fingers just reached the bottom of the model domain at the end of the simulations and ranged from 4.3 10^{-2} to 4.3 10^{8} y for the highest and lowest permeability, respectively. Parameters that were constant for all simulations are listed in figure 5.1.

Computations were carried out on a IBM RS/6000 SP with CPU times typically in the order of 20 h. Convergence of the non-linear equations was generally achieved after 2 or 3 iterations.

5.3 Results

Ten numerical simulations were carried out using the model setup described above with permeabilities ranging from 1.16 10^{-16} to 1.16 10^{-11} m^2 (table 5.2). Figure 5.2 shows the salinity pattern that developed for simulation number 5 (k = 1.16 10^{-13} m^2) after 52, 147, 242, and 338 y. After the break-up of the diffusive boundary layer, fingers of salt water descend to the bottom of the model and fresh water flows upward between them and discharges at the top. The coalescence of individual salt fingers can be observed as the number of fingers decreases from 14 at $t = 5$ y to 3 at $t = 338$ y. The horizontally-averaged concentrations (equation 5.12) for simulation 5 after 79 and 147 y are depicted in figure 5.3.

Table 5.2: Overview of numerical simulations. Calculated and normalized salinization velocities are listed for seawater fractions (f_s) = 0.1, 0.3, and 0.5, respectively.

Simulation	log(k)	Δz [m]	$\Delta\rho gk/\mu n$ [m/y]	Calculated salinization velocity [m/y]			Normalized salinization velocity		
				$f_s = 0.1$	$f_s = 0.3$	$f_s = 0.5$	$f_s = 0.1$	$f_s = 0.3$	$f_s = 0.5$
1	−10.94	0.002765	304	38.4	19.2	10.4	0.13	0.06	0.03
2	−11.94	0.02765	30.4	5.81	2.74	1.11	0.19	0.09	0.04
3	−12.09	0.0395	21.3	2.96	1.46	0.93	0.14	0.07	0.04
4	−12.33	0.0691	12.2	2.47	0.82	0.35	0.20	0.07	0.03
5	−12.94	0.2765	3.04	0.61	0.34	0.12	0.20	0.11	0.04
6	−13.09	0.395	2.13	0.33	0.20	0.10	0.16	0.09	0.05
7	−13.33	0.691	1.22	0.23	0.17	0.09	0.19	0.14	0.07
8	−13.94	2.765	0.304	0.046	0.024	0.009	0.15	0.08	0.03
9	−14.94	27.65	0.0304	0.0071	0.0048	0.0011	0.23	0.16	0.04
10	−15.94	276.5	0.00304	0.00058	0.00039	0.00025	0.19	0.13	0.08

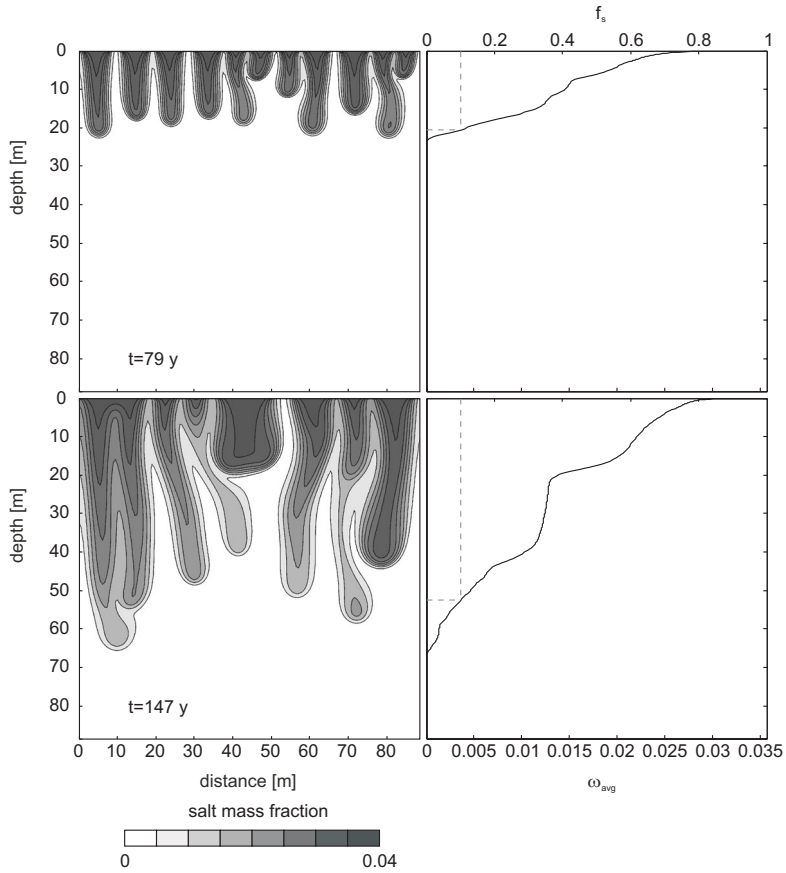

Figure 5.3: Salinization concentration patterns (left panels) and horizontally-averaged salt mass fraction vs. depth (right panels) for simulation number 5 after 79 and 147 y. The position of the salinity front $f_s = 0.1$ is indicated as an example.

Figures 5.4a and 5.4b show the depth and velocity of the salinity front $f_s = 0.1$ as a function of time for the simulations number 5 (the simulation of figures 5.2 and 5.3) and number 8 ($k = 1.16\ \ 10^{-14}$ m^2) respectively. A number of phases can be distinguished: (1) slow progression of the front during growth of the diffusive-boundary layer, (2) acceleration of the front when the boundary layer breaks up, (3) approximately-linear descent of the front with superimposed velocity variations with a factor of about 2 and (4) decreasing front velocity at the end of the simulation as the plumes reach the bottom of the model domain. The same general behaviour was observed for the other simulations.

The mean front velocity (v) during phase 3 was determined by fitting a straight

line through the time-depth data (figures 5.4a and 5.4b). Table 5.2 shows the calculated velocities and also the velocities normalized by $\Delta\rho gk/\mu n$. The scatter may be partly due to the fact that the number of fingers during the final stages of the simulations is rather small (= 3), which does not always allow a 'sharp' front to be defined (figure 5.4b).

The normalized salinization velocities are plotted as a function of f_s in figure 5.5, which shows that despite the scatter in the data there is a distinct relationship between normalized front velocity and f_s. Based on regression analysis of the 60 calculated front velocities, an empirical relationship was found that describes the front velocity as a function of permeability (k) and f_s during the phase of descent of the salt fingers:

$$v = \frac{\Delta\rho gk}{\mu n}(0.20f_s^2 - 0.45f_s + 0.22) \tag{5.14}$$

This relationship shows the expected dependency of f_s on the characteristic velocity $\Delta\rho gk/\mu n$. The significance of the equation largely resides in the fact that it relates the proportionality constant to the degree of salinization.

5.4 Discussion

5.4.1 Variations of salinity front velocity

Although the depth of a front increases approximately linearly with time, a pronounced deceleration during the initial phase of plume descent can be observed in all the models (figure 5.4). This is probably caused by the fact that during their descent, the fingers lose dissolved salt by lateral diffusion. Hence, as time progresses, the density contrast between the plume and the surrounding fresh water becomes smaller. An idea of how this process depends on permeability can be gained by comparing the timescales associated with advective and diffusive transport. The time needed for the salt plume to reach a given depth Z is approximately:

$$T_{adv} = Z/v_z \sim \frac{Z\mu n}{\Delta\rho gk} \tag{5.15}$$

A timescale of diffusive salt loss can be obtained as follows. The characteristic width ($1/2\lambda$) of fingers that emanate from a saline diffusive boundary layer at the seafloor is:

$$1/2\lambda \sim \frac{Ra_{cr}^{\delta}\mu D}{\Delta\rho gk} \tag{5.16}$$

An effective timescale for diffusion can now be defined as:

$$T_{diff} = \frac{(1/4\lambda)^2}{D} \sim \frac{(Ra_{cr}^{\delta})^2\mu^2 D}{4\Delta\rho^2 g^2 k^2} \tag{5.17}$$

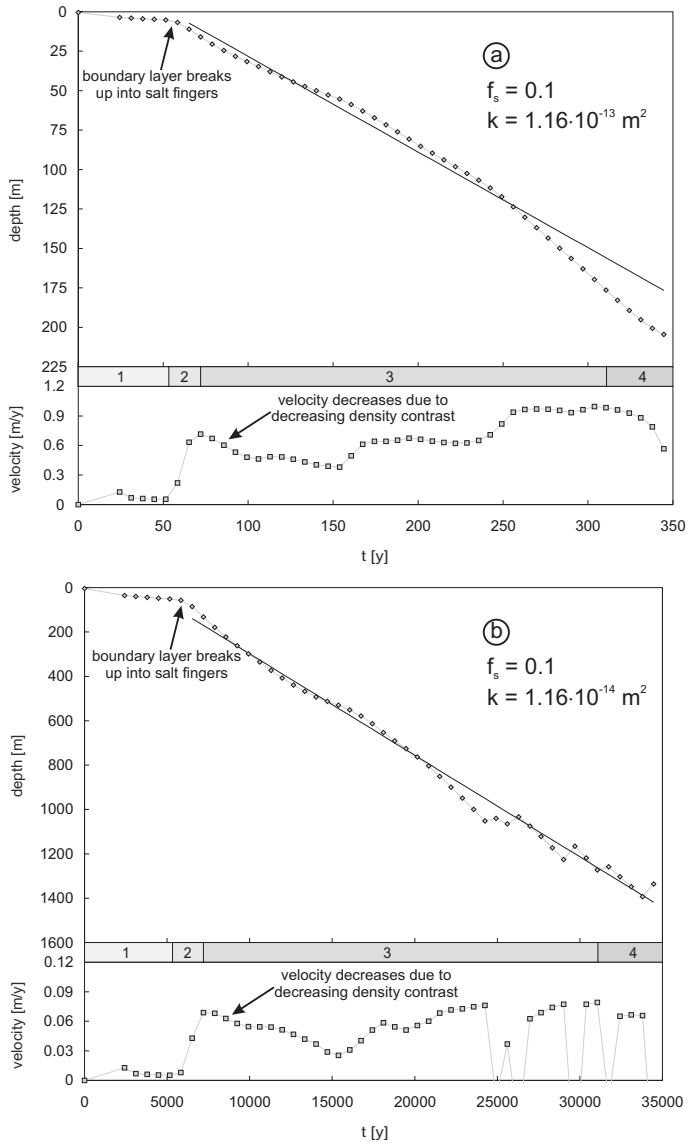

Figure 5.4: Graphs of depth (diamond symbols) and velocity (square symbols) of salinity front $f_s = 0.1$ vs. time for (a) simulation number 5 and (b) simulation number 8. Straight line indicates the time-depth relationship according to the average front velocity. Numbers in bars refer to the phases 1 to 4 described in the text.

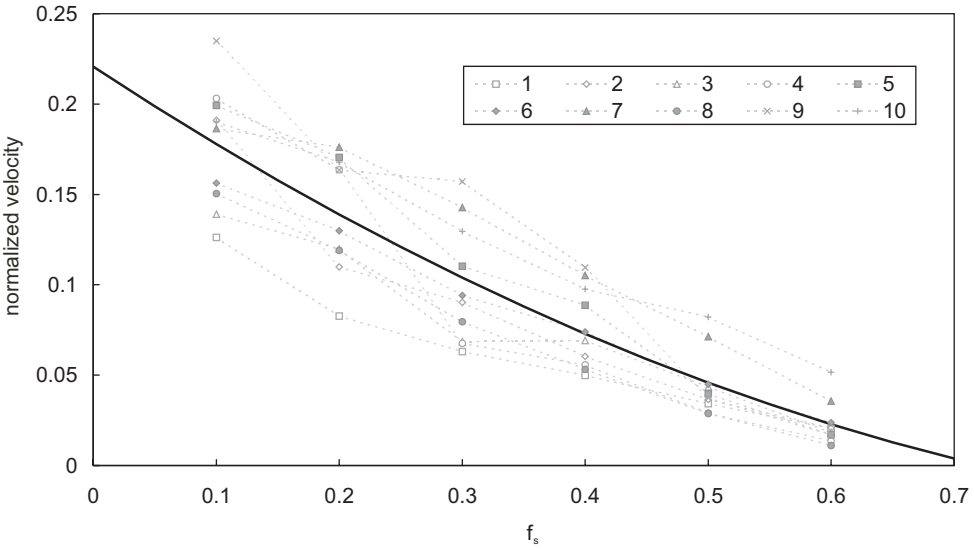

Figure 5.5: Graph of normalized salinization velocity vs. seawater fraction (f_s) for simulations 1 to 10. Numbers in legend are simulation numbers. Solid line shows the normalized salinization velocity vs. seawater fraction (f_s) according to equation 5.14.

The ratio of the timescales for advection and diffusion is then proportional to:

$$\frac{T_{adv}}{T_{diff}} \sim \frac{4Zn\Delta\rho gk}{(Ra_{cr}^{\delta})^2\mu D} \tag{5.18}$$

A high value of this ratio implies that once the plumes reach a certain depth Z, diffusive transport has become important. Because the ratio is proportional to k, reduction of the density contrast by diffusion associated with the saline fingers is most efficient for high permeabilities. The increasing importance of diffusion at high permeabilities may seem counterintuitive but it stems from the fact that the reduction in width of the fingers upon an increase in k and its effect of increasing diffusive transport is more important than the increase in the rate of finger descent. As diffusion decreases the density contrast between the plume and the ambient water, the velocity of the plumes will decrease concomitantly. This result can be corroborated by plotting the depth at which the deceleration first occurs as a function of permeability (figure 5.6). The data plot along a hyperbola and clearly show that for high k values the deceleration starts earlier than for low k values, as predicted by equation 5.18.

Although the initial slowing down of the plumes is clearly observed, front velocities eventually increase again. The data from these simulations suggest that phases of front acceleration coincide with phases of finger coalescence to larger scale fea-

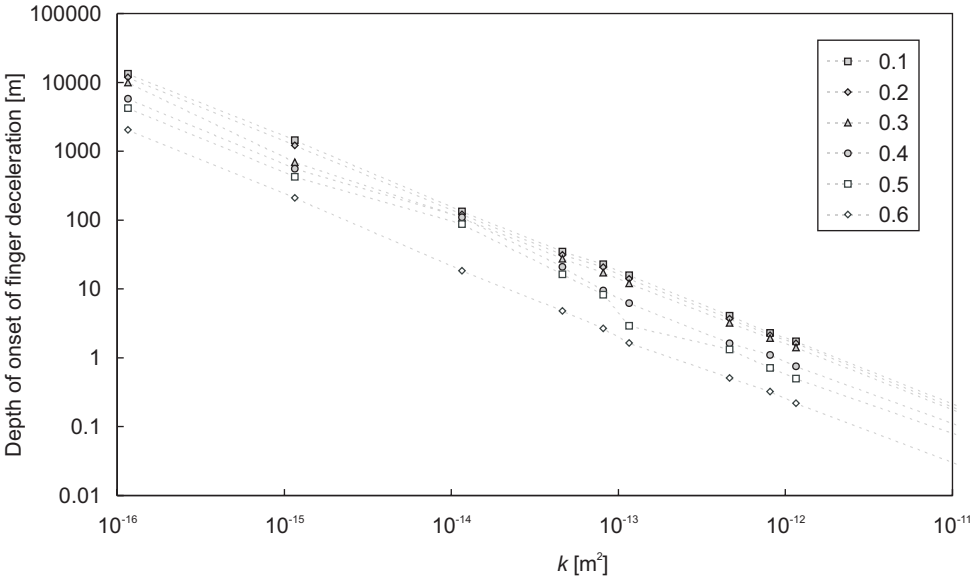

Figure 5.6: Graph of depth of onset of finger deceleration vs. permeability (k) for $f_s = 0.1$, 0.2, 0.3, 0.4, 0.5 and 0.6. Numbers in legend refer to f_s.

tures. Although front velocities increase slightly during the simulations, the overall increase of the salinity front velocity with depth appears to be linear.

5.4.2 Problems with application to the aquifer scale

Inspection of equations 5.8 and 5.14 shows that, as f_s approaches zero, the results discussed above are consistent with those of Wooding (1969) who obtained equation 5.8 by measuring the mean finger amplitude (or $f_s \approx 0$). Thus, the results of the numerical simulations from this study compare very well with the laboratory experiments and mathematical analysis of Wooding (1969). The advantage over relationships such as equation 5.8 is that equation 5.14 provides more insight into the salinity distribution with depth. However, when applying equation 5.14 to predict the time that is required to salinize a high-permeability, real-world aquifer a number of questions arise.

First, it is uncertain if the approximately-linear increase of front depth with time that was observed in these simulations can be extended to depths that exceed the depth range of the numerical models ($Ra = 6\,000$). During the final stage of the simulations, the number of fingers (< 3) becomes too small for any detailed analysis of front velocity variations. Therefore, it could not be ascertained from these simulations how processes such as deceleration owing to decreased density contrast

and finger coalescence influence the longer-term front velocity variations. Results from the Hele-Shaw experiments carried out by Wooding (1969) suggest that linear growth of individual fingers is maintained for Rayleigh numbers up to 3.6 10^5.

Second, and perhaps more important, the validity of the constitutive equations of the numerical model at high permeabilities must be questioned. It was already noted that the dimensions of the salt fingers are a function of permeability. At permeabilities of 10^{-11} m^2 and higher (corresponding conductivities > 10 m/d), the dimensions of fingers are on the order of millimeters and thus approach the size of individual pores. This means that the constitutive equations for pressure and salt mass fraction that average over a certain representative elementary volume (rev) can no longer be applied. This may explain the difficulties that Ackerer et al. (2000) experienced when simulating the concentration patterns that were observed in laboratory experiments where fingering was observed at a permeability on the order of 10^{-9} m^2.

Third, in the numerical simulations in this study, dispersion was independent of flow velocity since D included only diffusion. This was done to allow comparison with results from Hele-Shaw cells and numerical results of Wooding (1969). Normally, hydrodynamic dispersion is incorporated in transport simulations through the use of a dispersivity coefficient to represent heterogeneities (variations in the flow field) that are smaller than the element size of the numerical model. Representation of mechanical dispersion by an enhanced diffusion coefficient overestimates mixing at the sub-rev scale associated with small-scale heterogeneity in the flow field. Because these small-scale heterogeneities in the salinity distribution tend to exert a strong influence on the flow field at large k values, it is not clear how mechanical dispersion should be incorporated into models that simulate free convection in order to adequately represent the physics of the process.

Finally, equation 5.14 is based on the assumption of a homogeneous medium whereas in reality anisotropy and the presence of thin, fine laminae within permeable deposits will affect the front velocity.

5.5 Implication for the Dutch coastal aquifers

In chapters 1 and 2, it was concluded that the vast occurrences of brackish and saline groundwater in the Pleistocene aquifers are due to Holocene transgressions. The Pleistocene aquifer system has an average depth of about 200 m and a hydraulic conductivity of at least 10 m/d ($k \pm 10^{-11}$ m^2). The time required to have a horizontally-averaged concentration of 50 % seawater at 200 m would only be about 15 y according to equation 5.8. Gieske (1991) used a similar expression and obtained comparable values. Although the timescale reported here is merely an estimate of the order of magnitude, there is little doubt that in areas where confining units are absent or laterally-discontinuous, the coastal aquifer system was salinized within decades, confirming the Holocene origin of the brackish and saline groundwater.

Chapter 6

Salinization by free convection in a lithologically-heterogeneous subsurface

Abstract

Numerical modelling is used to study the migration pathways of seawater in a heterogeneous subsurface after a transgression. Three cases are presented: (1) inundation with coeval deposition of clay, (2) transgression of the sea on top of a pre-existing clay bed and (3) horizontal migration of brackish water in an aquifer below a clay layer. Both sedimentation and the presence of clay (cases 1 and 2) retard the onset and rate of free convection. Realistic sedimentation rates appear to be too low, however, to effectively prevent salinization of the inundated aquifer. The presence of a pre-existing clay bed potentially protects the underlying aquifer for thousands of years. The width of the plumes that eventually sink into the aquifer is higher than would be the case in an unconfined aquifer with the same permeability. Horizontal migration of seawater (case 3) extends over a distance of approximately 3.2 km within 1 ka under the conditions modelled. These experiments show that lateral intrusion of seawater can cause significantly-elevated salt concentrations in the course of centuries to millennia.

6.1 Introduction

Equation 5.14 presented in chapter 5, predicts that salinization of the Pleistocene aquifers in the coastal area of the Netherlands occurred within a time span of decades. This outcome applies to a geologically-uniform subsurface and temporally-constant boundary conditions. This chapter presents the result of numerical models that were employed to conceive how more complex stratigraphic conditions will affect salinization by free convection. Three cases were taken into account that are considered to be crucial to the development of salinity patterns in groundwater:

inundation by seawater with coeval deposition of clay

transgression on top of a clay layer

obstruction of free convection by subsurface clay layers

Each of these will be discussed in a separate section.

6.2 Deposition of clay at the seafloor

6.2.1 General

Early marine incursions during the Holocene occurred in a back-barrier tidal basin that received ample sediment supply (Beets et al., 2003). Deposition of clay layers mainly occurred in lagoons and tidal flats. The rate of salinization by free convection is expected to decrease when low-permeability sediments are deposited because these retard the downward movement of dissolved salts. The role of this process was investigated using an adapted version of the METROPOL-3 code.

6.2.2 Model setup

The growth of a sediment layer is taken into account by the adapted version of the METROPOL-3 code by adding rows of elements at the top of the model. Rows are added, incrementally, one at a time depending on a specified deposition rate. The boundary conditions at the upper model edge evolve according to a specified sea level relative to the base of the model, which may vary in time. Boundary conditions no longer apply to former boundary nodes that become part of the inner model domain after a row of elements has been added.

Two model simulations were carried out with the same boundary conditions and parameters as simulation number 5 in chapter 5 (figure 5.1, table 6.1). The permeability of this simulation ($k = 10^{-13}$ m^2) is low compared to the actual permeability of the Pleistocene fluvial sediments ($k > 10^{-11}$ m^2). Nevertheless, this simulation was selected because at a high permeability, modelling of free convection at the scale of real-world aquifers is impossible (chapter 5). The dimensions of the model domain of simulation number 5 approach the size of a real-world aquifer. Still, to constrain calculation time, a smaller grid of 40 m (127 elements) high and 75 m (150 elements) wide had to be used. The element height was 0.33 m except in the upper 1 m of the domain that had an element height of 0.1 m. Element width was uniform (0.5 m).

Table 6.1: Model parameters of the numerical simulations.

Parameter	Section 6.2		Section 6.3		Section 6.4	
	Sand	Clay	Sand	Clay	Sand	Clay
$\log k$	−13	−16	−13	−16	−11	−16
n [dimensionless]	0.3	0.3	0.3	0.43	0.3	0.3
$\log D$	−9	−9	−9	−10.3	−9	−9

One of the simulations was run without sedimentation. This simulation served as a reference to assess the impact of sedimentation. The other model simulated deposition of a clay layer ($k = 10^{-16}$ m^2) at a rate of 0.1 cm/y during the first 100 y. Added elements had a height of 1 cm, which means that every 10 y a mesh layer is introduced.

6.2.3 Results

Figure 6.1 shows the salinity patterns that develop for the model without sedimentation. The boundary layer breaks up after $\sim$ 50 y and plumes sink towards the aquifer bottom. After $\sim$ 200 y the aquifer is almost completely filled with seawater.

Break-up of the boundary layer is retarded for the model that includes sedimentation (compare figures 6.1 and 6.2). Moreover, the plumes that develop have lower concentrations because the clay layer at the top retards the introduction of dissolved salts. The relatively-low density contrast between the plumes and the ambient groundwater lowers the rate of plume descent. The extent of salinization after 317 y is therefore less compared to the model without sedimentation.

6.3 Transgression on top of a clay layer

6.3.1 General

Transport by diffusion in a low-permeability seafloor bed in the southern North Sea was discussed in chapter 3. No measurements of groundwater salinity in the underlying fine-grained sand layer were available. In this section, the development of salinity patterns in this layer is predicted with a numerical model. The results are considered representative for the behaviour in comparable geological settings.

6.3.2 Model setup

The model without deposition described in section 6.2 was adapted to include a clay layer in the upper 5 m of the model domain. Model parameters for the sand and clay layer are listed in table 6.1. The values of the diffusion coefficient and porosity of the clay layer follow from the results presented in chapter 3 (tables 3.1 and 3.3). The permeability of both the fine-grained aquifer and the clay layer at the sampling site is unknown. The selected $k = 10^{-13}$ m^2 for the aquifer is at the lower end of the reported permeability range for fine sand (Domenico and Schwartz, 1990). The adopted permeability of the clay is 1 000 times lower than that of the underlying sand.

After an initial model run, the width of the model domain was increased from 75 m (150 elements) to 150 m (300 elements) to warrant simulation of a significant number of salt plumes.

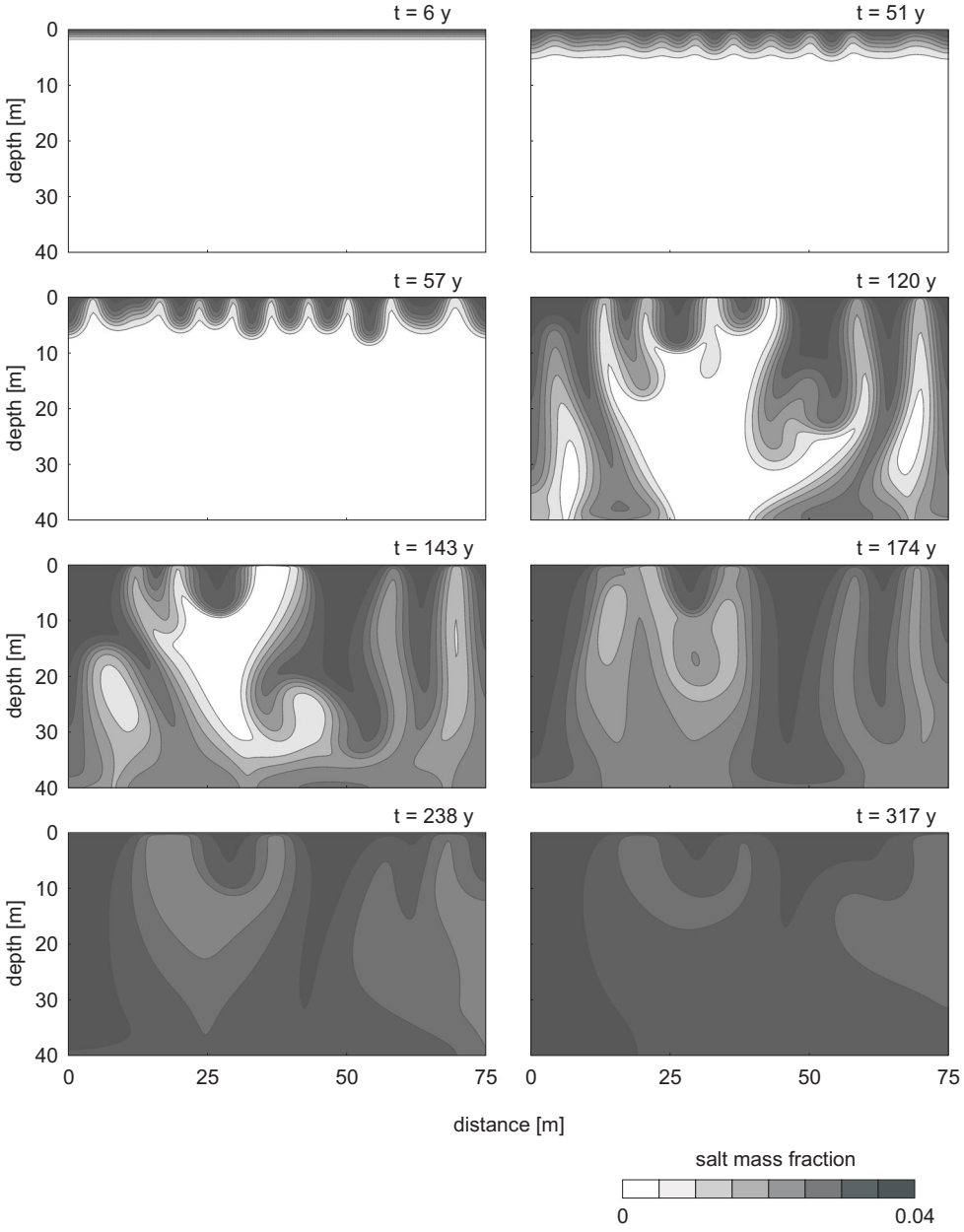

Figure 6.1: Simulated salinization concentration patterns without sedimentation after 6, 51, 57, 120, 143, 174, 238 and 317 y. The aquifer has $k = 10^{-13}$ m^2.

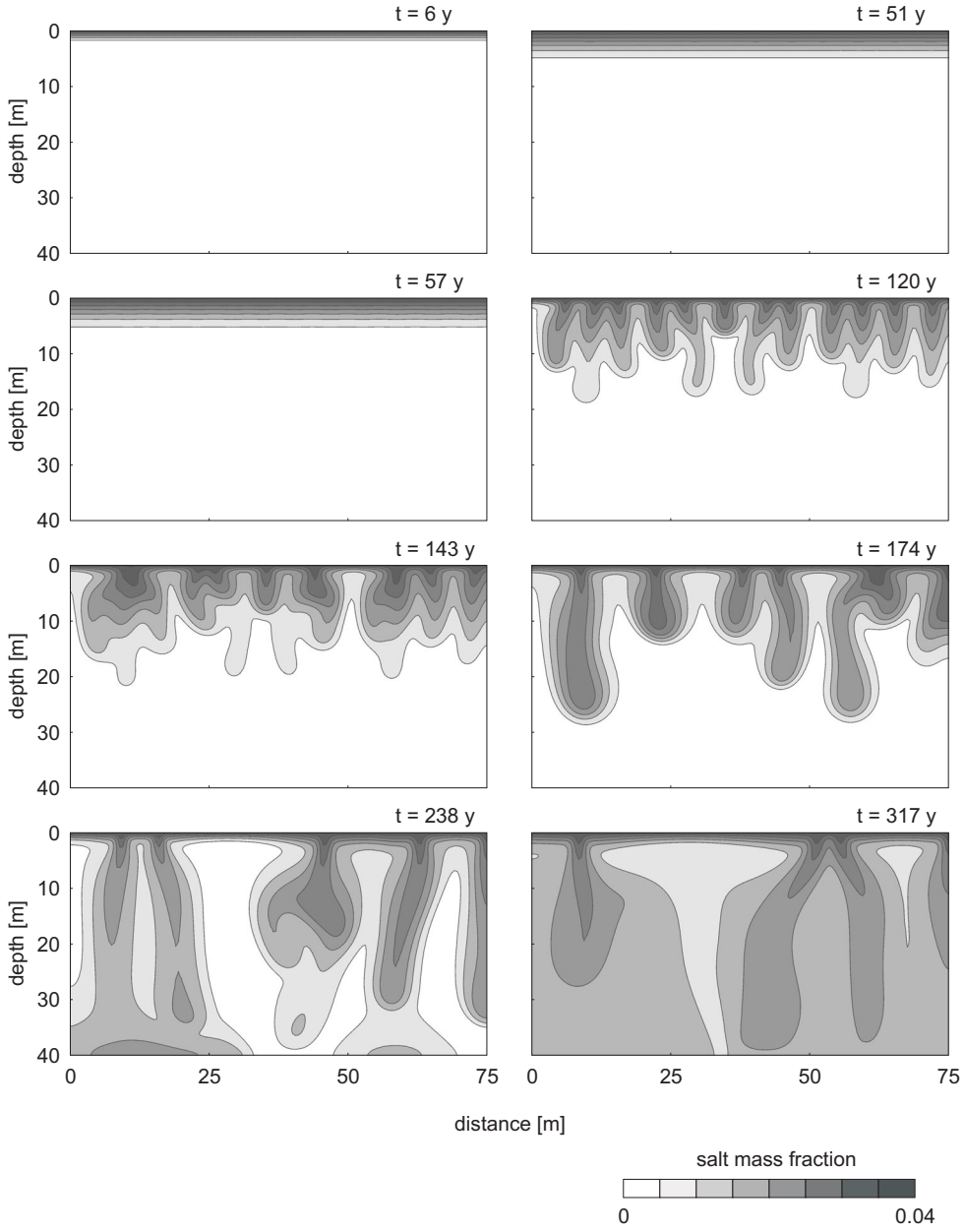

Figure 6.2: Simulated salinization concentration patterns with sedimentation after 6, 51, 57, 120, 143, 174, 238 and 317 y. The sedimentation rate is 0.1 cm/y during the first 100 y. The aquifer has $k = 10^{-13}$ m^2, the deposited clay has $k = 10^{-16}$ m^2.

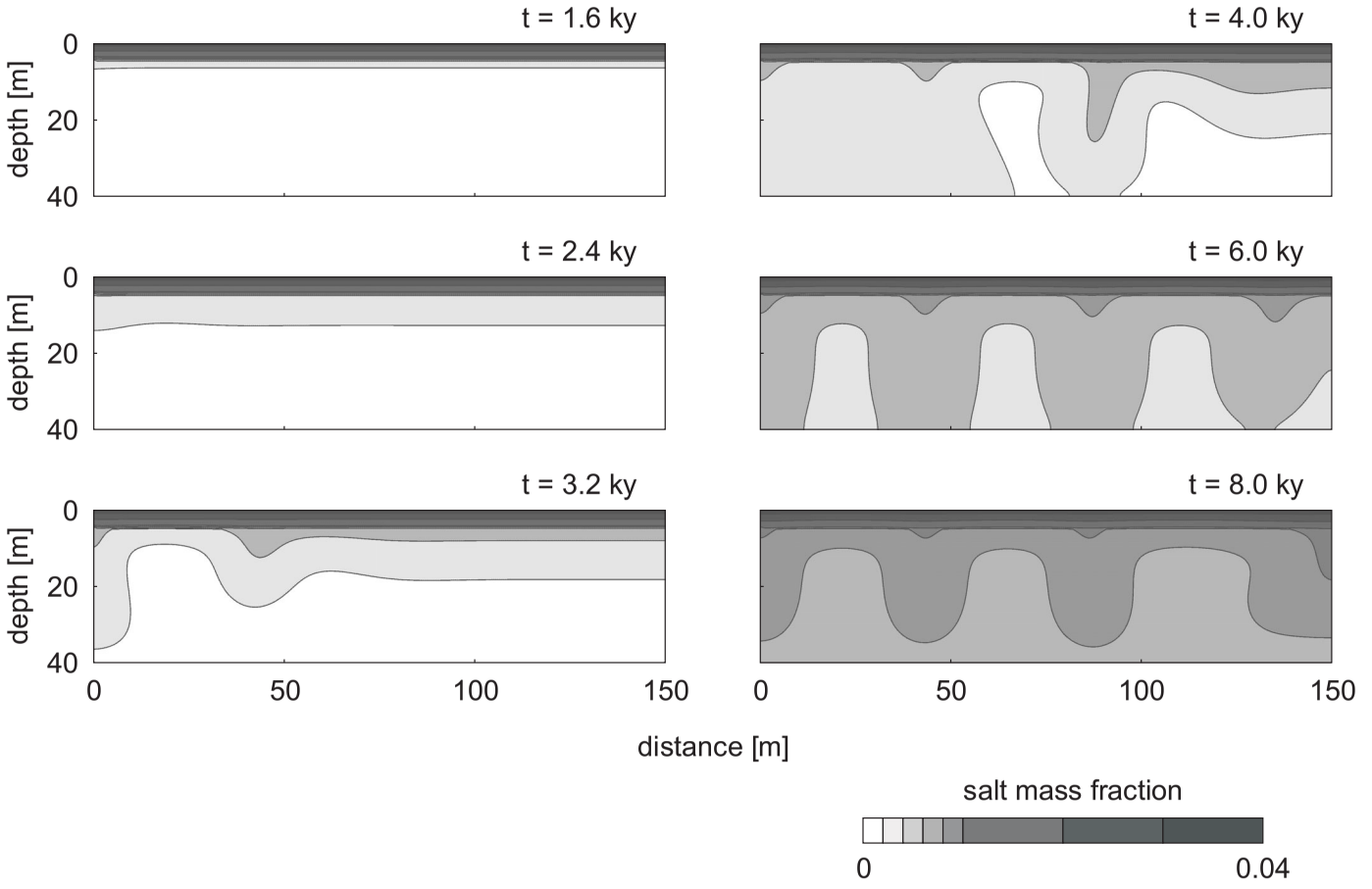

Figure 6.3: Simulated salinization concentration patterns in the geological setting described in chapter 3 after 1.6, 2.4, 3.2, 4.0, 6.0 and 8.0 ky. The aquifer has $k = 10^{-13}$ m^2, the clay has $k = 10^{-16}$ m^2. Note the non-uniform contour interval, which differs from the other figures in chapters 5 and 6.

6.3.3 Results

Introduction of dissolved salts into the aquifer proceeds slowly due to the low diffusion coefficient of the clay. Break-up of the boundary layer does not occur until 2.4 ka after inundation (figure 6.3). The wavelength of the plumes ($\sim$ 37 m) is higher than in the case of direct contact between seawater and the aquifer ($\sim$ 7 m, compare figures 6.1 and 6.3). This follows from the dependency of the wavelength on the density contrast (equation 5.10) that remains low below the clay layer due to the retarded supply of dissolved salts.

Just as in the case of coeval sedimentation of clay, the downward velocity of the salt plumes remains relatively low. The maximum salinity of groundwater in the aquifer below the clay amounts to almost one quarter of that of seawater after 8 ka.

6.4 Obstruction by subsurface clay layers

6.4.1 General

Proof of the retarding effect of subsurface clay layers on salinization is provided by several accounts of salinity inversions in the Netherlands (i.e., groundwater salinity decreasing with depth) in connection to the presence of aquitards (Pomper, 1981; Glasbergen and Mook, 1982; Gieske, 1991; Stuyfzand, 1993). In other cases no inversion is observed or the salinity decrease is insignificant, which implies that these layers have not always been effective in preventing the underlying aquifers from salinization. Two principle migration pathways of intruded seawater can then be envisaged (figure 6.4):

vertical passage of dissolved salts by diffusion in the presence of a laterally-continuous confining layer. Following an initial stage of free convection in the upper aquifer, transport becomes dominated by diffusion in the clay layer. Salinity patterns in the underlying aquifer then develop in a similar fashion as for the case discussed in section 6.3.

horizontal flow due to a rotating vertical interface in the case of a laterally-discontinuous confining layer. Seawater will sink to the bottom by free convection in the area where the two aquifers are connected. The vertical interface that is created in the lower aquifer has the tendency to rotate (Verruijt, 1980), which leads to the development of a salt water wedge in the aquifer below the confining layer.

For the second case a numerical model was used to test the effectiveness of horizontal migration of saline water as a salinization mechanism.

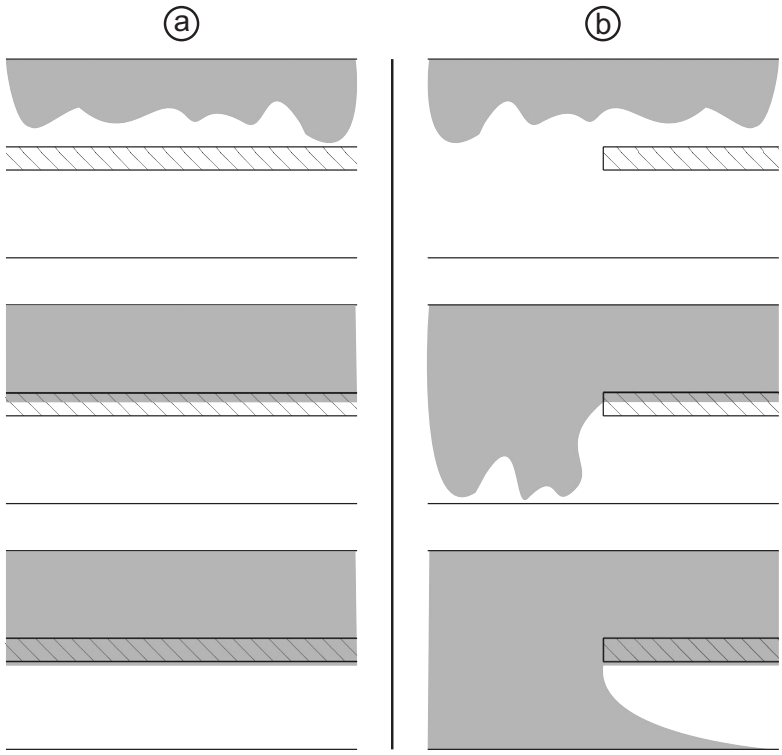

Figure 6.4: Schematic diagram of migration pathways of seawater (shaded) in the presence of a (a) continuous and (b) discontinuous subsurface clay layer.

6.4.2 Model setup

Numerical modelling was carried out with the adapted method of characteristics (MOC) code by Oude Essink (2001). This code was selected because it uses a Lagrangian approach for solute transport, which allows larger domains to be modelled because element size is not restricted by the mesh-Peclet condition (as opposed to METROPOL-3).

The model domain was 5 000 m (200 elements) wide and 50 m (100 elements) high. The domain represents the lower aquifer and the overlying clay layer, but does not include the upper aquifer. The hydraulic conductivity of the lower 45 m was 10 m/d ($k \approx 10^{-11}$ m^2), which is a conservative (i.e., on the low side) number for Dutch coastal aquifers. The upper 5 m of the model domain representing the clay unit were given a conductivity 5 orders of magnitude lower (figure 6.5, table 6.1). Heads and concentrations were specified on the left and upper boundaries (figure 6.5). The lower and right boundaries were closed. The closed boundary on the right

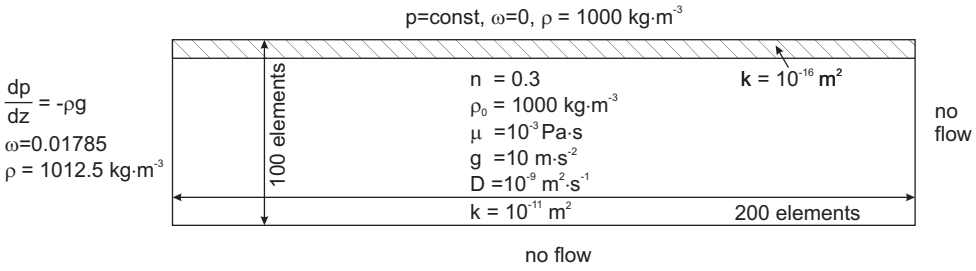

Figure 6.5: Geometry, parameter values and boundary conditions for the numerical model of a rotating interface in an aquifer below a clay layer.

model edge assumes that the clay layer has a finite extent equal to twice the model width and that the flow problem is symmetrical.

It is assumed that saline water first sinks to the bottom before any significant horizontal spreading occurs. In that case the initial salinity distribution approximates a vertical interface, which was implemented in the model by starting with fresh water ($\omega = 0$) throughout the model domain and a specified salt-mass fraction $\omega = 0.01785$ on the left boundary. This value, which is about half that of seawater, is based on the assumption of seawater mixing with pristine fresh groundwater during the sinking of the plumes.

6.4.3 Results

The development of the salt water wedge in the aquifer below the confining unit is shown in figure 6.6. Due to tilting and broadening of the interface the driving force decreases with time. Consequently, the velocity of front advancement becomes smaller, reducing the effectiveness of this process as a salinization mechanism over longer periods of time. After 1 ka, the toe of the salt front has travelled 3.2 km.

The relatively-low conductivity in the model ($\sim$ 10 m/d) compared to field values (up to 60 m/d) yields a conservative estimate of salinity front advancement. Moreover, the closed boundary on the right-hand side of the model forces the displaced fresh groundwater to discharge through the clay layer. More rapid horizontal outflow (open boundary) but might well be important under natural conditions. The simulation time of 1 ka is short compared to the time since the first marine incursions in the coastal area ($\sim$ 7.5 ka BP) and more extensive salinization is to be expected, albeit at an ever-decreasing rate.

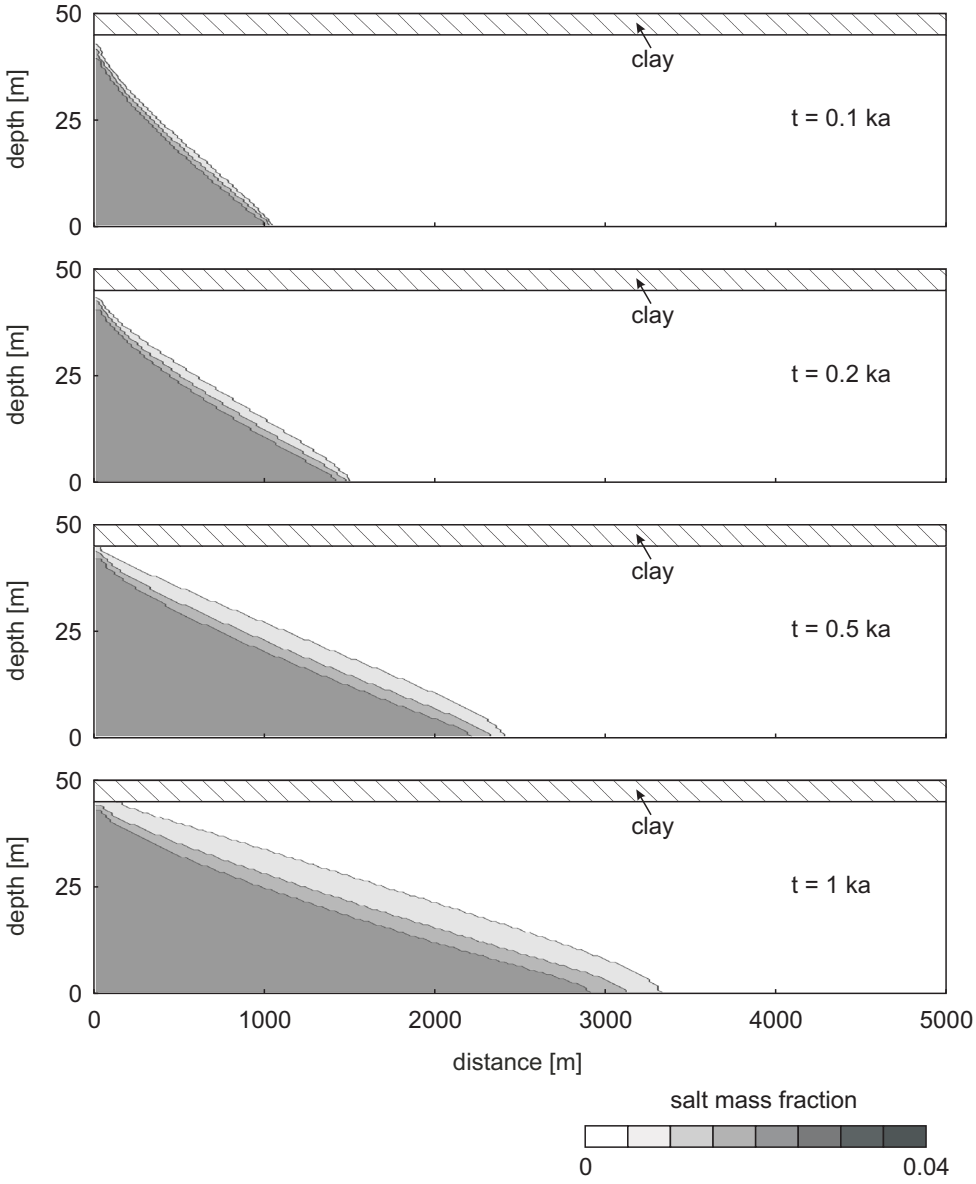

Figure 6.6: Simulated salinization concentration patterns due to interface rotation in an aquifer below a clay layer after 0.1, 0.2, 0.5 and 1 ka. The aquifer has $k = 10^{-11}$ m^2, the clay has $k = 10^{-16}$ m^2.

6.5 Discussion and conclusions

The schematic models presented in the previous sections extend the modelling approach undertaken in chapter 5 by taking into account a non-uniform lithology. Despite the limited number of simulations (and hence no sensitivity analysis), the results allow for evaluation of some generic aspects of the role of low-permeability strata in inhibiting groundwater salinization in the coastal area of the Netherlands during the Holocene.

Incorporation of clay deposition during inundation (section 6.2) still results in free convection, which, although at a smaller rate than for the case without sedimentation, causes elevated salt concentrations up to tens of meters deep. The time required to significantly increase groundwater salinity (decades to centuries) is longer, but appears to be shorter than the duration of the Holocene marine incursions (centuries to millennia). Realistic sedimentation rates (~ 1 mm/y) appear to be too low, however, to effectively prevent salinization of the inundated aquifer.

Spatial variability of depositional environments caused differences in grain size of clastic Holocene sediments. Channel sequences, dominated by a sandy facies, are separated by mud-rich inter-channel areas (e.g. De Mulder and Bosch, 1982; Beets et al., 2003). Decreasing energetic conditions with increasing distance from the coastline resulted in a higher clay content of inland sediments. This may account for the seaward gradient of groundwater salinity as described in chapter 1 (cf. figure 1.5) since the relative importance of clay deposition inland most-likely reduced salinization by free convection.

Transgression on top of a pre-existing confining unit similarly results in delayed and less extensive vertical salinization (section 6.3). A representative model for the geological setting presented in chapter 3 shows that the width of the salt plumes that develop below the clay becomes relatively high because break-up of the boundary layer is retarded. The predicted larger width of the plumes makes this geological setting an interesting target for investigation of free convection under field conditions as it possibly allows to delineate individual plumes, which have never been observed in a real-world aquifer. Offshore locations are especially suited because of the absence of interferences by anthropogenic activities (e.g. pumping).

The model of a rotating interface in an aquifer below a clay layer indicates that salinization driven by horizontal density gradients may extend over several kilometers (section 6.4). Low-permeability strata in the coastal area often also extend continuously over distances of several kilometers. Many interconnections between aquifers exist due to erosion and textural variations (Werkgroep Midden West-Nederland, 1976). Therefore, significant parts of aquifers below low-permeability deposits are susceptible to have been affected by this salinization mechanism.

The series of experiments seem to confirm the suggestion put forward in this thesis that the brackish and saline groundwater in the Pleistocene aquifers must be ascribed to the Holocene transgression. The models presented in this chapter employ a relatively-low permeability compared to the aquifers in the Dutch coastal area.

Hence, the simulated extent of salinization can be considered to be a conservative estimate. Nevertheless, high salt concentrations are predicted.

Chapter 7

Synthesis

The primary objective of this thesis was to develop quantitative understanding of the processes that caused salinization of groundwater in the Dutch coastal area during the Holocene transgression. In this final chapter, the main outcomes of the applied multi-disciplinary approach will be evaluated to determine to what extent they contribute to and improve current understanding. Some implications for practical hydrogeological studies will be discussed and finally, research topics that are currently not fully understood will be outlined. The results are proposed to have general applicability and contribute to the understanding of coastal hydrogeological systems in other areas.

7.1 Outcome and new insights

One of the main research topics in the literature on the coastal area of the Netherlands has been to identify the source of the brackish and saline groundwater in the Pleistocene aquifers. This study supports the conclusion from a number of previous studies that intrusion of Holocene seawater during periods of inundation of the present land surface has caused the extensive salinization (Versluys, 1931; De Vries, 1974; Gieske, 1991; Stuyfzand, 1993). New evidence is presented, which includes an inventory of isotope measurements, notably ^{14}C (chapter 2) and an elaborate analysis of the process of vertical seawater intrusion (chapters 5 and 6).

Meinardi (1991) suggested a major contribution of relic seawater from Pliocene and Early-Pleistocene marine sediments by upward diffusion and enhanced mixing by dispersion. Although this process almost certainly operated during Pleistocene continental phases, a contribution to the contemporary occurrence of brackish and saline groundwater in the Pleistocene aquifers was ruled out in chapter 1. This follows from the observation that, in the area that was affected by the Holocene transgression, salinity decreases with depth within the Pliocene and Early-Pleistocene strata. Therefore, diffusion of dissolved salts is currently directed downward. The occurrence and implication of the observed salinity drop had previously been recognized by Volker (1961), Pomper (1981) and Gieske (1991) in a limited number of

wells. The more comprehensive data set presented in chapter 1, however, provides evidence for the general occurrence of these inversions.

A matter of debate in the literature has also been what transport process led to such large-scale aquifer salinization. Versluys (1931) already argued that during the Holocene marine incursions, seawater would have sunk down into the freshwater aquifers due to the higher density of the former. Gieske (1991) used a simple expression for the rate of buoyancy-induced flow to demonstrate that this process can explain the occurrence of brackish and saline water up to 450 m depth given a period of inundation of only 60 y. Chapter 5 describes a series of numerical experiments that were carried out to investigate the long-term evolution of salinity patterns due to free convection in greater detail. From these experiments, an extension to the expression applied by Gieske (1991) was found that also takes into account the degree of salinization, which allows for an estimation of the approximate, horizontally-averaged, vertical salinity distribution.

The numerical analysis was extended in chapter 6 to investigate if the occurrence of low-permeability sediments has prevented extensive salinization of the coastal aquifer system. Deposition of clay during inundation retards the rate of free convection but still large parts of the aquifer are contaminated by seawater. Horizontal migration of intruded seawater in aquifers below subsurface clay layers appears to have been effective over distances of several kilometers and at least partly explains the occurrence of high-salinity groundwater below dissected clay layers in the coastal area.

In areas where the transgression of the sea was on top of confining deposits, salinization was significantly retarded. With flow rates greatly reduced or even zero, salt transport becomes dominated by diffusion. This is reflected by the vertical distribution of chloride in Holocene clay and peat below a former inland sea as shown by Volker (1961). New data from the Brown Bank in the southern North Sea (chapter 3) show that solute movement in an Eemian clay layer underlying the seafloor is also by diffusion. An important finding is that in this extremely-stiff clay, charged ions like Cl are moving at a lower rate than uncharged H_2O. The observed salinity profile suggests that relatively-fresh water is still preserved in the more permeable sand below the clay. Numerical simulation of the development of salinity patterns below the clay supports this hypothesis (chapter 6).

Observed salinity patterns in pore waters in low-permeability Holocene strata onshore are proof that flow is negligible in large parts of these units and that groundwater recharge and discharge is along preferential flow paths. This was demonstrated in chapter 4. More extensive documentation was published in contributions to conference proceedings that have not been included in this thesis (Post et al., 2002; Post and Kooi, 2003).

Previous studies have paid little attention to the role of evapotranspiration in the coastal area. As elaborated in chapter 2, evaporation is recognized in fresh groundwater that contributes to the present recharge of the aquifers. In chapter 4 it is further shown that seawater has also been subject to direct evaporation and

transpiration prior to infiltration. Field data from the island of Texel show that this process explains the development of anomalously-high salt contents (i.e., greater than in seawater). Even the highest Cl concentrations in groundwater from the coastal area ($m_{Cl} = 839$ mmol/l) can be attributed to this process.

7.1.1 Generalized paleohydrological evolution

Based on the findings presented, the following generalized paleohydrological evolution of the Dutch coastal area during the Holocene is proposed. Fresh groundwater was present in the Pleistocene aquifers after the Weichselian glacial stage and subjacent marine strata had been freshened up to depths of hundreds of meters. Sea level rose during the Holocene, which initially resulted in marine incursions in valleys in the Pleistocene land surface at approximately 7.5 ka BP. Barrier islands developed upon continued sea level rise, which migrated landward and were dissected by several tidal inlets. A dense network of tidal channels extended up to tens of kilometers inland that sometimes cut deep into the Pleistocene sediments and eroded the Holocene basal peat. Direct contact between seawater and the highly-permeable Pleistocene sediments caused rapid salinization of the fresh groundwater up to hundreds of meters deep by free convection. It is expected that free convection also played a role, although at a lower rate, in inter-channel areas where deposition of fine-grained sediments occurred. The time scale associated with this process is in the order of decades to centuries. The upper parts of the Pliocene to Early-Pleistocene marine strata have also been subject to this type of salinization during the Holocene. Relics of the original seawater in these sediments are found below intruded Holocene seawater.

Salt marshes were ubiquitous during the Holocene. In these environments concentration of seawater via direct evaporation and plant transpiration occurred. The increased density of the concentrated seawater presumably led to acceleration of the rate of salinization by free convection. Remnants of hypersaline groundwater still occur in both aquitards and aquifers.

Closure of the tidal channels resulted in decreasing marine influence in the back-barrier basin around 5 ka BP. Subsequently, peat growth started on a large scale and some freshening of the underlying sediments likely occurred. Renewed marine conditions were established due to erosion of large peat areas since 3.5 ka BP. Slow salinization by diffusion occurred in areas where seawater flooded Holocene confining units, but free convection dominated in areas where these units were eroded. Present data do not allow for assessment of the relative importance of the earliest Holocene transgressions compared to later marine incursions.

Since Medieval times man has created a series of flow systems related to the topography of the polder landscape. These flow systems further modified the salinity distribution, leading to the complex spatial concentration patterns observed today.

7.1.2 Practical implications

Despite the scholarly nature of the topics that were addressed in this thesis, the outcomes presented here have implications for practical hydrogeological research in coastal areas.

Discerning past and contemporary salinization is often difficult or even impossible, especially when only salinity or resistivity data are collected. Problems of this type occur for example in the identification of sources of well salinization and delineation of the extent of contaminant plumes. The preservation of relics of seawater in the western part of the Netherlands testifies to the fact that the current hydrogeological situation is simply a phase in the long-term development of aquifer systems. The brackish and saline groundwater formed in an environment totally unlike that of today and water quality patterns continue to adapt to their contemporary boundary conditions. As a result ambiguity is introduced into the interpretation of present-day observations. Knowledge of the geological history of the area under investigation is then essential to recognize the potential contribution of past hydrological processes to the present situation.

Proper conception of the slow adaptation of groundwater salinity patterns to coastline migration is also essential for seawater intrusion models. The presence of fresh water offshore complicates the selection of initial and boundary conditions and needs to be considered in calculations of sustainable yield.

Analysis of the pore water composition in confining units allows for quantification of flow rates and model parameters such as hydraulic conductivity and diffusion coefficients. Collection of the samples does not require highly-specialized techniques or equipment. Still, studies of this type are rarely employed in practical hydrological applications.

Pliocene and Early-Pleistocene marine strata are generally considered to be the impermeable base of the hydrogeological system in the western part of the Netherlands. However, this assumption is questionable given the presence of Holocene seawater in these layers. Possible interactions should be considered in modelling studies that span periods of centuries, such as those that predict the effect of climate change and sea level rise.

7.2 Remaining challenges

The present study employed different earth-scientific disciplines including hydrochemistry, isotope hydrology, geophysics, quantitative hydrogeology (hydraulic modelling) and Quaternary geology to investigate salinization of the Dutch coastal aquifers. None of the methodologies provide complete understanding of the hydrogeological system under consideration when applied separately. The strength of the adopted 'holistic' approach, however, is that theories are checked for consistency as they must stand up to the outcomes of all the individual disciplines. This is an

important extension of previous studies in the coastal area that mainly addressed the subject from a single direction.

Nevertheless, some of the topics that were discussed in this thesis are still not fully understood. These will be elaborated below.

Current understanding of free convection is based on mathematical models and laboratory experiments. It is unclear to what extent our knowledge applies in real-world aquifers. Ongoing free convection under field conditions has been observed for the first time only recently by Andersen (2001) after the study site of a controlled seawater intrusion experiment was flooded during a storm. More data are required to study aspects such as boundary layer break-up, finger dimensions and salinity front propagation. Obtained insights will have relevancy to areas inundated by seawater, which are currently being created deliberately at a number of locations in the Netherlands in nature restoration projects and at waste disposal sites from which dense contaminant plumes emanate.

The observed pore water salinity in the Brown Bank Formation provides indirect evidence for the occurrence of relatively-fresh water below the North Sea. More data are required to map the spatial extent of these occurrences. Numerical simulation of the salinization patterns in the aquifer below the clay layer indicates that the dimensions of the salt plumes are probably in the order of meters. Consequently, this geological setting is an interesting potential target for the study of ongoing free convection.

Migration of charged solutes in the clay from the Brown Bank below the North Sea was shown to be retarded with respect to water, but uncertainty remained on the cause hereof. Transport of water and its dissolved solids in clay layers is susceptible to effects of anion-exclusion and pore geometry, which give rise to osmotic phenomena. The role of this process in natural settings is still unclear and may have implications for disposal of radioactive waste and other contaminants.

Our understanding of the hydrogeological behaviour of low-permeability Holocene strata is inadequate. Observed spatial salinity variations in the pore waters of these layers imply complicated flow patterns, which contrast with the often-made assumption of an uniform vertical flow field. This scale issue has important bearing on ecological and pollution-oriented applications that require detailed knowledge of the small-scale flow field, such as the quantification of high nutrient loads to surface waters in groundwater discharge areas. It requires the development of methods to characterize groundwater flow in greater detail than those provided by sparse observation wells.

The inability of radiocarbon (^{14}C) to accurately date intruded seawater calls the need for alternative methods. Radiogenic ^{4}He, which derives from U and Th decay, is being evaluated as a dating tool in coastal areas (Ekwurzel et al., 2001; Loosli et al., 2001). Furthermore ^{226}Ra, with a half-life of 1 602 y can in some cases aid in validation of radiocarbon ages (Loosli et al., 2001). The coastal area of the Netherlands provides a potentially-interesting case for application of these relatively-new techniques.

Freshening of the Pliocene and Early-Pleistocene marine strata is expected to have occurred by diffusion during large parts of the Pleistocene when fresh water circulation occurred in the overlying aquifers (Meinardi, 1991). Moreover, compaction-driven flow caused migration of the connate seawater. Modern numerical codes that simulate groundwater flow can take into account changes in basin geometry due to subsidence, coeval deposition and associated sediment compaction. Numerical modelling could be combined with geochemical investigations and would allow for more accurate quantification of the paleohydrological evolution of the relic Cenozoic seawater.

Little is known about the impact of the ice ages on groundwater flow systems. In the literature, solute migration related to permafrost in the Dutch coastal area during Quaternary glacial stages has been postulated only by Pomper (1978). Its influence on the evolution of groundwater salinity was never evaluated in detail and may well be underappreciated given its suspected role in brine formation (e.g. Bottomley et al., 1999; Bein and Arad, 1992; Herut et al., 1990). Moreover, anomalous Sr isotope ratios in secondary calcite from the Amsterdam Saalian glacial basin might imply circulation of groundwater up to hundreds of meters deep (C.J. Beets, personal communication). This raises the question to what extent the development of large flow systems in front of the former ice sheets contributed to flushing of marine strata of Early-Pleistocene age and older.

Finally, as a general remark, care must be taken to avoid that hydrogeological research becomes too much of a modelling exercise. The advent of sophisticated numerical models has shifted the focus away from field hydrogeology. Field data are indispensable for a proper conception of the hydrogeological system under investigation. Models provide a means to test concepts against physical and chemical theory. Used in the right way, the conjunctive use of both measurements and models leads to better understanding and new insights.

References

Ackerer, P., Younes, A., Oswald, S. E., Kinzelbach, W., 2000. On modelling of density driven flow. In: Stauffer, F., Kinzelbach, W., Kovar, K., Hoehn, E. (Eds.), Calibration and Reliabity in Groundwater modelling (Proceedings of the ModelCARE 99 Conference held at Zurich, Switzerland, September 1999). Vol. 265. IAHS, pp. 377–384.

Andersen, M. S., 2001. Geochemical processes at a seawater-freshwater interface. Ph.D. thesis, Technical University of Denmark.

Appelo, C. A. J., 1994. Cation and proton exchange, pH variations, and carbonate reactions in a freshening aquifer. Water Resources Research 30 (10), 2793–2805.

Appelo, C. A. J., Geirnaert, W., 1991. Processes accompanying the intrusion of salt water. In: De Breuck, W. (Ed.), Hydrogeology of salt water intrusion: A selection of SWIM papers. Vol. 11 of International Contributions to Hydrogeology. Verlag Heinz Heise, Hannover, Germany, pp. 291–303.

Appelo, C. A. J., Postma, D., 1994. Geochemistry, groundwater and pollution. A.A. Balkema, Rotterdam, The Netherlands.

Bachmat, Y., Elrick, D. E., 1970. Hydrodynamic instability of miscible fluids in a vertical porous column. Water Resources Research 6, 156–171.

Barbecot, F., Marlin, C., Gibert, E., Dever, L., 2000. Hydrochemical and isotopic characterisation of the Bathonian and Bajocian coastal aquifer of the Caen area (northern France). Applied Geochemistry 15, 791–805.

Barker, A. P., Newton, R. J., Bottrell, S. H., Tellam, J. H., 1998. Processes affecting groundwater chemistry in a zone of saline intrusion into an urban sandstone aquifer. Applied Geochemistry 13 (6), 735–749.

Bath, A. H., Edmunds, W. M., Andrews, J. N., 1978. Paleoclimatic trends deduced from the hydrochemistry of a Triassic sandstone aquifer, United Kingdom. In: Isotope hydrology 1978. Vol. II. International Atomic Energy Agency, Neuherberg, pp. 545–568.

Beekman, H. E., 1991. Ion chromatography of fresh- and seawater intrusion. Ph.D. thesis, Vrije Universiteit, Amsterdam.

Beets, C. J., 1992. Calibration of late Cenozoic marine strontium isotope variations and its chronostratigraphic and geochemical implications. Ph.D. thesis, Vrije Universiteit, Amsterdam.

Beets, D. J., De Groot, T. A. M., Davies, H. A., 2003. Holocene tidal back-barrier development at decelerating sea-level rise: a 5 millennia record, exposed in the

western Netherlands. Sedimentary Geology 158, 117–144.

Beets, D. J., Van der Valk, L., Stive, M. J. F., 1992. Holocene evolution of the coast of Holland. Marine Geology 103, 423–443.

Bein, A., Arad, A., 1992. Formation of saline groundwaters in the Baltic region through freezing of seawater during glacial periods. Journal of Hydrology 140, 75–87.

Berner, R. A., 1980. Early diagenesis: A theoretical approach. Princeton University Press, Princeton, New York, USA.

Berry, F. A. F., 1967. Role of membrane hyperfiltration on origin of thermal brines, Imperial Valley, California. AAPG Bulletin 51, 454–455.

Boisson, J. Y., Bertrand, L., Heitz, J. F., Moureau-Le Golvan, Y., 2001. In situ and laboratory investigations of fluid flow through an argillaceous formation at different scales of space and time, Tournemire tunnel, southern France. Hydrogeology Journal 9 (1), 108–123.

Boswinkel, J. A., Ritsema, I. L., oktober 1984 1984. Grondwaterkaart van Nederland: Rotterdam 37 West, 37 Oost (Groundwater map of the Netherlands: Rotterdam 37 West, 37 East). Tech. Rep. Rapportno. GWK 35, Dienst Grondwaterverkenning TNO.

Bottomley, D. J., Katz, A., Chan, L. H., Starinsky, A., Douglas, M., Clark, I. D., Raven, K. G., 1999. The origin and evolution of Canadian Shield brines: evaporation or freezing of seawater? New lithium isotope and geochemical evidence from the Slave craton. Chemical Geology 155, 295–320.

Boudreau, B. P., 1997. Diagenetic models and their implementation, modelling transport and reactions in aquatic sediments. Springer-Verlag, Berlin Heidelberg, Germany.

Broers, H. P., Griffioen, J., 1992. Het grondwaterkwaliteitsmeetnet van de provincie Noord-Brabant: opzet en eerste resultaten (Groundwater quality monitoring network in the province of Noord-Brabant: design and preliminary results). H_2O 25 (26), 728–735.

Burnett, W. C., Taniguchi, M., Oberdorfer, J., 2001. Measurement and significance of the direct discharge of groundwater into the coastal zone. Journal of Sea Research 46, 109–116.

Cameron, D., Van Doorn, D., Laban, C., Streif, H. J., 1993. Geology of the southern North Sea Basin. In: Hillen, R., Verhagen, H. J. (Eds.), Coastlines of the Southern North Sea. Coastlines of the World Series. American Society of Civil Engineers, New York, USA, pp. 14–26.

Clark, I. D., Fritz, P., 1997. Environmental isotopes in hydrogeology. Lewis Publishers, Boca Raton, USA.

Csonka, J., Otte, W. M. A., November 1985 1985. Geo-elektrisch onderzoek Waddeneilanden (Geo-electrical research on the Frisian islands). Tech. Rep. Rapportnr. GF 145, Dienst Grondwaterverkenning TNO.

De Breuck, W., 1991. Hydrogeology of Salt Water Intrusion. Vol. 11 of International contributions to Hydrogeology. Verlag Heinz Heise, Hannover, Germany.

De Gans, W., De Groot, T., Zwaan, H., 1986. The Amsterdam basin, a case study of a glacial basin in The Netherlands. In: INQUA Symposium on the genesis and lithology of glacial deposits. Amsterdam, pp. 205–216.

De Gans, W., Van Gijssel, K., 1996. The late Weichselian morphology of the Netherlands and its influence on the Holocene coastal development. Mededelingen Rijks Geologische Dienst 57, 11–25.

De Groot, M. M., Van der Linden, F. J., 1987. Hydrologisch onderzoek in de Horstermeerpolder (Hydrological investigation of the Horstermeerpolder). Master's thesis, Vrije Universiteit, Amsterdam.

De Louw, P. G. B., Griffioen, J., Van den Eertwegh, G. A. P. H., 2000. High nutrient and chloride loads to surface waters in polder areas due to groundwater seepage. In: Sililo, O. (Ed.), Groundwater: Past Achievements and Future Challenges. A.A. Balkema, Cape Town, South Africa, pp. 418–486.

De Mulder, E. F. J., Bosch, J. H. A., 1982. Holocene stratigraphy, radiocarbon datings and paleogeography of Central and Northern North-Holland (The Netherlands). Mededelingen Rijks Geologische Dienst 36 (3), 111–160.

De Ruiter, J. C., 1988. Hydrologische systeemanalyse in Centraal Zuid-Holland (Hydrological systems analysis in the Central Zuid-Holland area). Tech. rep., Vrije Universiteit.

De Vries, D. M., 1935. Plantengezelschappen als kenteeken van het keukenzoutgehalte van den bodem (Plant communities as indicators of the halite content of the soil). Nederlands Kruidkundig Archief 45, 97–121.

De Vries, J. J., 1974. Groundwater flow systems and stream nets in the Netherlands. Ph.D. thesis, Vrije Universiteit, Amsterdam.

De Vries, J. J., 1981. Fresh and salt groundwater in the Dutch coastal area in relation to geomorphological evolution. Geologie en Mijnbouw 60, 363–368.

Degueldre, C., Scholtis, A., Laube, A., Turrero, M. J., Thomas, B., 2003. Study of the pore water chemistry through an argillaceous formation: a paleohydrochemical approach. Applied Geochemistry 18, 55–73.

Den Hartog, C., 1958. De vegetatie van het Balgzand en de oeverterreinen van het Balgkanaal (Vegetation of the Balgzand area and shores of the Balgzand canal). Vol. 27 of Wetenschappelijke mededelingen van de K.N.N.V. Hoogwoud Bureau K.N.N.V.

Desaulniers, D. E., Cherry, J. A., Fritz, P., 1981. Origin, age and movement of pore water in argillaceous Quaternary deposits at four sites in southwestern Ontario. Journal of Hydrology 50, 231–257.

Desaulniers, D. E., Kaufmann, R. S., Cherry, J. A., Bentley, H. W., 1986. ^{37}Cl-^{35}Cl variations in a diffusion-controlled groundwater system. Geochimica et Cosmochimica Acta 50, 1757–1764.

Doherty, J., 2002. PEST, model-independent parameter estimation. Tech. rep., Watermark Numerical Computing.

Domenico, P. A., Schwartz, F. W., 1990. Physical and chemical hydrogeology. John Wiley and Sons, New York, USA.

Drabbe, J., Badon Ghijben, W., 1888. Nota in verband met de voorgenomen putboring nabij Amsterdam (Report concerning projected well drilling near Amsterdam). Tijdschrift Koninklijk Instituut v Ingenieurs, Verh. 1888-1889 , 8–22.

Drever, J. I., 1997. The geochemistry of natural waters. Prentice Hall, Upper Saddle River, USA.

Dubois, E., 1903. Feiten ter opsporing van de bewegingsrichting en den oorsprong van het grondwater onzer zeeprovincien (Facts for the detection of the direction of migration and origin of the groundwater in our sea provinces). Verslagen en Mededelingen Koninklijke Nederlandse Akademie van Wetenschappen, Afdeling Wis- en Natuurkunde 12 (1), 187–212.

Dufour, F. C., 1998. Grondwater in Nederland (Groundwater in the Netherlands). Nederlands Instituut voor Toegepaste Geowetenschappen TNO, Delft, The Netherlands.

Edmunds, W. M., 2001. Palaeowaters in European coastal aquifers - the goals and main conclusions of the PALAEAUX project. In: Edmunds, W. M., Milne, C. J. (Eds.), Palaeowaters in Coastal Europe: evolution of groundwater since the late Pleistocene. Vol. 189. The Geological Society of London, London, Great Britain, pp. 1–16.

Edmunds, W. M., Buckley, D. K., Darling, W. G., Milne, C. J., Smedley, P. L., Williams, A. T., 2001. Palaeowaters in the aquifers of the coastal regions of southern and eastern England. In: Edmunds, W. M., Milne, C. J. (Eds.), Palaeowaters in Coastal Europe: evolution of groundwater since the late Pleistocene. Vol. 189. The Geological Society of London, London, Great Britain, pp. 71–92.

Edmunds, W. M., Smedley, P. L., 2000. Residence time indicators in groundwater: the East Midlands Triassic sandstone aquifer. Applied Geochemistry 15, 737–752.

Eggenkamp, H. G. M., 1994. The geochemistry of chlorine isotopes. Ph.D. thesis, Utrecht University.

Eggenkamp, H. G. M., Middelburg, J. J., Kreulen, R., 1994. Preferential diffusion of ^{35}Cl relative to ^{37}Cl in sediments of Kau Bay, Halmahera, Indonesia. Chemical Geology 116, 317–325.

Ekwurzel, B., Moran, J. E., Hudson, G. B., Bissani, M., Blake, R., Krimissa, M., Mosleh, N., Marah, H., Safsaf, N., Hsissou, Y., Bouchaou, L., 2001. An isotopic investigation of salinity and water sources in the Souss-Massa Basin, Morocco. In: Ouazar, D., Cheng, A. H. D. (Eds.), The first international conference on salt water intrusion and coastal aquifers. Essaouira, Morocco.

Elder, J. W., 1967. Transient convection in a porous medium. Journal of Fluid Mechanics 27, 906–923.

Elder, J. W., 1968. The unstable thermal interface. Journal of Fluid Mechanics 32, 69–96.

Engelen, G. B., De Ruiter-Peltzer, J. C., 1986. A case study of regional hydrological systems and fresh-salt water interaction in the Western part of The Netherlands. In: Boekelman, R. H., Van Dam, J. C., Evertman, M., Ten Hoorn, W. H. C. (Eds.), 9th Salt Water Intrusion Meeting. Delft University of Technology, Delft,

pp. 177–191.

Fabricius, C., Olofson, B., 1996. Salinization of private wells from de-icing chemicals - A pilot project in central Sweden. In: 14^{th} Salt Water Intrusion Meeting. Vol. Rapporter och meddelanden nr 87. Sveriges Geologiska Undersokning, Malmo, Sweden, pp. 220–229.

Fan, Y., Duffy, C. J., Oliver, D. S., 1997. Density-driven groundwater flow in closed desert basins: field investigations and numerical experiments. Journal of Hydrology 196, 139–184.

Faure, G., 1986. Principles of isotope geology. John Wiley and sons, New York, USA.

Fleischer, E., Goldberg, M., Gat, J. R., Magaritz, M., 1977. Isotopic composition of formation waters from deep drillings in southern Israel. Geochimica et Cosmochimica Acta 41 (4), 511–525.

Fritz, S. J., Marine, I. W., 1983. Experimental support for a predictive osmotic model of clay membranes. Geochimica et Cosmochimica Acta 47, 1515–1522.

Gautschi, A., 2001. Hydrogeology of a fractured shale (Opalinus Clay): Implications for deep geological disposal of radioactive wastes. Hydrogeology Journal 9 (1), 97–107.

Gebhart, B., Jaluria, Y., Mahajan, R. L., Sammakia, B., 1988. Buoyancy-induced flows and transport. Hemisphere Publishing Corporation, Washington D.C., USA.

Geenen, A., 1993. 3-Dimensionale interpolatie van het chloride-gehalte van het grondwater in de Amsterdamse Waterleidingduinen (Three-dimensional interpolation of the chloride content of groundwater in the Amsterdam Water Supply dune area). Tech. rep., Gemeentewaterleidingen Amsterdam.

Gehrels, J. C., 1999. Groundwater level fluctuations. Ph.D. thesis, Vrije Universiteit, Amsterdam.

Geirnaert, W., 1972. The hydrogeology and hydrochemistry of the lower Rhine fluvial plain. Leidse Geologische Mededelingen 49 (1), 59–84.

Geyh, M. A., 2000. An overview of 14C analysis in the study of groundwater. Radiocarbon 42 (1), 99–114.

Gieske, J. M. J., 1991. De oorsprong van het brakke grondwater in het IJsselmeergebied: diffusie, dispersie, of dichtheidsstroming? (Origin of brackish groundwater in the IJsselmeer area: diffusion, dispersion or density-driven flow? H_2O 24 (7), 189–193.

Glasbergen, P., 1981. Extreme salt concentrations in deep aquifers in the Netherlands. In: Van Duijvenbooden, W., Glasbergen, P., Van Lelyveld, H. (Eds.), Quality of groundwater, Proceedings of an International Symposium, Noordwijkerhout, The Netherlands, 23-27 March 1981. Vol. 17 of Studies in Environmental Science. Elsevier Scientific Publishing Company, Noordwijkerhout, The Netherlands, pp. 687–695.

Glasbergen, P., Mook, W. G., 1982. Toepassing van natuurlijke isotopen in regionaal hydrologisch onderzoek (Application of natural isotopes in regional hydrological research). Tech. Rep. R.I.D.-mededelingen 82-9, National Institute for Water Supply.

Graf, D. L., 1982. Chemical osmosis, reverse chemical osmosis, and the origin of subsurface brines. Geochimica et Cosmochimica Acta 46, 1431–1448.

Griffioen, J., 1994. Uptake of phosphate by iron hydroxides during seepage in relation to development of groundwater composition in coastal areas. Environmental Science and Technology 28, 675–681.

Griffioen, J., De Louw, P. G. B., Boogaard, H. L., Hendriks, R. F. A., 2002 2002. De achtergrondbelasting van het oppervlaktewatersysteem met N, P en Cl en enkele ecohydrologische parameters in Westelijk Nederland (Loads of N, P and Cl and selected ecological parameters to surface waters in the Western Netherlands). Tech. Rep. Rapportno NITG 02-166-A, NITG-TNO.

Groen, J., 2002. The effects of transgressions and regressions on coastal and offshore groundwater. Ph.D. thesis, Vrije Universiteit, Amsterdam.

Groen, J., Post, V. E. A., Kooi, H., Hemker, C. J., 2000a. Paleo-hydrology of the sedimentary plain of Suriname. In: Dassargues, A. (Ed.), Tracers and modelling in hydrogeology. Vol. 262 of International Association of Hydrological Sciences (IAHS) Publications. International Association of Hydrological Sciences (IAHS), Liege, Belgium, pp. 417–424.

Groen, J., Velstra, J., Meesters, A. G. C. A., 2000b. Salinization processes in paleowaters in coastal sediments of Suriname: evidence from δ^{37}Cl analysis and diffusion modelling. Journal of Hydrology 234, 1–20.

Halamickova, P., Detwiler, R. J., Bentz, D. P., Garboczi, E. J., 1995. Water permeability and chloride ion diffusion in Portland cement mortars: relationship to sand content and critical pore diameter. Cement and Concrete Research 25 (4), 790–802.

Harrar, W. G., Williams, A. T., Barker, J. A., Van Camp, M., 2001. Modelling scenarios for the emplacement of palaeowaters in aquifer systems. In: Edmunds, W. M., Milne, C. J. (Eds.), Palaeowaters in Coastal Europe: evolution of groundwater since the late Pleistocene. Vol. 189. The Geological Society of London, London, Great Britain, pp. 213–229.

Harting, P., 1852. De bodem onder Amsterdam, onderzocht en beschreven (Investigation and description of the subsurface of Amsterdam). Verhandelingen der Eerste Klasse van het Koninklijk-Nederlandsche Instituut. 3 (5), 73–232.

Hartog, N., Griffioen, J., Van der Weijden, C. H., 2002. Distribution and reactivity of O_2-reducing components in sediments from a layered aquifer. Environmental Science and Technology 36, 2338–2344.

Hathaway, J. C., Poag, C. W., Valentine, P. C., Miller, R. E., Schultz, D. M., Manheim, F. T., Kohout, F. A., Bothner, M. H., Sangrey, D. A., 1979. Core drilling on the Atlantic shelf. Science 206, 515–527.

Heijboer, D., Nellestijn, J., 2002. Klimaatatlas van Nederland, de normaalperiode 1971-2000 (Climate atlas of the Netherlands, normal period 1971-2000). Uitgeverij Elmar B.V., Rijswijk, The Netherlands.

Hendry, M. J., Wassenaar, L. I., 1999. Implications of the distribution of δD in pore waters for groundwater flow and the timing of geologic events in a thick aquitard

system. Water Resources Research 35 (6), 1751–1760.

Hendry, M. J., Wassenaar, L. I., 2000. Controls on the distribution of major ions in pore waters of a thick surficial aquitard. Water Resources Research 36 (2), 503–513.

Hendry, M. J., Wassenaar, L. I., Kotzer, T., 2000. Chloride and chlorine isotopes (^{36}Cl and δ^{37}Cl) as tracers of solute migration in a thick, clay-rich aquitard system. Water Resources Research 36 (1), 285–296.

Herut, B., Starinsky, A., Katz, A., Bein, A., 1990. The role of seawater freezing in the formation of subsurface brines. Geochimica et Cosmochimica Acta 54, 13–21.

Hettling, H. K., 1985. Isotopic groundwater study of the Loosdrecht lakes area (The Netherlands). Tech. Rep. W.O.L. rapport 1985-4, Vrije Universiteit.

Hinsby, K., Harrar, W. G., Nyegaard, P., Konradi, P. B., Rasmussen, E. S., Bidstrup, T., Gregersen, U., Boaretto, E., 2001. The Ribe Formation in western Denmark - Holocene and Pleistocene groundwaters in a coastal Miocene sand aquifer. In: Edmunds, W. M., Milne, C. J. (Eds.), Palaeowaters in Coastal Europe: evolution of groundwater since the late Pleistocene. Vol. 189. The Geological Society of London, London, Great Britain, pp. 29–48.

Hiscock, K. M., Dennis, P. F., Saynor, P. R., Thomas, M. O., 1996. Hydrochemical and stable isotope evidence for the extent and nature of the effective Chalk aquifer of north Norfolk, UK. Journal of Hydrology 180, 79–107.

Hobma, T. W., Van de Graaf, M., Hoogeboom, B., Van de Leemkule, M., 1993. Ecohydrologie en hydrochemie van de Brabantse Wal en aangrenzende polders rond Clafven (Ecohydrology and hydrochemistry of the Brabantse wal and adjacent polder area near the village of Calfven). Tech. rep., Vrije Universiteit, Faculty of Earth Sciences.

Holzbecher, E. O., 1998. Modeling density-driven flow in porous media. Springer, Berlin Heidelberg, Germany.

Hoogendoorn, J. H., 1985. De zoet-zout-verdeling van het grondwater in Nederland deel 3A - Een case study (Distribution of fresh and saline groundwater in the Netherlands part 3A - a case study). Tech. Rep. OS 85-33, Dienst Grondwaterverkenning TNO.

Howard, K. W. F., Beck, P. J., 1993. Hydrogeochemical implications of groundwater contamination by road de-icing chemicals. Journal of Contaminant Hydrology 12 (3), 245–268.

Hubbert, M. K., 1940. The theory of ground-water motion. Journal of Geology 48 Part 1, 785–944.

IAEA/WMO, 2001. Global Network of Isotopes in Precipitation. The GNIP Database. Accessible at: http://isohis.iaea.org.

Johnson, R. L., Cherry, J. A., Pankow, J. F., 1989. Diffusive Contaminant transport in a natural clay: A field example and implications for clay-lined waste disposal sites. Environmental Science and Technology 23 (3), 340–349.

Jørgensen, N. O., 2002. Origin of shallow saline groundwater on the island of Laeso, Denmark. Chemical Geology 184, 359–370.

Jørgensen, N. O., Holm, P. M., 1994. Isotope studies ($^{18}O/^{16}O$, D/H and $^{87}Sr/^{86}Sr$) of saline groundwater in Denmark. In: Soveri, J., Suokko, T. (Eds.), Future Groundwater Resources at Risk. Proceedings of the FGR 94 Conference held at Helsinki, June 1994. Vol. IAHS Publication 222. IAHS, Wallingford, UK, pp. 231–238.

Keijzer, T. J. S., 2000. Chemical osmosis in natural clayey minerals. Ph.D. thesis, Utrecht University.

Koch, M., 1994. The dynamics of density driven finger instabilities in stochastically heterogeneous porous media. In: Peters, A., Wittum, G., Herrling, B., Meissner, U., Brebbia, C. A., Gray, W. G., Pinder, G. F. (Eds.), Computational Methods in Water Resources. Vol. X. Kluwer Academic Publishers, Dordrecht, The Netherlands, pp. 481–488.

Kohout, F. A., Hathaway, J. C., Folger, D. W., Bothner, M. H., Walker, E. H., Delaney, D. F., Frimpter, M. H., Weed, E. G. A., Rhodehamel, E. C., 1977. Fresh groundwater stored in aquifers under the continental shelf: implications from a deep test, Nantucket Island, Massachusetts. Water Resources Bulletin 13, 373–386.

Kolditz, O., Ratke, R., Diersch, H. J., Zielke, W., 1998. Coupled groundwater flow and transport: 1. Verification of variable density flow and transport models. Advances in Water Resources 21, 27–46.

Kooi, H., De Vries, J. J., 1998. Land subsidence and hydrodynamic compaction of sedimentary basins. Hydrology and Earth System Sciences 2, 159–171.

Kooi, H., Garavito, A. M., Bader, S., 2003. Numerical modelling of chemical osmosis and ultrafiltration across clay formations. Journal of Geochemical Exploration 7, 333–336.

Kooi, H., Groen, J., Leijnse, A., 2000. Modes of seawater intrusion during transgressions. Water Resources Research 36 (12), 3581–3589.

Laban, C., 1995. The Pleistocene glaciations in the Dutch sector of the North Sea. Ph.D. thesis, University of Amsterdam.

Leijnse, A., 1992. Three-dimensional modeling of coupled flow and transport in porous media. Ph.D. thesis, Notre Dame University.

Loosli, H. H., Aeschbach-Hertig, W., Barbecot, F., P., B., Darling, W. G., Dever, L., Edmunds, W. M., Kipfer, R., Purtschert, R., Walraevens, K., 2001. Isotopic methods and their hydrogeochemical context in the investigation of palaeowaters. In: Edmunds, W. M., Milne, C. J. (Eds.), Palaeowaters in Coastal Europe: evolution of groundwater since the late Pleistocene. Vol. 189. The Geological Society of London, London, Great Britain, pp. 193–212.

Lorie, J., 1899. Onze brakke, ijzerhoudende en alkalische bodemwateren (Our brackish, ferrous and alkaline soil waters). Verhandelingen Koninklijke Nederlandse Akademie van Wetenschappen, 2e sectie 6 (8), 39.

Maathuis, H., Yong, R. N., Adi, S., Prawiradisastra, S., 1996. Development of groundwater management strategies in the coastal region of Jakarta, Indonesia. Tech. Rep. SRC Publ. R-1250-1-E-96, International Development Research Centre (IDRC), Environment and Natural Resources Division.

Manzano, M., Custodio, E., Loosli, H., Cabrera, M. C., Riera, X., Custodio, J., 2001. Palaeowater in coastal aquifers of Spain. In: Edmunds, W. M., Milne, C. J. (Eds.), Palaeowaters in Coastal Europe: evolution of groundwater since the late Pleistocene. Vol. 189. The Geological Society of London, London, Great Britain, pp. 107–138.

Meinardi, C. R., 1974. The origin of brackish groundwater in the lower parts of the Netherlands. Tech. Rep. R.I.D.-mededelingen 74-6, National Institute for Water Supply.

Meinardi, C. R., 1975. Brackish groundwater bodies as a result of geological history and hydrological conditions. Tech. Rep. R.I.D.-mededelingen 75-1, National Institute for Water Supply.

Meinardi, C. R., 1991. The origin of brackish groundwater in the lower parts of The Netherlands. In: Breuck, W. d. (Ed.), Hydrogeology of salt water intrusion: A selection of SWIM papers. Vol. 11 of International contributions to hydrogeology. Verlag Heinz Heise, Hannover, Germany, pp. 271–290.

Molt, E. L., 1961. De Rijn (The river Rhine). Water 45 (11), 143–155.

Mook, W. G., 1968. Geochemistry of the stable carbon and oxygen isotopes of natural waters in the Netherlands. Ph.D. thesis, Groningen University.

Mook, W. G., 2000. Environmental Isotopes in the hydrological cycle: Volume I Introduction theory methods review. Vol. 1. UNESCO/IAEA, Vienna, Austria.

Novakowski, K. S., Van der Kamp, G., 1996. The radial diffusion method 2. A semi-analytical model for the determination of effective diffusion coefficients, porosity, and adsorption. Water Resources Research 32 (6), 1823–1830.

Oetting, G. C., Banner, J. L., Sharp Jr., J. M., 1996. Regional controls on the geochemical evolution of saline groundwaters in the Edwards aquifer, central Texas. Journal of Hydrology 181, 251–283.

Ortega-Guerrero, A., Cherry, J. A., Aravena, R., 1996. Origin of pore water and salinity in the lacustrine aquitard overlying the regional aquifer of Mexico City. Journal of Hydrology 197, 47–69.

Oswald, S. E., Kinzelbach, W., 2000. A three-dimensional physical model for verification of variable-density flow codes. In: Stauffer, F., Kinzelbach, W., Kovar, K., Hoehn, E. (Eds.), Calibration and Reliabity in Groundwater modelling (Proceedings of the ModelCARE 99 Conference held at Zurich, Switzerland, September 1999). Vol. 265 of IAHS Publication. IAHS, pp. 399–404.

Oude Essink, G. H. P., 1996. Impact of sea level rise on groundwater flow regimes. Ph.D. thesis, Delft University of Technology.

Oude Essink, G. H. P., 2001. Salt Water Intrusion in a Three-dimensional Groundwater System in The Netherlands: a Numerical Study. Transport in Porous Media 43 (1), 137–158.

Ouwerkerk, J., 1993. Beschrijving van de chemie van het grondwater van Zeeland en van Walcheren en Zuid-Beveland in het bijzonder (Description of groundwater chemistry in the province of Zeeland with special reference to Walcheren and Zuid-Beveland). Tech. rep., Provincie Zeeland, directie Milieu en Waterstaat.

Parkhurst, D. L., Appelo, C. A. J., 1999. User's guide to PHREEQC (version 2.0) - A computer program for speciation, batch-reaction, one-dimensional transport, and inverse geochemical calculations. Vol. Water-Resources Investigations Report 99-4259. U.S. Geological survey, Denver, Colorado, USA.

Person, M., Urbano, L., Taylor, J., Willett, M., Swenson, J., Dugan, B., 2001. Pleistocene hydrology of Nantucket Island, Massachusetts. In: Ouazar, D., Cheng, A. D. H. (Eds.), First International Conference on Saltwater Intrusion and Coastal Aquifers. Essaouira, Morocco, p. 5.

Phillips, F. M., Bentley, H. W., Davis, S. N., Elmore, D., Swanick, G. B., 1986. Chlorine 36 dating of very old groundwater 2. Milk river aquifer, Alberta, Canada. Water Resources Research 22 (13), 2003–2016.

Piekarek-Jankowska, H., 1996. Hydrochemical effects of submarine groundwater discharge to the Puck Bay (Southern Baltic Sea, Poland). Geographia Polonica 67, 103–119.

Plummer, L. N., Prestemon, E. C., Parkhurst, D. L., 1994. An interactive code (NETPATH) for modeling NET geochemical reactions along a flow PATH version 2.0. Vol. Water Resources Investigation Report 94-4169. U.S. Geological Survey, Reston, Virginia, USA.

Plummer, L. N., Sprinkle, C. L., 2001. Radiocarbon dating of dissolved inorganic carbon in groundwater from confined parts of the Upper Floridan aquifer, Florida, USA. Hydrogeology Journal 9 (2), 127–150.

Pomper, A. B., 1978. An estimation of chloride intrusion in the Midwest Netherlands during the Pleistocene Epoch. In: Proceedings 5th Salt Water Intrusion Meeting - Medmenham, Great Britain. Medmenham, Great Britain, pp. 114–125.

Pomper, A. B., 1981. A possible explanation of the occurrence of inversions in the chloride content of groundwater in the western Netherlands. In: Sixth salt water intrusion meeting. Vol. 29 of Geologisches Jahrbuch Reihe C: Hydrogeologie, Ingenieurgeologie. pp. 205–215.

Pomper, A. B., 1983. The geohydrological situation of the western part of the Netherlands. Geologie en Mijnbow 62 (3), 519–528.

Pons, L. J., 1992. Holocene peat formation in the lower parts of the Netherlands. In: Verhoeven, J. T. A. (Ed.), Fens and bogs in the Netherlands: vegetation, history, nutrient dynamics and conservation. Kluwer Academic Publishers, Dordrecht, The Netherlands, pp. 7–79.

Post, V. E. A., Bloem, E., Ooteman, K., Slob, E., Groen, J., Groen, M., 2002. The use of CVES to map the subsurface salinity distribution: a case study from The Netherlands. In: Boekelman, R. H., Hornschuh, J. C. S., Olsthoorn, T. N., Oude Essink, G. H. P., Peute, L., Stark, J. M. (Eds.), Proceedings 17th Salt Water Intrusion Meeting, Delft 6-10 May 2002. Delft, The Netherlands, pp. 283–290.

Post, V. E. A., Kooi, H., 2003. Pore water analyses of low-permeability sediments as a tool for reconstruction of hydrological processes. In: Marin, L. E., Cheng, A. (Eds.), The second international conference on Salt Water Intrusion and Coastal Aquifers in Monitoring, Modeling and Management. Merida, Mexico, p. 4.

Remenda, V. H., Van der Kamp, G., Cherry, J. A., 1996. Use of vertical profiles in δ^{18}O to constrain estimates of hydraulic conductivity in a thick, unfractured till. Water Resources Research 32, 2979–2987.

Ridder, T. B., Baard, J. H., Buishand, T. A., 1984. De invloed van monstermethoden en analysetechnieken op gemeten chemische concentraties in regenwater (Effects of sampling and analysis techniques on measured chemical concentrations in precipitation). Tech. Rep. Technische rapporten T.R. -55, KNMI.

Rozanski, K., 1985. Deuterium and oxygen-18 in European groundwaters-links to atmospheric circulation in the past. Chemical Geology (Isotope Geoscience Section) 52, 349–363.

Sauter, F. J., Leijnse, A., Beusen, A. H. W., 1993. Metropol's user guide. Vol. Report 725205003. National Institute of Public Health and Environmental Protection (RIVM), Bilthoven, The Netherlands.

Schincariol, R. A., Schwartz, F. W., 1990. An experimental investigation of variable density flow and mixing in homogeneous and heterogeneous media. Water Resources Research 26 (10), 2317–2329.

Schincariol, R. A., Schwartz, F. W., Mendoza, C. A., 1994. On the generation of instabilities in variable density flow. Water Resources Research 30 (4), 913–927.

Schincariol, R. A., Schwarz, F. W., Mendoza, C. A., 1997. Instabilities in variable density flows: Stability and sensitivity analyses for homogeneous and heterogeneous media. Water Resources Research 33, 31–41.

Schot, P. P., Molenaar, A., 1992. Regional changes in groundwater flow patterns and effects on groundwater composition. Journal of Hydrology 130 (1-4), 151–170.

Schulz, H. D., Zabel, M. (Eds.), 2000. Marine geochemistry. Springer-Verlag, Berlin - Heidelberg, Germany.

Shennan, I., Lambeck, K., Flather, R., Horton, B., McArthur, J., Innes, J., Lloyd, J., Rutherford, M., Wingfield, R., 2000. Modelling western North Sea paleogeographies and tidal changes during the Holocene. In: Shennan, I., Andrews, J. (Eds.), Holocene Land-Ocean Interaction and Environmental Change around the North Sea. Vol. 166. The Geological Society of London, London, Great Britain, pp. 299–319.

Simmons, C. T., Narayan, K. A., 1997. Mixed convection processes below a saline disposal basin. Journal of Hydrology 194, 263–285.

Simmons, C. T., Narayan, K. A., Wooding, R. A., 1999. On a test case for density-dependent groundwater flow and solute transport models: The salt lake problem. Water Resources Research 35 (12), 3607–3620.

Sjöberg, E. L., Georgala, D., Rickard, D. T., 1984. Origin of interstitial water compositions in postglacial black clays (northeastern Sweden). Chemical Geology 42, 147–158.

Stuyfzand, P. J., April 1991 1991. De samenstelling van regenwater langs Hollands kust (The composition of rain water along the coast of Holland). Tech. Rep. SWE 91.010, KIWA.

Stuyfzand, P. J., 1993. Hydrochemistry and hydrology of the coastal dune area of

the western Netherlands. Ph.D. thesis, Vrije Universiteit, Amsterdam.

Stuyfzand, P. J., Stuurman, R. J., 1994. Recognition and genesis of various brackish to hypersaline groundwaters in the Netherlands. In: Barrocu, G. (Ed.), Proceedings 13th Salt Water Intrusion Meeting (SWIM), June 5-10 1994. Villasimius (Cagliari) Italy, pp. 125–136.

Suzuoki, T., Kumura, T., 1973. D/H and $^{18}O/^{16}O$ fractionation in ice-water systems. Mass Spectroscopy 21, 229–233.

Vaikmäe, R., Edmunds, W. M., Manzano, M., 2001. Weichselian palaeoclimate and palaeoenvironment in Europe: background for palaeogroundwater formation. In: Edmunds, W. M., Milne, C. J. (Eds.), Palaeowaters in Coastal Europe: evolution of groundwater since the late Pleistocene. Vol. 189. The Geological Society of London, London, Great Britain, pp. 163–191.

Van Dam, J. C., 1976. Possibilities and limitations of the resistivity method of geoelectrical prospecting in the solution of geohydrological problems. Geoexploration 14, 179–193.

Van der Hoeven, P. C. T., 1982. Observations of surface water temperature and salinity, State Office of Fishery Research (RIVO): 1861 - 1981. Tech. Rep. Scientific report W.R. 82-8, Koninklijk Nederlands Meteorologisch Instituut.

Van der Kamp, G., Van Stempvoort, D. R., Wassenaar, L. I., 1996. The radial diffusion method 1. Using intact cores to determine isotopic composition, chemistry, and effective porosities for groundwater in aquitards. Water Resources Research 32 (6), 1815–1822.

Van der Kemp, W. J. M., Appelo, C. A. J., Walraevens, K., 2000. Inverse chemical modeling and radiocarbon dating of palaeogroundwaters; the Tertiary Ledo-Paniselian Aquifer in Flanders, Belgium. Water Resources Research 36 (5), 1277–1287.

Van der Meij, J. L., Minnema, B., 1999. Modelling of the effect of a sea-level rise and land subsidence on the evolution of the groundwater density in the subsoil of the northern part of the Netherlands. Journal of Hydrology 226, 152–166.

Van der Molen, W. H., 1989. Het zoute grondwater in West-Nederland: een gevolg van dichtheidsstromingen? (The saline groundwater in the western Netherlands: a result of density-driven flow? H_2O 22 (11), 330–346.

Van der Schaaf, S., 1998. Anisotropie und Selbstregulierung bei Versickerungsverlusten in Hochmooren (Anisotropy and self adjustment in seepage losses from raised bogs). Telma 28, 131–144.

Van der Weijden, C. H., Middelburg, J. J., 1989. Hydrogeochemistry of the river Rhine: long term and seasonal variability, elemental budgets, base levels and pollution. Water Research 23 (10), 1247–1266.

Van Dongen, P. G., Boswinkel, J. A., 1982. De zoet-zoutverdeling van het grondwater in Nederland deel 2B - De interpretatie van boorgatmetingen met betrekking tot de overgangszone van zoet naar zout grondwater (Distribution of fresh and saline groundwater in the Netherlands part 2B - Interpretation of well logs concerning the transition zone from fresh to saline groundwater). Tech. Rep. OS 82-09, Dienst

Grondwaterverkenning TNO.

Van Duijvenbooden, W., Kooper, W. F., 1981. Effects on groundwater flow and groundwater quality of a waste disposal site in Noordwijk, The Netherlands. In: Van Duijvenbooden, W., Glasbergen, P., Van Lelyveld, H. (Eds.), Quality of Groundwater. Vol. 17 of Studies in Environmental Science. Elsevier Scientific Publishing Company, Noordwijkerhout, The Netherlands, pp. 253–260.

Van Huissteden, J., Van de Plassche, O., 1998. Sulphate reduction as a geomorphological agent in tidal marshes ('Great Marshes' at Barnstable, Cape Cod, USA). Earth Surface Processes and Landforms 23, 223–236.

Van Rees Vellinga, E., Toussaint, C. G., Wit, K. E., 1981. Water quality and hydrology in a coastal region of the Netherlands. Journal of Hydrology 50, 105–127.

Van Rossum, P., 1998. Mobilisatie en herkomst van arseen in de bodem van de provincie Noord-Holland (Mobilisation and origin of arsenic in the subsurface of the province of Noord-Holland). Tech. rep., Vrije Universiteit.

Van Weert, F. H. A., Van Gijssel, K., Leijnse, A., Boulton, G. S., 1997. The effects of Pleistocene glaciations on the geohydrological system of Northwest Europe. Journal of Hydrology 195, 137–159.

Van Wieringen, J., Willemsen, G., 1982. Kationenuitwisseling in het grondwater onder de polder Groot-Mijdrecht (Cation exchange in groundwater below the Groot-Mijdrecht polder area). Master's thesis, Vrije Universiteit, Amsterdam.

Vermeulen, A. J., 1977. Immissieonderzoek met behulp van regenvangers: opzet, ervaringen en resultaten (Immission studies using rain collectors: design, experiences and results). Tech. rep., Provinciale Waterstaat van Noord-Holland.

Verruijt, A., 1980. The rotation of a vertical interface in a porous medium. Water Resources Research 16 (1), 239–240.

Versluys, J., 1931. Subterranean water conditions in the coastal regions of the Netherlands. Economic Geology 26, 65–95.

Volker, A., 1961. Source of brackish ground water in Pleistocene formations beneath the Dutch polderland. Economic Geology 56, 1045–1057.

Volker, A., Van der Molen, W. H., 1991. The influence of groundwater currents on diffusion processes in a lake bottom: an old report reviewed. Journal of Hydrology 126, 159–169.

Voss, C. I., Souza, W. R., 1987. Variable density flow and solute transport simulation of regional aquifers containing a narrow freshwater-saltwater transition zone. Water Resources Research 23 (10), 1851–1866.

Walraevens, K., 1987. Hydrogeologie en hydrochemie van het Ledo-Paniseliaan in Oost- en West-Vlaanderen. Ph.D. thesis, Ghent University.

Walraevens, K., Van Camp, M., Lermytte, J., Van der Kemp, W. J. M., Loosli, H. H., 2001. Pleistocene and Holocene groundwaters in the freshening Ledo-Paniselian aquifer in Flanders, Belgium. In: Edmunds, W. M., Milne, C. J. (Eds.), Palaeowaters in Coastal Europe: evolution of groundwater since the late Pleistocene. Vol. 189. The Geological Society of London, London, Great Britain, pp. 49–70.

Wang, J. H., Robinson, C. V., Edelman, I. S., 1953. Self diffusion and structure of

liquid water with ^{2}H, ^{3}H and ^{18}O as tracers. Journal of the American Chemical Society 75, 466–470.

Wang, R., 1994. Survey of a fresh water aquifer in Shengsi sea area. Hydrogeology and Engeneering Geology 3, 5–10.

Werkgroep Midden West-Nederland, 1976. Hydrologie en waterkwaliteit van Midden West-Nederland (Hydrology and water quality of the Midden West-Nederland area). Vol. 9. Instituut voor Cultuurtechniek en Waterhuishouding, Wageningen, The Netherlands.

Wigley, T. M. L., Plummer, L. N., Pearson, F. J., 1978. Mass transfer and carbon isotope evolution in natural water systems. Geochimica et Cosmochimica Acta 42, 1117–1139.

Wintgens, P., 1911. Beitrag zu der Hydrologie von Nordholland (Contribution to the hydrology of the province of Noord-Holland). Ph.D. thesis, T.H. Dresden.

Wooding, R. A., 1962. The stability of an interface between miscible fluids in a porous medium. Zeitschr. Angew. Math. Phys. 13, 255–266.

Wooding, R. A., 1969. Growth of fingers at an unstable diffusing interface in a porous medium or Hele-Shaw cell. Journal of Fluid Mechanics 39, 477–495.

Wooding, R. A., Tyler, S. W., White, I., 1997a. Convection in groundwater below an evaporating salt lake: 1. Onset of instability. Water Resources Research 33, 1199–1217.

Wooding, R. A., Tyler, S. W., White, I., Anderson, P. A., 1997b. Convection in groundwater below an evaporating salt lake: 2. Evolution of fingers or plumes. Water Resources Research 33, 1219–1228.

Yaqing, W., Xiaobai, C., Guanglan, M., Shaoqing, W., Zhenyan, W., 2000. On changing trends of δD during seawater freezing and evaporation. Cold Regions Science and Technology 31, 27–31.

Yechieli, Y., Ronen, D., 1996. Self-diffusion of water in a natural hypersaline solution (Dead Sea brine). Geophysical Research Letters 23, 845–848.

Yurtsever, Y., 1997. Role and contribution of environmental tracers for study of sources and processes of groundwater salinization. In: Hydrochemistry (Proceedings of the Rabat symposium, April 1997). Vol. IAHS Publication 244. IAHS, pp. 3–12.

Zagwijn, W., Beets, D. J., Van den Berg, M., Van Montfrans, H. M., Van Rooijen, P., 1985. Atlas van Nederland, deel 13: Geologie (Atlas of the Netherlands, part 13: geology). Vol. 13. Staatsuitgeverij, 's Gravenhage, The Netherlands.

Zagwijn, W. H., 1974. The paleogeographic evolution of the Netherlands during the Quaternary. Geologie en Mijnbouw 53 (6), 369–385.

Zagwijn, W. H., 1983. Sea level changes in the Netherlands during the Eemian. Geologie en mijnbouw 62 (3), 437–450.

Zagwijn, W. H., 1986. Nederland in het Holoceen (The Netherlands during the Holocene). Vol. 1 of Geologie van Nederland. Sdu uitgeverij, 's Gravenhage, The Netherlands.

Zagwijn, W. H., 1989. The Netherlands during the Tertiary and the Quaternary: A

case history of Coastal Lowland evolution. Geologie en Mijnbouw 68, 107–120.

Zagwijn, W. H., Doppert, J. W. C., 1978. Upper Cenozoic of the southern North Sea basin: paleoclimatic and paleogeographic evolution. Geologie en Mijnbouw 57, 577–588.

Zagwijn, W. H., Van Staalduinen, C. J., 1975. Toelichting bij geologische overzichtskaarten van Nederland (Supplement to the geological map of the Netherlands). Rijks Geologische Dienst, Haarlem, The Netherlands.

Samenvatting

De ruimtelijke verdeling van zoet- en zout grondwater komt in veel kustgebieden niet overeen met de verdeling die men op basis van het huidige stromingspatroon zou verwachten. Zout grondwater bevindt zich vaak landinwaarts van de huidige kustlijn, terwijl onder de zeebodem soms nog relatief zoet grondwater wordt aangetroffen. Dit is het gevolg van veranderingen in de ligging van de kustlijn die zich in de loop van de geologische geschiedenis hebben voorgedaan.

In het laaggelegen deel van Nederland is op grote schaal brak- en zout grondwater aanwezig. De herkomst van dit water en de processen die het voorkomen ervan hebben beïnvloed, zijn onderwerp geweest van een groot aantal publicaties die echter geen eenduidige theorie hebben opgeleverd over de ontstaanswijze van het brakke- en zoute grondwater.

Het doel van dit proefschrift was om tot een beter begrip te komen van de processen die hebben geleid tot verzilting van het grondwater in het Nederlandse kustgebied. Hierbij is gebruikt gemaakt van chloride- en isotoopanalyses, geo-electrische metingen, numerieke transportmodellen en kennis van de geologische geschiedenis van het gebied.

In hoofdstuk 1 wordt de geologische ontstaansgeschiedenis behandeld en een overzicht gegeven van de grootschalige ruimtelijke variaties van het zoutgehalte van grondwater. Deze verdeling laat tot een diepte van ongeveer 50 m onder zeeniveau een grillig patroon zien, wat deels kan worden toegeschreven aan stroomsystemen die zijn ontstaan onder invloed van door de mens gecreëerde hoogteverschillen. De processen en oorzaken die mogelijk tot de hoge zoutconcentraties in het grondwater hebben geleid worden geëvalueerd en hieruit volgt dat het voorkomen van het brakke- en zoute grondwater het gevolg is van transgressies gedurende het verleden. Op grond van de afname van de Cl-concentratie met de diepte in de mariene pakketten van Pliocene tot Vroeg-Pleistocene ouderdom wordt geconcludeerd dat connaat zeewater uit deze afzettingen niet de bron kan zijn voor het brakke- tot zoute grondwater in de bovenliggende Pleistocene watervoerende pakketten. Een eventuele herkomst uit het Eemiën wordt uitgesloten op basis van de ^{14}C-activiteit. Het brakke- en zoute grondwater moet daarom uit het Holoceen stammen. Door de hoge doorlatendheid van de zandige ondergrond ontstond een instabiele situatie toen de zee het gebied, waarin zich aanvankelijk zoet water in de ondergrond bevond, bedekte, zodat het zwaardere zeewater in de bodem kon zakken. Dit proces wordt aangeduid als vrije convectie. Kleilagen die zich in de ondergrond bevonden of werden afgezet tij-

dens de transgressies, zorgden er in een aantal gebieden voor dat het onderliggende zoete grondwater beschermd werd tegen verzilting. Verzoeting van de watervoerende pakketten begon op te treden nadat de zee zich had teruggetrokken en er hoogteverschillen in het landschap ontstonden. Aanvankelijk gebeurde dit door natuurlijke processen zoals veengroei en duinafzetting, maar later ook door menselijke ingrepen zoals het aanleggen van polders en het bedijken van waterlopen.

In hoofdstuk 2 wordt getracht met behulp van natuurlijke isotopen de hydrologische processen die het grondwater hebben beïnvloed te reconstrueren. Uit ^{2}H- en ^{18}O-waarden blijkt dat verdamping en menging van zoet water met zeewater de belangrijkste processen zijn waarmee de waargenomen variaties in meetwaarden kunnen worden verklaard. Het zoete water wat met zeewater mengde heeft lagere δ^{18}O-waarden dan het zoete grondwater dat het gemengde water later verdrongen heeft. Dit impliceert dat infiltratie van door verdamping beïnvloed zoet water pas begon op te treden nadat de ondergrond verzilt was. De zeer geringe ^{14}C-activiteit van Plioceen- tot Vroeg-Pleistoceen brak water vergeleken met het bovenliggende Holocene brakke water in peilbuis 31E-0176 bewijst dat een hoge ^{14}C-activiteit indicatief is voor een Holocene ouderdom. Dit wordt bevestigd door het ontbreken van een afname van ^{14}C met de Cl-concentratie, die zichtbaar zou zijn als de ^{14}C-activiteit het gevolg was van menging van Holoceen zoet water met Plioceen- tot Vroeg-Pleistoceen zeewater. Een nauwkeurige bepaling van de leeftijd van de brakke- en zoute grondwatermonsters is onmogelijk. De reden hiervoor is dat de koolstof die in het water is opgelost voor het grootste deel afkomstig is van bronnen in het sediment zoals organisch materiaal en calciet, hetgeen blijkt uit geochemische massabalansberekeningen. De berekende leeftijd van een watermonster is hierdoor extreem gevoelig voor de veronderstelde leeftijd van de koolstofbron, welke onmogelijk geschat kan worden door de enorme ruimtelijke variatie die deze bezit. Van het brakke water in peilbuis 31E-0176 zijn tevens nieuwe monster genomen waarin de ^{87}Sr/^{86}Sr-ratio is bepaald. De gemeten waarden duiden, net als de ^{14}C-activiteit en de Cl-concentraties op een Pliocene- tot Vroeg-Pleistocene herkomst van het brakke grondwater in het onderste filter en een Holocene herkomst van het brakke grondwater daarboven.

De resultaten van het onderzoek naar het zoutgehalte van het poriënwater in een drietal kleilagen onder de bodem van de Noordzee worden gepresenteerd in hoofdstuk 3. De bemonsterde locaties bevinden zich op de Doggersbank, de Boldersbank en de Bruine Bank. Onder de Doggersbank worden tot een diepte van circa 2 m onder de zeebodem Cl-concentraties aangetroffen die hoger zijn dan zeewater ($m_{\mathrm{Cl}} = 566$ mmol/l). Beneden deze diepte neemt de Cl-concentratie abrupt af. Ook onder de Boldersbank zijn twee monsters aangetroffen met een Cl-concentratie die hoger is dan zeewater, maar de afname met de diepte is veel geringer. Het profiel onder de Bruine Bank liet de duidelijkste afname zien en hier is een diepere boring gezet zodat de gehele kleilaag bemonsterd kon worden. De Cl-concentratie laat een afname zien van 562 mmol/l aan de bovenkant van de kleilaag (1.2 m onder de zeebodem) naar 250 mmol/l aan de onderkant van de kleilaag (5.9 m onder de zeebodem). Ook de gemeten δ^{2}H-, δ^{18}O- en δ^{37}Cl-waarden laten een duidelijke afname zien. De

waargenomen patronen geven aan dat er neerwaartse diffusie plaatsvindt. Met behulp van een eenvoudig model is dit proces gesimuleerd zodat de diffusiecoëfficienten van Cl, ^{2}H en ^{18}O berekend konden worden. Hieruit volgt dat de diffusiecoëfficient van Cl ongeveer een factor 10 lager is dan die van ^{2}H en ^{18}O. Uit experimenten met ongestoorde kleimonsters blijkt eveneens dat Cl langzamer diffundeert dan ^{18}O, maar omdat de omstandigheden in het laboratorium afweken van die in het veld is het verschil minder groot. De diffusiecoëfficient van Cl die uit het model volgt is veel lager dan diffusiecoëfficienten die in de literatuur worden gerapporteerd. De oorzaak hiervoor is wellicht de sterke uitdroging en compactie van de kleilaag gedurende het Weichselien, maar door welk mechanisme het transport van Cl wordt vertraagd is niet helemaal duidelijk.

Het onderzoek op Texel, dat besproken wordt in hoofdstuk 4, had tot doel het voorkomen van grondwater met een Cl-concentratie hoger dan zeewater te verklaren. Grondwater met een dergelijk hoog zoutgehalte komt op verschillende plaatsen langs de Nederlandse kust voor. In een aantal peilbuizen en een gestoken kleikern zijn de chemische samenstelling en de isotopen ^{2}H, ^{18}O en ^{37}Cl van het water bepaald. De Cl-concentraties in de peilbuizen zijn lager dan wat in voorgaande jaren is gemeten maar nog steeds anderhalf maal zo hoog als het zeewater rondom Texel. De Cl-concentraties van het poriënwater in de kleilaag zijn het hoogst op 4.2 m onder maaiveld ($m_{\mathrm{Cl}} = 612$ mmol/l) en nemen geleidelijk af richting de boven- ($m_{\mathrm{Cl}} = 100$ mmol/l) en onderkant ($m_{\mathrm{Cl}} = 538$ mmol/l) van de kleilaag. De isotopen vertonen een vergelijkbaar patroon. Ultrafiltratie (of omgekeerde osmose) en bevriezing van zeewater worden uitgesloten als mogelijke oorzaken van de verhoogde zoutgehaltes. De waargenomen δ^{2}H- en δ^{18}O-waarden wijzen er op dat verdamping van zeewater, zowel direct als door planten, het meest waarschijnlijke proces is dat tot de vorming van hypersalien grondwater heeft geleid. Mogelijk hebben oplossing van neergeslagen zoutkristallen, zoutuitscheiding door planten en droge depositie ook een bijdrage geleverd. Na inpoldering van het gebied, 170 j geleden, is de kleilaag verzoet wat met een model gesimuleerd. Overeenkomst tussen model en velddata werd bereikt door, behalve diffusie, een neerwaartse advectieve flux van 6 mm/j te beschouwen. Uit het model volgt dat het zougehalte van de kleilaag voor verzoeting tussen de 1 en 1.4 mol/l bedroeg. Dit betekent dat zelfs de hoogste Cl-concentraties die in het Nederlandse kustgebied zijn aangeroffen ($m_{\mathrm{Cl}} = 839$ mmol/l) aan evapotranspiratie toegeschreven kunnen worden.

In hoofdstuk 5 wordt getracht inzicht te verkrijgen in het verloop van verzilting door vrije convectie die optreedt wanneer zeewater een gebied overstroomt waar zich zoet grondwater in de ondergrond bevindt. Er ontstaat eerst een grenslaag die groeit door diffusie totdat deze een kritische dikte bereikt en instabiel wordt, waarna zoutpluimen naar beneden zakken. Theoretische verbanden die de zaksnelheid van individuele pluimen beschrijven houden geen rekening met het afnemende dichtheidsvershil tussen de pluimen en het omliggende zoete grondwater tijdens het zakken en het samengaan van pluimen. De uitgevoerde numerieke experimenten hadden tot doel het effect van deze processen op de verziltingssnelheid te bepalen in

een systeem met een hoog Rayleigh getal ($Ra = 6\,000$). Uit de experimenten volgt een uitdrukking voor de zaksnelheid van het horizontaal gemiddelde zoutgehalte wat consistent is met bestaande uitdrukkingen voor de zaksnelheid van individuele pluimen. Nieuw is dat hiermee het zoutgehalte als functie van diepte en tijd geschat kan worden. De toepasbaarheid in aquifers wordt bemoeilijkt doordat bij hoge permeabiliteit de dimensies van de zoutpluimen die van de poriën naderen waardoor de geldigheid van de vergelijkingen in het geding komt. Bovendien spelen heterogeniteit en hydronamische dispersie een rol. Desalniettemin is een schatting te geven van de tijd die nodig was om de Pleistocene aquifers in het Nederlandse kustgebied te verzilten. Deze ligt in de orde van tientallen jaren, hetgeen relatief kort is vergeleken met de duur van de Holocene transgressies.

In hoofdstuk 6 wordt een aantal numerieke experimenten besproken die tot doel hadden het effect van een inhomogene ondergrond op het verziltingspatroon door vrije convecntie te bestuderen. Drie verschillende situaties zijn beschouwd: (1) overstroming door de zee met gelijktijdige sedimentatie, (2) een transgressie in een gebied met een reeds aanwezige kleilaag aan de oppervlakte en (3) horizontale verplaatsing van brak water in een aquifer onder een kleilaag. Zowel sedimentatie als de aanwezigheid van een kleilaag (scenario's 1 en 2) vertragen het optreden van vrije convectie. Realistische sedimentatiesnelheden zijn echter te laag om vrije convectie te voorkomen. De aanwezigheid van een kleilaag aan de oppervlakte vertraagt het optreden van vrije convectie met mogelijk duizenden jaren. De pluimen die in dat geval ontstaan zijn veel breder dan de pluimen die in een aquifer met dezelfde permeabiliteit onstaan waar een kleilaag ontbreekt. In het beschouwde geval van horizontale verplaatsing van brak grondwater (scenario 3) wordt een afstand overbrugd van ongeveer 3.2 km in 1 000 j. Omdat de kleilagen in het kustgebied op vele plaatsen zijn doorsneden, betekent dit dat in grote delen van de Pleistocene aquifers verhoogde zoutconcentraties verwacht mogen worden als gevolg van laterale zoutindringing.

In de synthese worden de belangrijkste uitkomsten van het onderzoek samengevat en vergeleken met inzichten uit de literatuur. Op basis van de resultaten wordt de grootschalige paleohydrologische ontwikkeling van het Nederlande kustgebied gedurende het Holoceen geschetst. Daarnaast worden enkele praktische implicaties besproken. De verkegen inzichten kunnen bijvoorbeeld van belang zijn bij het onderscheiden van natuurlijke en menselijke oorzaken van verhoogde zoutgehaltes, het modelleren van zeewaterintrusie en grootschalige stromingssystemen en het gebruik van poriënwateranalyses voor het schatten van fluxen en doorlatendheden. Tenslotte wordt ingegaan op aspecten waarvan de huidige kennis ontoereikend is. Deze omvatten het gedrag van vrije convectie in aquifers, het voorkomen van relatief zoet grondwater onder de zeebodem, transportprocessen in kleilagen, de toepassing van nieuwe dateringstechnieken voor brak- en zout grondwater en het verzoeten van Pliocene- en Vroeg-Pleistocene mariene pakketten.

Dankwoord (Acknowledgements)

Wie zee houdt, wint de reis. Maar in m'n eentje had ik de reis niet gehaald.

Mijn ouders Henk en Mieke verdienen het om als eerste genoemd te worden. De kansen die ik in mijn leven heb gekregen, heb ik voor een groot deel aan hen te danken dus dat geldt ook voor dit proefschrift.

Collega-promovendi Victor Bense, Elmer van den Berg en Boris van Breukelen waren hardstikke aardige jongens. Rik Jonker en Gu Oude Essink trouwens ook. De afgelopen jaren waren in vele opzichten uniek, soms bijna surrealistisch, maar bovenal de moeite waard en dat was grotendeels dankzij hen.

Dat geldt ook voor Henk Kooi en Koos Groen. Maar Henk was copromotor en een zeer competente ook nog, dus noem ik hem apart. Gelukkig stuurde hij me bij toen ik er even geen zin meer in had. En Koos was altijd enthousiast, soms een beetje verstrooid, zat vol goede ideeën en bezorgde me een paar leuke klusjes tussendoor.

Promotor Co de Vries bestudeerde het zoute grondwater in Nederland ook al voor zijn proefschrift, maar koos uiteindelijk een ander onderwerp omdat er toen nog te weinig rekenkracht bestond voor een kwantitatieve aanpak. Nadat de rekenlineaal had plaatsgemaakt voor de supercomputer ontstond in 1998, mede dankzij TNO-NITG, een mogelijkheid voor een hernieuwde poging, die hij aan mij toevertrouwde.

Nadat Gijs Remmelts van afdeling verhuisde, nam Jasper Griffioen de taak van contactpersoon bij TNO-NITG op zich. Hij toonde veel interesse in mijn werk en voorzag talrijke manuscripten van inhoudelijk commentaar.

Jasper maakte ook deel uit van de leescommissie, die verder bestond uit Prof. Mike Edmunds, Dr. Cees Meinardi, Dr. Theo Olsthoorn en Dr. Kay Beets. Kay was ook degene die mij liet kennismaken met de toepassing van Sr-isotopen in de hydrogeologie en dat moest bekopen met een ijs- en ijskoude middag in het veld.

Hetty Schäfer en Nel Slimmen hebben in het laboratorium heel wat te stellen gehad met mijn grondwatermonsters, die eigenlijk veel te zout waren. Het CIO in Groningen verzorgde de isotopenanalyses, waarbij de behulpzame Bert Kers een voorname rol speelde. Harm-Jan Streurman, die alle monsters uit het CIO-archief uit het hoofd leek te kennen, was onmisbaar bij het opsporen van oude analyses.

Ik heb veel hulp gekregen van studenten: Arno Hooijboer stortte zich met volle overgave op de klei van de Bruine Bank, Kevin Ooteman en Esther Bloem verwerkten tegenslag na tegenslag in de polders bij Weesp (maar gaven niet op!), Sander Brink haalde alles uit de kast om het lastige probleem van het zoete grondwater in Amstelveen op te lossen en Joeri Jacobs en Fred Hartendorf namen de boot naar

Texel. Over studenten gesproken: dankzij Annemieke, Hedwig en Imke werd het klusje voor de SWM in Suriname nog onvergetelijker.

Zowel voor, tijdens als na al het veldwerk stond Michel Groen paraat met goede adviezen, een verfrissende blik en een helpende hand. Lester Reiniers van de provincie Noord-Holland leverde een essentiële logistieke bijdrage aan de monstername in het veld en was altijd bereid om zijn gegevens met mij te delen. Hetzelfde geldt voor Jeroen de Maat van de provincie Zeeland. Ook veel anderen stelden hun data beschikbaar, zoals Reinder Boekelman van de TU Delft, Jos Dijkmans, Hans Huisman en Peter Jellema van TNO-NITG (ook dank aan Arthur van Ewijk!), Arjen Kok van Vitens, Paul Schot van de Universiteit Utrecht en Pieter Jan Stuyfzand van het KIWA.

Hanneke Gieske en Cees Laban van TNO-NITG en de bemanning van de 'Zirfaea' stelden ons in staat om de kleimonsters van de Noordzeebodem te bemachtigen. Garth van der Kamp beantwoordde de vele vragen die ik per e-mail op hem afvuurde over de radiale diffusie-experimenten. De alleskunners van de instrumentenmakerij zorgden ervoor dat de diffusiecellen ook werkelijkheid werden.

Leermeester Tony Appelo wil ik niet alleen bedanken voor het meedenken en de inhoudelijke discussies, maar ook voor de leuke cursussen en zijn goede gezelschap aan de dis.

Voor gezelligheid zorgden ook vele studenten en collega's, met name de rest van de harde kern van de C4-gang: Patrick Bogaart, Mark Bokhorst, Rob Houtgast, Govert Nugteren en Mirjam Vriend. Dat was ook wel nodig in die gang, die maandenlang de uiterlijke verschijning had van de diepste schacht van een kolenmijn.

Bij paranimfen Jan en Jolanda stond de deur altijd open, ook al was ik meestal (op doktersadvies) tenminste 30 minuten aan het klagen.

Ik zou de opsomming nog veel langer kunnen maken, toch laat ik het hier bij. Mijn excuses aan degenen die onvermeld blijven, want ook hen ben ik dankbaar.

Tenslotte is er nog één naam die niet mag ontbreken en dat is die van Fran.

A recipe for free convection

You don't need a supercomputer to set up a free convection experiment: it is as easy as baking a cake. The photograph below shows the slices of a marble cake made up of alternating layers of batter with and without cacao that were originally stratified horizontally. Density differences due to differential heating during baking gave rise to convective flow, which can be seen from the well-developed finger patterns.

The recipe for this cake, reproduced here with the kind permission of the publisher J.H. Gottmer / H.J.W. Becht BV, is from the *Cookery book of the Amsterdam domestic science school* by C.J. Wannée, originally published in 1909.

200 g of butter
200 g of sugar
pinch of salt
7 g of vanilla sugar
4 eggs
200 g of self-raising flower, sieved
4 tablespoons of cacao
2 tablespoons of sugar

All ingredients must be at room temperature.

Butter a 27 cm cake tin and dust with flour. Preheat the oven to 160 °C or gas mark 2–3. Using an electrical mixer, whisk the butter, sugar, salt and vanilla sugar to a lightly-colored, creamy mass. Mix in the eggs one by one. After each egg is taken up by the batter, keep mixing another 2 minutes before adding the

next one. Gradually add the flour to the batter. Mix the cacao and the sugar with 4 tablespoons of hot water until smooth. Mix the cacao mixture with half of the batter. Pour alternating layers of the two batters into the cake tin. Start and finish with the normal batter. Put the tin on a wire rack just below the middle of the preheated oven and bake for 75 minutes until golden brown. Let cool in the tin for a short while. Remove the tin and leave to cool completely.